universität wien

DISSERTATION

Titel der Dissertation

Assessment of innovative *in situ* techniques for groundwater and soil remediation: nanoremediation and thermal desorption

Verfasserin

Diplom LebChem Susanne Laumann

angestrebter akademischer Grad

Doktorin der Naturwissenschaften (Dr. rer. nat.)

Wien, 2013

Studienkennzahl lt. Studienblatt:	A 791426
Dissertationsgebiet lt. Studienblatt:	Dr.-Studium der Naturwissenschaften Erdwissenschaften
Betreuerin / Betreuer:	Univ. Prof. Dr. Thilo Hofmann

Table of Contents

Acknowledgments

I would like to express my gratitude to Prof. Thilo Hofmann for giving me the opportunity to work in his group. His support, guidance and encouragement helped me to gain and maintain confidence in my work and made this thesis possible.

I particularly would like to thank Dr. Vesna Micić Batka for her invaluable support. Her immense encouragement kept me motivated throughout my PhD and I really appreciated her honesty, reliability, and dedication when discussing my work.

I am thankful to Prof. Gregory V. Lowry for sharing his knowledge on nanoremediation and for the fruitful discussions during his time in Vienna.

I thank Dr. Johann Fellner and David Clement as well as Dr. Thomas Reichenauer, Dr. Georg Waldner, Philipp Schöftner, Dr. Nadezhda Kataeva, and Dr. Jörg Schotter for the nice cooperation within the MEMOS and the NanoSan projects.

I also would like to thank the Austrian Federal Ministry of Agriculture, Forestry, Environment and Water, who funded the MEMOS and the NanoSan projects and therefore made this research possible.

I am grateful to Petra Körner and Wolfgang Obermaier for their invaluable help in the laboratory and to Dr. Frank von der Kammer and Dr. Melanie Kah for their support and advice over the last four years.

I would like to thank the entire Department for the amazing time I had during my PhD and the cooking group for keeping me alive. I especially want to thank Elisabeth Neubauer, Christian Müllegger, Andrea Bichler and Stephanie Haslinger. You made Vienna feel like home!

Last but not least I want to thank my family, Jakob Hüsing, Jochen Erpenbeck, Mirko Bachmeyer, Johanna Gründker, Lina Klingebeil and Monika Hohenbrink for their support, help and care.

Abstract

Contamination of soil and groundwater by organic and inorganic contaminants is a serious environmental issue in many industrial countries. Chlorinated solvents are among the most frequently found contaminants in soil and groundwater. Once released into the environment, they can contaminate large volumes of soil and groundwater and persist in the subsurface for decades. Consequently, sustainable and effective remediation strategies are needed to clean up such contaminated land and to improve environmental quality.

The overall objective of this PhD thesis was to investigate the use of two selected innovative remediation techniques: nanoremediation and *in situ* thermal desorption. More specifically, the objectives were (1) to close some of the gaps in knowledge with respect to the mobility of nZVI in the subsurface that currently limit the practical use of nanoremediation for *in situ* groundwater treatment and (2) to evaluate the effectiveness of *in situ* thermal desorption in a contaminated soil by means of material flow analysis. The main findings can be summarized as follows:

Nanoremediation

- The mobility of commercially available, polyacrylic acid coated nZVI (PAA-nZVI) was significantly reduced in carbonate-containing porous media and in the presence of high dissolved calcium concentrations.
- The maximum predicted travel distance of PAA-nZVI was reduced from approximately 1.6 m in quartz sand to just a few centimeters in pure carbonate sand.
- Modification of the aquifer grain surfaces by means of a polyelectrolyte coating (natural organic matter, humic acid, carboxymethyl cellulose, and lignin sulfonate) affects the PAA-nZVI mobility in carbonate porous media.
- The co-injection of polyelectrolytes has been shown to increase the mobility of PAA-nZVI in carbonate-containing porous media and also in the presence of high dissolved calcium concentrations (as typically found in carbonate-rich aquifers).
- Lignin sulfonate, an environmentally friendly and inexpensive agent, was identified as the most suitable polyelectrolyte for field applications.
- The greatest increase in PAA-nZVI mobility in carbonate sand was achieved with co-injected lignin sulfonate concentrations of 50 mg L^{-1} or more. At these concentrations the maximum PAA-nZVI travel distance in carbonate porous media was double that measured in the absence of lignin sulfonate.

***In situ* thermal desorption (ISTD)**

- At the investigated field site, ISTD was effective in removing the majority of chlorinated solvents from soil. The target remediation value in soil vapor (10 mg m^{-3}) was achieved after nine months of remediation, demonstrating the efficiency of ISTD for this particular site.
- Material flow analysis is shown to be a suitable tool for evaluation of soil remediation performance. It reveals contaminant emissions into the environment, before and during remediation and provides an overview of processes occurring throughout soil remediation.

The results presented in this PhD thesis demonstrate that the optimization of innovative techniques is necessary in order to effectively remediate contaminated land. The comprehensive assessment of a remediation performance is another important step in the further development and optimization of innovative remediation techniques. This assessment should consider all environmental effects of the remediation in order to achieve the best environmental management practices.

Kurzfassung

Boden- und Grundwasserkontaminationen durch organische und anorganische Schadstoffe sind ein weitverbreitetes Problem in vielen Industrieländern. Chlorierte Kohlenwasserstoffe gehören dabei zu den am häufigsten vorkommenden Schadstoffen. Gelangen diese in die Umwelt, sind großflächige Kontaminationen des Untergrundes möglich. Zur Sanierung derart kontaminierter Standorte ist es notwendig nachhaltige und innovative Sanierungsverfahren zu entwickeln und zur Marktreife zu bringen.

Das Ziel dieser Dissertation war es zwei ausgewählte innovative Sanierungsverfahren für die Grundwasser- und Bodensanierung zu untersuchen, eine Sanierung in der Praxis wissenschaftlich zu begleiten und diese Verfahren zu optimieren. Bei den Verfahren handelt es sich um die Sanierung mit Nanoeisenpartikeln und die thermische *in situ* Sanierung. Zum einen wurde das Transportverhalten von Nanoeisenpartikeln genauer untersucht, da die geringe Mobilität der Nanoeisenpartikel derzeit einen breiten Einsatz in der Grundwassersanierung verhindert. Zum anderen wurde die Effektivität der thermischen *in situ* Sanierung in der ungesättigten Bodenzone an einem Feldstandort mit Hilfe einer Stoffflussanalyse bewertet. Die Ergebnisse der Dissertation können folgendermaßen zusammengefasst werden:

Sanierung mit Nanoeisenpartikeln

- Die Mobilität von kommerziell erhältlichen mit Polyacrylsäure modifizierten Nanoeisenpartikeln (PAA-nZVI) nimmt in carbonatreichen Aquiferen und in Gegenwart von hohen Calciumkonzentrationen ab.
- Die maximale Transportreichweite beträgt 1,6 m im Quarzsand und verringert sich auf wenige Zentimeter im Carbonatsand.
- Die Modifizierung der Oberfläche des Aquifermaterials mit Polyelektrolyten (natürliches organisches Material, Huminsäure, Carboxymethylcellulose und Ligninsulfonat) beeinflusst das Transportverhalten der Nanoeisenpartikel in carbonatreichen Aquiferen.
- Die Coinjektion von Polyelektrolyten zusammen mit den Nanoeisenpartikeln führt zu einer erhöhten Partikelmobilität bei hohen Calciumkonzentrationen und in carbonatreichen Aquiferen.
- Von den verwendeten Polyelektrolyten ist Ligninsulfonat an einem Feldstandort zu bevorzugen, da es nicht toxisch, in großen Mengen verfügbar und preisgünstig ist.

- Der größte Einfluss auf die Partikelmobilität wird bei Ligninsulfonatkonzentrationen ≥ 50 mg/l beobachtet. Die Coinjektion dieser Ligninsulfonatmenge führt zu einer Verdopplung der Transportreichweite der Nanoeisenpartikel in carbonatreichen Aquiferen.

***In situ* thermische Sanierung**

- Durch die *in situ* thermische Sanierung in der ungesättigten Bodenzone wurde ein Großteil der Schadstoffe am untersuchten Feldstandort entfernt. Der Sanierungszielwert in der Bodenluft (10 mg/m^3) wurden nach neun Monaten erreicht. Dies verdeutlicht die hohe Effizienz der thermischen Sanierung an diesem kontaminierten Standort.
- Die Stoffflussanalyse ist ein geeignetes Mittel zur Evaluierung einer Sanierungsmaßnahme. Sie ermöglicht es, Schadstoffemissionen in die Umwelt während und nach Sanierung zu quantifizieren und gibt einen Überblick über Prozesse, die während der Sanierung im Boden stattfinden.

Die Ergebnisse dieser Dissertation zeigen, dass die Weiterentwicklung von innovativen Sanierungsverfahren notwendig ist, um kontaminierte Standorte effektiv zu sanieren. Eine umfassende Evaluierung von verschiedenen Verfahren ist ein weiterer wichtiger Schritt zur Optimierung und Weiterentwicklung von innovativen Sanierungstechniken. Um eine nachhaltige Sanierung sicherzustellen, sollte diese Evaluierung alle Auswirkungen auf die Umwelt berücksichtigen.

1. General introduction

1.1. Subsurface contamination

Contamination of soil and groundwater by organic and inorganic contaminants is a serious environmental issue in many industrial countries. The European Environment Agency (EEA) estimates that nearly three million sites in its member states are potentially polluted. Soil and groundwater contamination at approximately 250,000 of these sites requires clean up (EEA, 2007). The U.S. Environmental Protection Agency (U.S. EPA) estimates that a similar number of hazardous waste sites (294,000) are present in the United States (Karn et al., 2009). Major causes for soil and groundwater contamination are recent and historic industrial and agricultural activities. Improper disposal of municipal and industrial wastes additionally causes elevated concentrations of a wide range of contaminants in the environment. The most frequently encountered soil and groundwater contaminants are heavy metals, mineral oil and chlorinated solvents (Karn et al., 2009; Lowry, 2007; EEA, 2007).

Chlorinated solvents such as tetrachloroethene (PCE) and trichloroethene (TCE) have been produced in large quantities since the middle of the 20th century. These compounds are used in a variety of applications, mainly as metal degreasers, chemical intermediates, and in dry cleaning. Once released into the environment, chlorinated solvents can contaminate large volumes of soil and groundwater and persist in the subsurface for decades. Remediation of such contaminated sites is challenging due to the specific physicochemical properties of chlorinated solvents, as they belong to the dense non-aqueous phase liquids (DNAPLs; Stroo et al., 2003). DNAPLs rapidly migrate through the subsurface since they are typically denser and less viscous than water (Kueper et al., 2003). Disconnected droplets and ganglia of DNAPLs (residual DNAPL) are formed in both soil and groundwater at the tailing end of the migrating DNAPL body (U.S. EPA, 2004). Furthermore, DNAPLs can come to rest in larger accumulations (DNAPL pools), which tend to form above finer-grained horizons such as clay (Figure 1.1). Residual and pooled DNAPLs can evaporate into the soil air and dissolve into groundwater, leading to a long-term contamination of soil, soil vapor, and groundwater.

The amount of chlorinated solvents present at contaminated sites can be quite large, approaching hundreds to tens of thousands of kilograms (Brusseau et al., 2013). Consequently national and regional legislation has been implemented to enforce the clean up of contaminated land and the protection of groundwater resources, as well as to promote environmental

quality and public health (Cundy et al., 2008). This requires sustainable and effective remediation strategies.

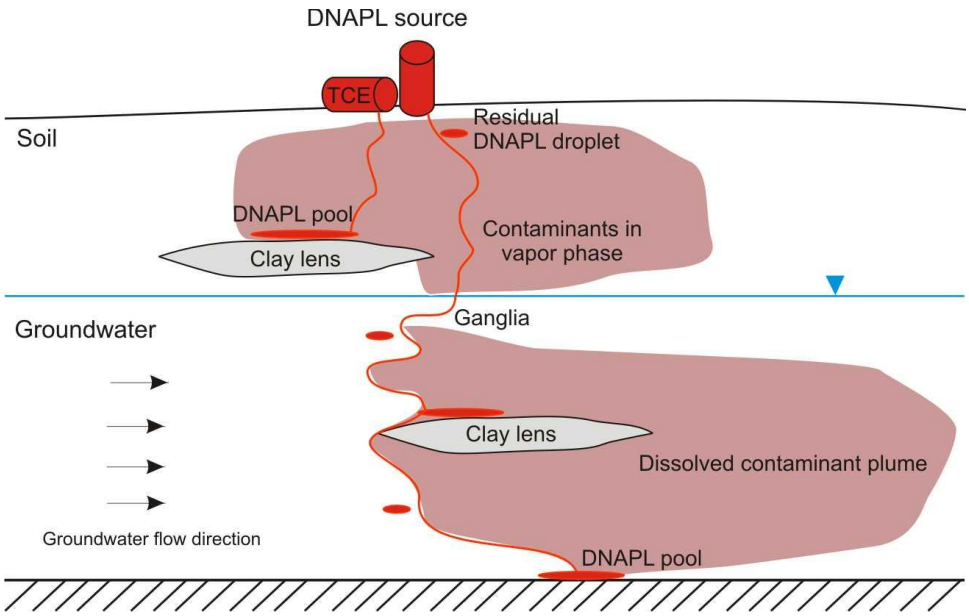

Figure 1.1. DNAPL release, transport, and distribution in the subsurface (modified after Mackay and Cherry (1989) and U.S. EPA (2004)).

1.2. Conventional techniques for soil and groundwater remediation

The most commonly applied remediation technique for contaminated groundwater in the past thirty years has been pump-and-treat (P&T; Mackay and Cherry, 1989; Stroo et al., 2012). P&T involves extraction of contaminated groundwater via groundwater wells and on-site treatment by, for example, activated carbon. The effectiveness of a P&T system is reduced by mass-transfer limitations due to slow dissolution of residual and pooled DNAPLs, slow desorption/diffusion rates of contaminants, and heterogeneities in terms of hydraulic conductivity (Mackay and Cherry, 1989). These effects result in tailing (the slower rate of decline in dissolved contaminant concentration with continued P&T operation) and rebound (the increase in contaminant concentration that can occur if pumping is discontinued). Both tailing and rebound hamper the site remediation by P&T (U.S. EPA, 1996; Voudrias, 2001). Therefore, even though they may operate for decades at a single site, P&T systems are often not able to achieve clean up goals (Karn et al., 2009; Stroo et al., 2003).

Soil remediation conventionally involves excavation of the contaminated soil. Excavation is, however, not always practical and can be extremely costly, especially at sites with deep sub-

surface contamination or contamination beneath aboveground infrastructure. At such sites soil vapor extraction (SVE) appears to be a common alternative (Nobre and Nobre, 2004).

SVE is a remediation technique for relatively permeable and homogenous soils affected by volatile and semi-volatile contaminants, such as chlorinated solvents (U.S. EPA, 1997a; Khan et al., 2004; Nobre and Nobre, 2004). SVE involves the application of a vacuum in the contaminated soil and subsequent extraction of the contaminated soil vapor, which is then treated before being released to the environment. For soils contaminated by TCE and PCE, SVE has become the default remediation practice (Brusseau et al., 2013). Nevertheless, it is observed that the effectiveness of SVE is typically reduced during later stages of operation (Brusseau et al., 2013). Factors contributing to this are soil heterogeneities, non-uniform contaminant distribution and associated limited accessibility of contaminants, higher soil-moisture content and mass-transfer limitations (Brusseau, 1991; Massmann et al., 2000; Poulsen et al., 1996). The latter are caused by, for example, slow desorption/diffusion rates and the limited volatilization of contaminants at normal soil temperatures (Brusseau et al., 2010; Heron et al., 1998; Park et al., 2005). In many cases, SVE can therefore not meet cleanup criteria in a reasonable time, which results in long remediation times and high remediation costs.

Overall, P&T and SVE systems can no longer be considered as the best remediation approaches for contaminated groundwater and soil. The high costs and long operating time of these conventional methods drive the need to develop innovative and more effective *in situ* remediation technologies.

1.3. Innovative remediation techniques

Innovative remediation techniques are remediation approaches that either increase the performance of a conventional method or represent a more effective alternative, making them faster and more cost-effective. These remediation techniques involve physical, chemical and biological processes, or their combinations. Some examples of innovative remediation techniques are microbial techniques (such as bioventing), solvent flushing, *in situ* chemical oxidation, *in situ* thermal remediation, permeable reactive barriers, and nanoremediation. Many innovative technologies are currently available for treatment of contaminated sites; the selection, however, depends on the contaminant present, the site characteristics, regulatory requirements, and remediation time and costs (Khan et al., 2004; Mulligan et al., 2001).

This thesis focuses on two innovative *in situ* techniques, one applicable for groundwater and one for soil contamination: nanoremediation and thermal remediation, respectively.

1.3.1. Nanoremediation for groundwater contamination

Nanotechnology in remediation, also referred to as nanoremediation, has received increasing attention as an efficient *in situ* treatment technique for contaminated groundwater. Nanomaterials enable fast and efficient transformation and detoxification of contaminants, due to their high chemical reactivity and high specific surface area (>20 m^2 g^{-1}; Karn et al., 2009; Zhang, 2003). Several reactive nanomaterials such as nanoscale zero-valent iron (nZVI; Liu et al., 2005; Zhang, 2003), bimetallic nanoparticles (using e.g., nZVI with palladium or nickel; Schrick et al., 2002; Wang and Zhang, 1997), metal oxides and hydroxides (such as ferrihydrite and titanium dioxide; Chen et al., 2005; Tosco et al., 2012), and zeolites (Georgi et al., 2010; Gonzalez-Olmos et al., 2013) are currently being explored for remediation. All of these nanomaterials have different modes of action, including contaminant reduction, oxidation and adsorption. This thesis focuses on nZVI, as a nanomaterial with the highest potential for contaminant transformation, particularly for chlorinated solvent detoxification, and as currently the most widely used nanomaterial for *in situ* groundwater treatment (Grieger et al., 2010; Karn et al., 2009).

Zero-valent iron is a strong reducing agent, which can be used for treatment of a variety of contaminants, primarily chlorinated solvents (Gillham and O'Hannesin, 1994; Liu et al., 2005) but also pharmaceuticals (Stieber et al., 2011), pesticides (Elliott et al., 2009; Joo and Zhao, 2008; Sayles et al., 1997), polychlorinated biphenyls (Chuang et al., 1995; Lowry and Johnson, 2004), radionuclides (Cundy et al., 2008; Gu et al., 1998), and heavy metals (Cantrell et al., 1995; Kanel et al., 2005). For *in situ* groundwater remediation, zero-valent iron has first been applied in its granular form in permeable reactive barriers (U.S. EPA, 1998). Although reactive barriers can effectively remove contaminants from groundwater, they remediate the contaminant plume but not the source zone (Li et al., 2006). Their application is limited due to construction restrictions and therefore excludes remediation of contaminated sites with aboveground infrastructure or remediation of deep aquifers (Li et al., 2006; O'Carroll et al., 2013).

nZVI has potential to overcome these limitations, by direct emplacement of nZVI in form of a water suspension within the contaminated source zone (Figure 1.2). There are, however, still critical aspects of the nZVI-based remediation that until now prevented the widespread

market and regulatory acceptance of this technique. Critical aspects include the reactivity and longevity of the particles as well as the nZVI emplacement within the contaminated source zone (Lowry, 2007; O'Carroll et al., 2013).

Reactivity and longevity of nZVI are affected by particle properties (i.e., specific surface area, age of the particles, and surface coating), pH and redox conditions at the investigated site, concentrations of reactive groundwater constituents, and concentrations of the contaminant itself (Liu et al., 2005; Liu and Lowry, 2006; Liu et al., 2007; Phenrat et al., 2009b). Natural groundwater constituents such as nitrate and oxygen can, for example, compete with the target contaminants, thereby reducing the effectiveness of nZVI towards contaminant reduction (O'Carroll et al., 2013). In addition, reactivity and longevity of nZVI under near-natural conditions (i.e., in porous media) have rarely been investigated. Therefore, understanding and evaluating the factors that control nZVI reactivity and longevity, and improving particle properties to overcome potential obstacles are part of ongoing research.

The emplacement of nZVI within the contaminated source zone is essential for the widespread implementation of this remediation technique, since the attractiveness of nanoremediation lies in its potential to be used *in situ*. If the particles are not delivered to the contaminated source zone, their potential as a highly reactive remediation agent cannot be utilized (Lowry, 2007). Successful emplacement depends on the injection technique, the injection velocity and the mobility of nZVI in the subsurface. All of these aspects are also part of current investigations.

The simplest nZVI injection technique involves the utilization of existing groundwater monitoring wells (Figure 1.2). In order to achieve a hydraulic gradient, parallel sets of injection and extraction wells can be used (Johnson et al., 2013). Other methods for nZVI injection include direct push, pressure pulse technology, pneumatic fracturing, and hydraulic fracturing (U.S. EPA, 2008; Grieger et al., 2010). In general, very high injection velocities compared to natural groundwater flow or induced fractures are needed to successfully deliver nZVI to the contaminated source zone (Tratnyek and Johnson, 2006).

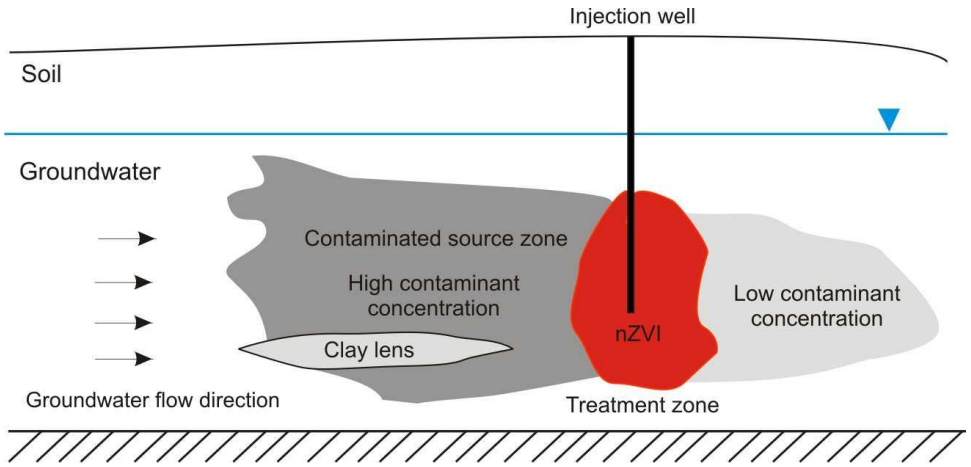

Figure 1.2. Schematic representation of an *in situ* groundwater remediation using nZVI (modified after Tratnyek and Johnson, 2006).

The mobility of nZVI in the subsurface has been shown to be a major obstacle to the nZVI application for *in situ* groundwater remediation (Crane and Scott, 2012; Grieger et al., 2010). Previous studies have demonstrated that nZVI-based particles are not mobile in porous media; transport distances rage from a few centimeters in sand columns (Schrick et al., 2004) to just a few meters measured in a three-dimensional field-scale system (Johnson et al., 2013) and a field demonstration in fractured sandstone (Zhang and Elliott, 2006).

The limited nZVI mobility is a result of extensive particle aggregation and deposition onto aquifer grains. Particle sedimentation, pore blocking, ripening, and straining are additional processes that can reduce particle mobility (Bradford et al., 2002; Ryan and Elimelech, 1996; Yao et al., 1971). All of these processes are influenced by particle properties, including the particle size, composition, and surface charge (Phenrat et al., 2007; Phenrat et al., 2009a), and site-specific hydrochemical and hydrogeological conditions. Hydrogeochemical factors include the groundwater chemistry (i.e., water composition, ionic strength, and pH; Kim et al., 2012; Saleh et al., 2008) and the properties of the aquifer material (such as grain size distribution, surface charge heterogeneities, surface roughness, and mineral and organic matter content; He et al., 2009; Kim et al., 2012).

A common tool for minimizing particle aggregation and deposition onto the aquifer grains is surface modification of nZVI particles with polymers, polyelectrolytes, or surfactants (Phenrat et al., 2009a; Raychoudhury et al., 2010). These different types of surface coatings provide different modes of stabilizing nZVI against aggregation and deposition, which include electrostatic, steric and electrosteric stabilization (Lowry, 2007). Anionic polyelectro-

lytes, for example, impart a negative surface charge on the nZVI, providing electrosteric repulsions and therefore hindering nZVI deposition onto the aquifer matrix.

The stability and mobility of coated nZVI, however, still remain affected by the site-specific groundwater chemistry. High ionic strength and especially the presence of divalent cations reduce the electrostatic double layer repulsions between particles as well as between particles and aquifer grains, increasing aggregation and deposition (Petosa et al., 2010; Saleh et al., 2008). Lower pH values (below 7) can change the conformation of the adsorbed polyelectrolyte layer on the nZVI surface and decrease the charge in this layer (Kim et al., 2012). This results in a loss of electrosteric repulsion, causing increased particle aggregation and thereby reduced mobility.

Surface charge heterogeneities encountered in aquifers are an additional factor that significantly controls particle deposition in porous media (Elimelech et al., 2000; Yang et al., 2010). Negatively charged silicates and alumosilicates are dominant minerals in porous media. The oxides of iron, aluminum, and manganese are an important group of accessory minerals and the most common source of surface charge heterogeneity in aquifers (Johnson et al., 1996; Ryan and Elimelech, 1996). These minerals are positively charged at pH values typically encountered in groundwater and therefore represent favorable deposition sites for negatively charged surface-modified nZVI particles. Studies on the transport of latex microspheres have demonstrated that particle deposition onto heterogeneously charged surfaces is orders of magnitude higher than on surfaces having no charge heterogeneity (Song et al., 1994). The same effect can be expected for nZVI particles. The influence of surface charge heterogeneities on the nZVI transport has, however, rarely been addressed to date, since studies investigating nZVI transport were mainly carried out with homogenously charged quartz as a model aquifer material (Kim et al., 2009; Raychoudhury et al., 2012; Saleh et al., 2008).

The reduced particle mobility in heterogeneous porous media will limit the practical use of nanoremediation for *in situ* groundwater treatment. One way to overcome this problem is to reduce surface charge heterogeneity of the aquifer grains by means of polyelectrolyte coating. Polyelectrolytes can adsorb onto the favorable deposition sites (e.g., positively charged iron oxides or edges of clay minerals) in the porous media and hence increase the repulsion between the particles and the aquifer matrix (Kim et al., 2012). Previous studies have mainly investigated the effects of polyelectrolytes on the transport of non-coated particles (Johnson et al., 2009; Jones and Su, 2012; Kretzschmar and Sticher, 1997; Pelley and Tufenkji, 2008).

Only limited information is available on the effects that polyelectrolytes have on the transport of surface-modified nZVI used for *in situ* groundwater remediation.

1.3.2. *In situ* thermal remediation for soil contamination

Thermal remediation techniques are applied in order to enhance the performance of SVE. They are effective in removing semi-volatile and volatile contaminants, including chlorinated solvents (Heron et al., 1998), mercury (Kunkel et al., 2006), polychlorinated biphenyls (Stegemeier and Vinegar, 2001), BTEX aromatics (benzene, toluene, ethylbenzene, and xylenes, (Roland et al., 2011), and oil and petroleum products (Heron et al., 2005; Roland et al., 2007). The advantageous effects of thermal treatment are based on the influence of temperature on physical and chemical parameters of the contaminants. Increasing temperature results in reduced density, increased vapor pressure, reduced adsorption onto solid phases, and increased diffusion of the contaminants in the aqueous and gaseous phase (Heron et al., 1998; Roland et al., 2011; U.S. EPA, 1997b). In addition, the boiling points are reduced due to the formation of an azeotropic mixture with the pore water. An azeotropic mixture of, for example, TCE and water boils at 73°C, which is 14°C less than the pure TCE (with the boiling point of 87°C) and significantly less than the boiling point of water (U.S. EPA, 2004). All these temperature effects will aid to the recovery of contaminants from soil and to the achievement of remediation target values within a shorter time period (Heron et al., 2005).

Application of heat to the contaminated soil can be carried out via steam, water, and hot air injection, electrical resistance heating, radio frequency heating and thermal conductive heating (Heron et al., 1998). Which of these techniques is to be applied depends on the target contaminants and the properties of the porous media at the contaminated site (Park et al., 2005). Air, water, and steam injection, for example, require sites with relatively permeable zones. Electrical resistance heating and radio frequency heating increase the removal rates of contaminants from low-permeable soils (U.S. EPA, 1997a). Electrical resistance heating can, however, only be applied in humid soils (Roland et al., 2008) and is limited to the boiling temperature of water. This thesis focuses on the application of thermal conductive heating in complex and heterogeneous soils. Much higher temperatures in the subsurface have been achieved by applying this technique (Kunkel et al., 2006).

Thermal conductive heating, also known as *in situ* thermal desorption (ISTD), is an efficient remediation technique for heterogeneous and medium- to low-permeable soils (Lemming et al., 2013; Triplett Kingston et al., 2010). The advantages of ISTD compared to the other

thermal treatment technologies are its easy implementation, its robust usage and the relatively low costs (Roland et al., 2008; U.S. EPA, 1997a).

ISTD involves the simultaneous application of heat and vacuum to soils with an array of heating elements and SVE wells (Figure 1.3). The heat is transferred to the subsurface by thermal conduction from the heating elements (Stegemeier and Vinegar, 2001). This makes ISTD less sensitive to subsurface heterogeneities, since the thermal conductivity of different soil types varies only over a very narrow range, changing by only a factor of four from clay to sand (Kunkel et al., 2006). On the other hand, soils are not efficient heat conductors, thus high temperature heat sources are needed for effective energy conduction into the subsurface (U.S. EPA, 2004). The heating elements therefore usually operate at temperatures up to 600°C.

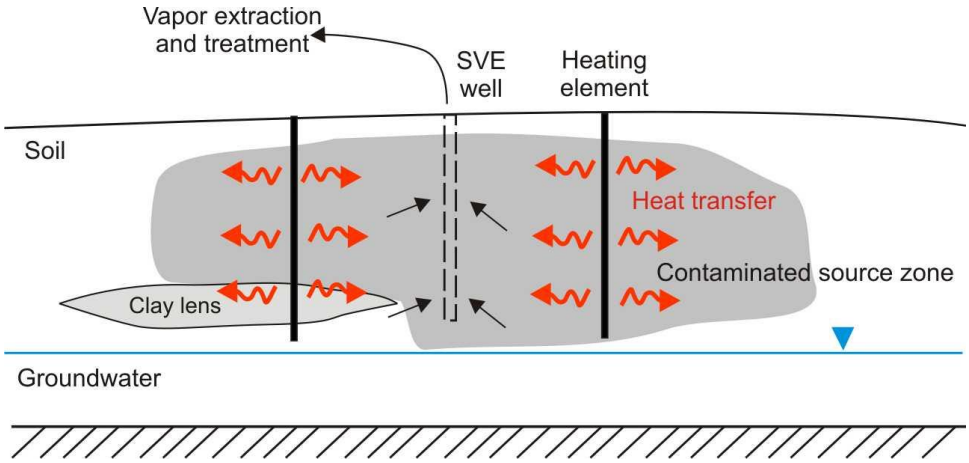

Figure 1.3. Schematic representation of an *in situ* thermal desorption system in soil (modified after U.S. EPA, 2004).

ISTD has already achieved market and regulatory acceptance and was applied at several sites contaminated by chlorinated solvents (e.g., Heron et al., 2009; Triplett Kingston et al., 2010; LaChance et al., 2006). The performance of this remediation technique has mainly been evaluated based on the achievement of the target remediation values and the measurements of the contaminant concentration in the soil, taken before and after remediation (Heron et al., 2009; Park et al., 2005; Stegemeier and Vinegar, 2001). A detailed assessment of an *in situ* thermal remediation practice, including the overall emission of the contaminants into the environment before and during remediation has not been performed to date.

1.4. Assessment of a remediation performance

The success of a remediation practice is defined by the achievement of the remediation goals. These usually include remediation target values such as contaminant concentration in soil vapor or contaminant mass flux in groundwater. For a better understanding of the effectiveness of a remediation technique and its environmental impact, it is necessary to include information about the contaminant mass present before, during, and after the remediation and the contaminant emissions into the environment during the course of remediation.

Mass balance calculations as a tool to evaluate the performance of a remediation are often limited to the amount of contaminants removed during the remediation (Heron et al., 2009; Park et al., 2005; Stegemeier and Vinegar, 2001). This is mainly due to the difficulty in quantifying the contaminant mass in soil prior to remediation. Soils are heterogeneous and the spatial distribution of contaminants such as chlorinated solvents is therefore often heterogeneous. This results in steep concentration gradients. In addition, the sampling density at contaminated sites is usually low in relation to the complex distribution of contaminants (Hofmann et al., 2010; Xie et al., 2011). This results in high values of relative uncertainty, which has to be taken into account in the assessment of a remediation performance.

Material flow analysis is a method based on the law of conservation of mass for systematic assessment of the flows and stocks of materials within a system defined in both space and time (Brunner and Rechberger, 2004). It is a frequently applied decision-support tool in waste (Pires et al., 2011; Steubing et al., 2010) and resource management (Klinglmair and Fellner, 2010; Wang et al., 2007), as well as in life-cycle assessment (Brunner and Rechberger, 2004). Material flow analysis has potential to be used for assessing the effectiveness of a remediation practice by means of connecting and quantifying the sources, the pathways, and the intermediate and final sinks of materials within a defined system. To date, material flow analysis has not been used to assess the performance of a remediation process.

1.5. Objectives of the thesis

The overall objective of this thesis was to investigate the use of the two selected innovative techniques for groundwater and soil remediation: nanoremediation and *in situ* thermal desorption. More specifically, the objectives were (1) to close some of the gaps in knowledge with respect to the mobility of nZVI in the subsurface that currently limit the practical use of nanoremediation for *in situ* groundwater treatment (elaborated in *Studies 1 & 2*) and (2) to

perform a detailed assessment of the effectiveness of *in situ* thermal desorption in a contaminated soil by means of material flow analysis (*Study 3*).

Objective 1

Nanoremediation for *in situ* groundwater treatment and in particular the application of nanoscale zero-valent iron (nZVI) has received increasing attention as a beneficial remediation technique. However, this remediation technique suffers from the limited transport of nZVI in the subsurface.

Study 1:

Previous studies on nZVI transport have mainly been carried out in quartz porous media. Carbonates represent an important group of minerals in aquifers (Ryan and Elimelech, 1996; Mackay et al., 1986) and they can locally comprise more than 80% of porous aquifers. Their effect on the nZVI transport has not been addressed in any study to date.

The aim of this study was to assess the influence of carbonate minerals in porous media on the transport of commercially available, polyacrylic acid coated nZVI (PAA-nZVI, NANOFER 25S, NANOIRON, s.r.o., Czech Republic). In order to account for the subsurface heterogeneities, the PAA-nZVI transport was evaluated in five model porous media, starting from pure quartz sand and systematically increasing the carbonate sand content. In addition, the influence of high dissolved calcium concentrations (which are typically encountered in carbonate-rich aquifers) on the PAA-nZVI transport in quartz and carbonate sand was investigated.

Study 2:

Aquifer heterogeneities due to carbonate minerals in porous media and high concentrations of dissolved calcium significantly reduce the nZVI mobility. Since such heterogeneities are commonly encountered in aquifers there is a need to improve nZVI mobility in these environments.

In this study the effect of co-injection of different polyelectrolytes (natural organic matter, humic acid, carboxymethyl cellulose, and lignin sulfonate) on the mobility of polyacrylic acid coated nZVI (PAA-nZVI, NANOFER 25S, NANOIRON, s.r.o., Czech Republic) in quartz and carbonate sand has been elucidated. One of the polyelectrolytes (lignin sulfonate) was chosen to study in detail the effect of increasing polyelectrolyte concentration on PAA-nZVI

transport and the combined effect of high dissolved calcium concentrations and co-injected polyelectrolyte on PAA-nZVI transport.

Objective 2

***In situ* thermal desorption (ISTD)** has already been applied at several contaminated sites in order to remove chlorinated solvents from soil (Heron et al., 2009; Triplett Kingston et al., 2010). A detailed assessment of an *in situ* thermal remediation practice is, however, still lacking.

Study 3:

In this study, ISTD was applied to remove a chlorinated solvent source from unsaturated soil beneath an existing aboveground infrastructure. The aim of this study was to apply a material flow analysis in order to assess the effectiveness of ISTD and to reveal the total emission of chlorinated solvents into the environment before and during remediation.

2. Carbonate minerals in porous media decrease mobility of polyacrylic acid modified zero-valent iron nanoparticles used for groundwater remediation

Susanne Laumann, Vesna Micić, Gegory V. Lowry, Thilo Hofmann

Environmental Pollution, 2013, 179, 53-60.

Reported with permission from Elsevier

Abstract

The limited transport of nanoscale zero-valent iron (nZVI) in porous media is a major obstacle to its widespread application for *in situ* groundwater remediation. Previous studies on nZVI transport have mainly been carried out in quartz porous media. The effect of carbonate minerals, which often predominate in aquifers, has not been evaluated to date. This study assessed the influence of the carbonate minerals in porous media on the transport of polyacrylic acid modified nZVI (PAA-nZVI). Increasing the proportion of carbonate sand in the porous media resulted in less transport of PAA-nZVI. Predicted travel distances were reduced to a few centimeters in pure carbonate sand compared to approximately 1.6 m in quartz sand. Transport modeling showed that the attachment efficiency and deposition rate coefficient increased linearly with increasing proportion of carbonate sand.

2.1. Introduction

The application of nanoscale zero-valent iron (nZVI) for *in situ* groundwater remediation has received increasing attention as a beneficial and novel remediation technique; nZVI is a strong reducing agent capable of rapid dechlorination of chlorinated organics and immobilization of heavy metals in contaminated groundwater (Grieger et al., 2010; Karn et al., 2009; Zhang, 2003). A precondition for effective nZVI application is its successful delivery to the contaminated source zones. This has proved to be a major obstacle to widespread utilization of this technology (O'Carroll et al., 2013; Tratnyek and Johnson, 2006). The reported transport distances for nZVI-based particles range from centimeters (Schrick et al., 2004) to hundreds of meters (Saleh et al., 2008) in sand columns (predicted using colloid filtration theory), to just a few meters measured in a field demonstration in fractured sandstone (Zhang and Elliott, 2006).

The limited nZVI transport in porous media is due to particle aggregation and deposition onto the aquifer grains. Both of these processes depend on the particle properties, such as size, composition, ZVI content, and surface charge (Phenrat et al., 2007; Phenrat et al., 2009a), as well as on the site-specific hydrochemical and hydrogeological parameters. These include the groundwater chemistry (i.e., water composition, ionic strength, and pH; Kim et al., 2012; Phenrat et al., 2010a; Phenrat et al., 2010b; Saleh et al., 2008) and the properties of the aquifer material (such as grain size distribution, surface charge heterogeneities, and mineral and organic matter content, He et al., 2009; Kim et al., 2012; Phenrat et al., 2011; Song et al., 2011). Although these studies showed the effects of certain parameters on nZVI transport, predicting nZVI mobility in a specific type of porous media is still not possible, since the most influential chemical and physical heterogeneities have not been identified yet.

Particle aggregation and deposition can be reduced by nZVI surface modification with polymers, polyelectrolytes, and surfactants, or by incorporation of nZVI into silica or activated carbon matrices (Bleyl et al., 2012; Mackenzie et al., 2012; Phenrat et al., 2010b; Zhan et al., 2008). Adsorbed anionic polyelectrolytes, such as polyacrylic acid (PAA), impart a negative surface charge on the nZVI and provide electrostatic double layer repulsions and electrosteric repulsions to counter attractive magnetic and van der Waals forces (Phenrat et al., 2010b; Raychoudhury et al., 2012; Schrick et al., 2004). The repulsive forces hinder nZVI deposition onto negatively charged aquifer material, which is prevalent in most subsurface media (Kim et al., 2012), therefore promoting nZVI mobility.

Even though nZVI transport can be promoted by PAA-modification in negatively charged quartz media, it is still affected by the physical and chemical heterogeneities encountered in aquifers, including variations in grain size, surface charge, and type and content of natural organic matter and clay. Studies on the transport of latex and silica microspheres have demonstrated that chemical heterogeneities can be a major factor controlling colloid deposition in porous media (Chen et al., 2001; Johnson et al., 1996; Yang et al., 2010). The same effect is expected for much denser nZVI particles used for remediation. Previous studies investigating nZVI transport were mainly carried out in mineralogically uniform media and quartz as a model aquifer material (Kim et al., 2009; Raychoudhury et al., 2012; Saleh et al., 2008). In addition, the presence of kaolinite clay in porous media at 2 wt.% has been shown to significantly decrease the nZVI mobility, which was attributed to heteroaggregation between kaolinite and nZVI particles and charge heterogeneities on the clay surface (Kim et al., 2012). Carbonate minerals are common constituents of aquifers (e.g., Borden Aquifer,

Mackay et al., 1986) and they can (locally) comprise more than 80% of the porous aquifer (Geological Survey of Austria, 1994). What effect these minerals exert on the transport of nZVI has not been addressed in any study to date.

In this study we have evaluated the effect of carbonate minerals in porous media on the transport of commercially available PAA-nZVI (NANOFER 25S) for five model porous media, starting from pure quartz sand and systematically increasing the carbonate sand content. The comparison between the transport in homogenous (pure quartz) media and in media with mineralogical heterogeneities caused by the presence of carbonate has been performed in well-controlled column experiments. The experimental transport data were analyzed and modeled using colloid filtration theory and a one dimensional convection-dispersion equation. A detailed characterization of the NANOFER 25S suspension was conducted to support these calculations. To our knowledge, this is the first study investigating the transport of commercially available NANOFER 25S particles, including two prevailing aquifer materials, quartz and carbonate, under injection conditions applied in groundwater remediation.

2.2. Materials and methods

2.2.1. Nanoscale zero-valent iron particles

PAA-nZVI (NANOFER 25S) was supplied by NANOIRON, s.r.o. (Czech Republic) in form of an aqueous suspension (pH 11) with a mean primary particle diameter below 50 nm and a total iron concentration of ~20 wt.% (as given by the producer). The particles are modified by an inorganic iron oxide layer and an organic PAA coating (Kadar et al., 2011). The production method for NANOFER 25S certainly differs from that of nZVI commonly reported in scientific literature (reactive iron nanoparticles, RNIP, Toda Kogyo, Japan or borohydride reduced nZVI particles). These different production methods will likely result in different structural configurations of particles, size distributions, and specific surface area (Mueller and Nowack, 2010; U.S. EPA, 2005), the properties that can affect the deposition and transport of nZVI particles.

2.2.2. Porous media

Standard Ottawa sand (20–30 mesh, 0.4–0.85 mm, extra pure, Fisher Scientific, Austria) was used as the quartz porous medium. Limestone (with ~97.0% $CaCO_3$, ~2% $MgCO_3$, and <1% aluminum and iron oxides, Appendix, Table A-1) was obtained from the Dachstein For-

mation (Lower Austria, Austria). The limestone was crushed with a jaw crusher and then sieved to between 0.5 and 1 mm, in order to obtain a size fraction as similar as possible to that of the Ottawa sand.

2.2.3. Preparation and characterization of PAA-nZVI suspension

The PAA-nZVI stock suspension (~8 g L^{-1}) was prepared by suspending the aqueous suspension of NANOFER 25S (50 g) provided by the producer in a 1 mM $NaHCO_3$ solution (pH 8.3), using an ultrasonic bath (Sonorex RK 106, Ø 240 mm, 130 mm high, 120 W indicated power, Bandelin electronic, Germany). Suspensions for the transport experiments and for particle characterization were prepared by further dilution of the PAA-nZVI stock suspension in 1 mM $NaHCO_3$ to the desired concentrations. The total iron (Fe) content was determined by inductively coupled plasma optical emission spectrometry (ICP-OES, Optima 5300DV, PerkinElmer, USA) after acid digestion.

Morphology and primary particle size were examined using scanning electron microscopy (SUPRA^{TM} 40 FE-SEM, Carl Zeiss, Germany). Aggregate size of PAA-nZVI in suspension was further determined by analyzing the obscuration time (pulse length) of a particle in a suspension being illuminated by a rotating laser beam, with a CCD camera positioned behind the measurement vessel as the detector (time of transition principle, 0.6–300 µm operation range, 0.2 µm resolution, limit of detection ~1000 particles mL^{-1}, Eytech^{TM}, Ambivalue, The Netherlands). Particle sedimentation was monitored by measuring the transmittance of monochromatic light (wavelength 880 nm) from the suspension (TurbiScan LAB, Quantachrome, Germany, Comba and Sethi, 2009), acquiring the transmittance data for 25 minutes over the entire height of the sample suspension (~55 mm) in steps of 40 µm.

Electrophoretic mobility and particle size were determined using dynamic light scattering and laser Doppler anemometry (Zetasizer Nano ZS, Malvern Instruments, UK) in the supernatant after two hours sedimentation. The electrophoretic mobility was determined as a function of pH (pH 2–10) and in the presence of monovalent and bivalent cations (in 1 mM $NaHCO_3$ and 0.3 mM $CaCO_3$, respectively). The electrophoretic mobility was converted into apparent zeta potential by applying the Smoluchowski relationship.

2.2.4. Preparation and characterization of porous media

The quartz sand (QS) was acid washed before use, as described by Yang et al. (2010), in order to remove metal oxide impurities from the grain surfaces. The carbonate sand (CS) was

rinsed with deionized water to remove any soluble solids and fine materials. Carbonate and quartz grains were mixed in varying proportions to obtain five different classes of porous media: (1) pure quartz sand (100% QS), (2) 90:10% QS:CS, (3) 50:50% QS:CS, (4) 10:90% QS:CS, and (5) pure carbonate sand (100% CS).

The streaming potentials of the porous media were measured with an Electrokinetic Analyzer (SurPASS, Anton Paar, Austria) equipped with a cylindrical cell. The cell was equilibrated by circulating the background solution (1 mM phosphate buffered saline, pH 7.4) in alternate directions for a period of ~15 minutes prior to each measurement. The streaming potential was converted into zeta potential using the Fairbrother-Mastin equation (Fairbrother and Mastin, 1924). In addition, the alteration of the surface charge as a function of pH (pH 5–10) has been studied in a 1 mM NaCl background solution.

2.2.5. Column experiments

Transport studies were performed in borosilicate glass columns (1 cm i.d., 10 cm length, Omnifit, Germany). A peristaltic pump (Ismatec, Germany) was used to feed background electrolyte and the PAA-nZVI suspension into the columns. In order to confirm the effects of different injection velocity for these particles, two experiments with different velocities that correspond to the injection velocities commonly applied at field sites (Phenrat et al., 2010b), $3x10^{-4}$ m s^{-1} and $6x10^{-4}$ m s^{-1} were performed in pure quartz and pure carbonate sand. The injection velocity of $6x10^{-4}$ m s^{-1} was chosen for the set of transport experiments involving five porous media with increasing carbonate content.

Each column was wet packed with porous media until ~8 cm height, and then flushed with at least ten pore volumes with a 1 mM $NaHCO_3$ background solution in order to remove background turbidity. Changes in the electrical conductivity and the pH due to dissolution of calcium carbonate are reported in Table A-2 (Appendix). A tracer test using NaBr was then conducted, and effluent bromide concentrations were analyzed by ion chromatography (ICS-1000, Dionex, Austria). The porosities of the media ranged between 0.38 (in pure quartz) and 0.46 (in pure carbonate). Following elution of the bromide tracer the entire PAA-nZVI suspension containing ~200 mg L^{-1} total Fe in 1 mM $NaHCO_3$ was introduced into the columns. In order to prevent aggregation and sedimentation, the particle suspension was sonicated prior to and during the injection (ultrasonic bath, Sonorex RK 106, Ø 240 mm, 130 mm high, 120 W indicated power, Bandelin electronic, Germany). The column effluent was collected every 30 seconds and analyzed for total Fe. The breakthrough curve for each transport exper-

iment was plotted as the normalized total Fe concentration (C/C_0) versus number of pore volumes. The presented data are the mean results from duplicate measurements.

2.2.6. Transport models

2.2.6.1. Colloid filtration theory

Colloid filtration theory (CFT) describes the deposition of particles in a porous medium involving two sequential steps: transport from the fluid to the grains of the medium, and attachment to the grains (Elimelech and O'Melia, 1990). These processes are described by the single-collector contact efficiency and the attachment efficiency. The single-collector contact efficiency (η_0), calculated following Tufenkji and Elimelech (2004) describes the transport of particles to a collector as a cumulative effect of diffusion (η_D), interception (η_I), and gravitational sedimentation (η_G): $\eta_0 = \eta_D + \eta_I + \eta_G$. The attachment efficiency (α) is the proportion of collisions between the particles and collectors that result in attachment. It was calculated empirically using the normalized iron concentration (C/C_0) at the plateau of the breakthrough curve (Kretzschmar et al., 1999; Yao et al., 1971), by applying the following equation:

$$\alpha = -\frac{2d_c}{3(1-n)\eta_0 L}\ln\ \frac{C}{C_0} \qquad (2.1)$$

In Equation (1), d_c represents the average diameter of the collector, n the porosity of the porous medium, and L the length of the column (8 cm in this case). The particle deposition rate coefficient (k_{CFT}) was then calculated after Kretschmar et al. (1999) and Tufenkji and Elimelech (2004):

$$k_{CFT} = -\frac{v}{L}\ln\ \frac{C}{C_0}\ = -\frac{3\,(1-n)}{2d_c}v\alpha\eta_0 \qquad (2.2)$$

where v is the pore water velocity.

The transport distance (L_T) of PAA-nZVI at which 50% and 99.9% of particles are removed (C/C_0 = 0.5 and 0.001, respectively) was calculated using the column properties (the average diameter of the collector and the porosity), the single-collector contact efficiency, and the attachment efficiency (Elimelech et al., 1995) as:

$$L_T = -\frac{2d_c}{3(1-n)\alpha\,\eta_0}\ln\ \frac{C}{C_0} \qquad (2.3)$$

2.2.6.2. One dimensional transport equation

The transport of particles through a saturated porous media under steady state flow conditions can be described by the convection-dispersion equation (CDE), including a term for first-order particle removal (Kretzschmar and Sticher, 1998):

$$\frac{\partial C}{\partial t} = D\frac{\partial^2 C}{\partial x^2} - v\frac{\partial C}{\partial x} - k_{CDE}C \qquad (2.4)$$

where t is the elapsed time, x is the travel distance, D is the dispersion coefficient for PAA-nZVI particles, and k is the first-order particle removal rate coefficient. The dispersion coefficient and first-order removal (k_{CDE}) values were obtained by fitting the convection-dispersion equation to the PAA-nZVI breakthrough curves, using the velocity applied in column experiments (CXTFIT, STANMOD software, version 2.08.1130). The removal rate coefficient (k_{CDE}) was compared to the deposition rate coefficient (k_{CFT}) calculated using colloid filtration theory.

Mineralogical variations within the subsurface can be incorporated into the model simulations by considering a two-patch charge heterogeneity. In the patchwise heterogeneity model (PHM) the surface area of the porous media is divided into favorable and unfavorable fractions (Song et al., 1994), which in this study comprise the carbonate and quartz sands, respectively. The heterogeneity parameter λ is defined as the proportion of favorable deposition sites in the porous medium, which is in our study equal to the proportion of carbonate sand. The average deposition rate coefficient (k_{PHM}) is then expressed as a linear combination of the deposition rates onto pure quartz (k_{QS}) and pure carbonate (k_{CS}) sand (Chen et al., 2001):

$$k_{PHM} = \lambda k_{CS} + (1-\lambda)k_{QS} \qquad (2.5)$$

2.3. Results and discussion

2.3.1. PAA-nZVI characterization

The SEM images of the PAA-nZVI particles showed irregularly-shaped aggregates ranging in size from 200 nm to >1 µm (Figure 2.1). Irregular shaped particles have been previously observed for other nZVI particles (e.g., RNIP, Toda Kogyo, Japan; Liu et al., 2005; Nurmi et al., 2005). Deviation between the primary particle size given by the manufacturer (~50 nm) and the observed aggregates are a result of particle aggregation and sample preparation, i.e., drying the PAA-nZVI suspension on the grid (Domingos et al., 2009). The SEM images

therefore provide the information about the morphology of the primary particles and aggregates, but the estimated aggregate size may not be representative of the actual particle size in the suspension. For that purpose the PAA-nZVI suspension was in addition characterized with the available complementary techniques to obtain a more thorough characterization.

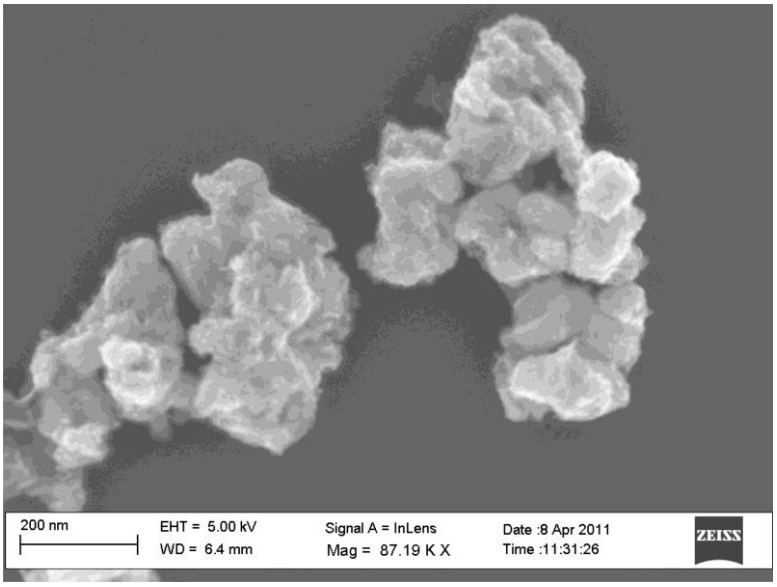

Figure 2.1. SEM image of PAA-nZVI.

The laser obscuration time measurement of the PAA-nZVI suspension (~100 mg L^{-1} total Fe in 1 mM $NaHCO_3$, pH 8.3) resulted in a mean particle size of 1.6±1.4 µm. This revealed a predominance of large aggregates in the particle suspension, and also indicated a polydisperse system with a broad particle size distribution. Determination of the dispersion state was further investigated by means of particle sedimentation in the PAA-nZVI suspension (with ~200 mg L^{-1} total Fe in 1 mM $NaHCO_3$, pH 8.3). This resulted in a sedimentation rate of 0.35 mm min^{-1} and corresponds to a PAA-nZVI diameter of 1.2 µm of the settled fraction based on Stokes Law (PAA-nZVI density: 7.87 g cm^{-3}, fluid density: 1 g cm^{-3}, fluid viscosity: 1 kg m^{-1} s^{-1}). This size is in agreement with the mean particle size delivered by the laser obscuration time method. The total Fe concentration in the stable fraction (supernatant after 2 hours of sedimentation) was a factor of ten smaller (~20 mg L^{-1}) than in the initial suspension, demonstrating that ~90% of the particles had already settled by this time. The hydrodynamic diameter of the stable PAA-nZVI particles determined by dynamic light scattering was 235±3 nm. The zeta potential of these stable PAA-nZVI particles was -41.1±0.5 mV (at neutral pH and in the presence of 1 mM $NaHCO_3$). With decreasing pH the zeta potential increased, reaching the isoelectric point at pH~3 (Figure 2.2). The zeta potential of these particles was additionally measured in the presence of a 0.3 mM $CaCO_3$ background solution, and

the particles exhibited a less negative charge over the whole pH range investigated. This indicated that calcium screened the PAA-nZVI surface charge, an effect that has previously been observed for polyaspartate-, triblock copolymer-, and surfactant-modified nZVI particles (Saleh et al., 2008).

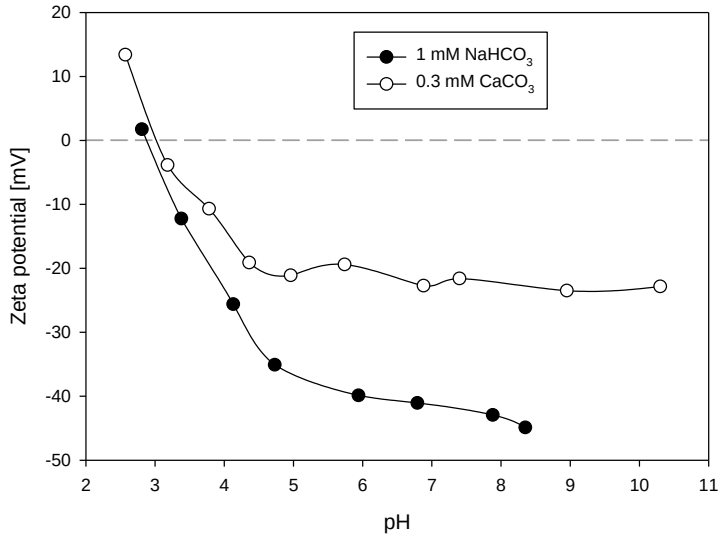

Figure 2.2. Zeta potential of the stable fraction (supernatant after sedimentation) of PAA-nZVI as a function of pH and in the presence of monovalent (sodium) and bivalent (calcium) cations.

2.3.2. Surface charge of porous media

The streaming potentials for the five classes of porous media (0–100% CS) were determined at a pH of 7.4 and ionic strength of 1 mM. The results showed that the pure quartz sand was negatively charged (-50 mV), with the zeta potential becoming less negative with increasing proportions of carbonate sand (Figure 2.3a). Pure carbonate sand carried a weak negative charge under the same experimental conditions (-16 mV, 100% CS, Figure 2.3a).

Previous studies have reported that the zeta potential of a heterogeneous porous medium at a given pH is a linear combination of the zeta potential values of the two original materials (Elimelech et al., 2000; Johnson, 1999). It should therefore be expected that

$$\zeta_{tot} = \lambda\zeta_{CS} + (1-\lambda)\zeta_{QS} \qquad (2.6)$$

where ζ_{QS} is the zeta potential of quartz sand, ζ_{CS} that of carbonate sand, and λ is the heterogeneity parameter (in our study, equal to the proportion of carbonate sand).

Our results showed that the zeta potential increased approximately linearly with increasing carbonate content (solid line, Figure 2.3a). The values obtained for the mixtures containing

10 and 50% carbonate sand were, however, slightly less negative than the linear combination of the zeta potentials of pure quartz and carbonate sands (dashed line, Figure 2.3a).

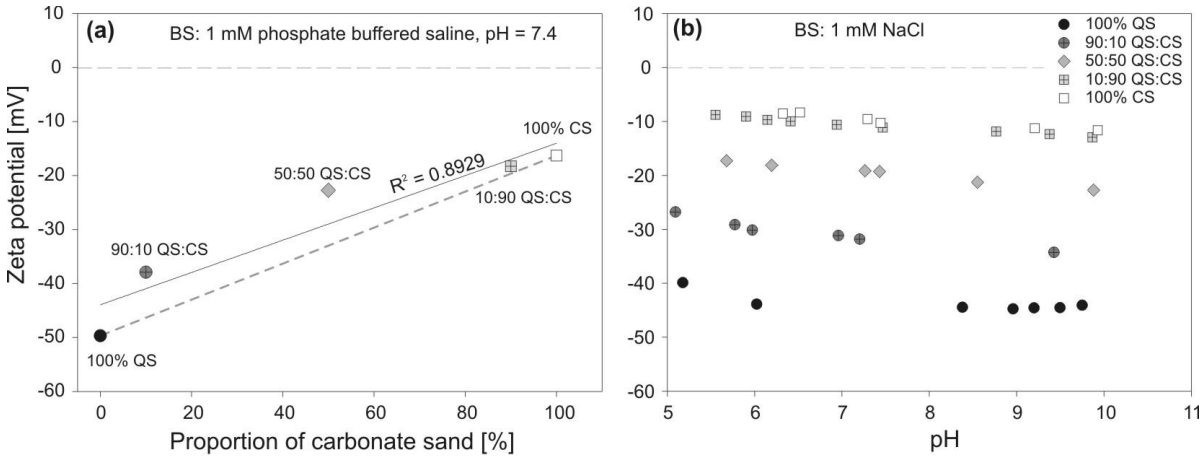

Figure 2.3. Zeta potential of the porous media as a function of (a) the proportion of carbonate sand, and (b) the pH. The solid line in a is a linear fit of the results, whereas the dashed line indicates the linear combination of the zeta potentials of pure quartz (QS) and pure carbonate (CS) sand, according to Equation 2.6. Note that different background solutions (BS) were used in the experiments a (phosphate buffered saline, ionic strength = 1 mM) and b (NaCl, ionic strength = 1 mM), which resulted in a slight difference in the zeta potential values at pH~7.

The zeta potential was further determined as a function of pH in all investigated media (Figure 2.3b). Quartz sand carried a high negative charge over the whole pH range investigated, with the zeta potential increasing slightly from -45 mV (at pH 10) to -39 mV (at pH 5). The surface charge of the quartz and carbonate mixtures exhibited a less negative zeta potential in this pH range. The surface charge of pure carbonate sand increased slightly from an initial -12 mV (at pH 10) to -8 mV (at pH 5.7). We hereby acknowledge that at pH values below 8.27 calcite starts dissolving at atmospheric CO_2 pressure and values obtained below this value represent conditions at thermodynamic non-equilibrium.

The differences in zeta potential for quartz and carbonate sand at pH 7.4 (Figure 2.3a and b) resulted from the different background solutions applied. Carbonate sand and especially quartz sand, were more negatively charged in the presence of the phosphate buffer (Figure 2.3a) than in the presence of NaCl (Figure 2.3b). This can be explained by phosphate adsorption onto the porous media surface, resulting in decreased zeta potentials, as previously reported for the surface charge of quartz sand under different phosphate concentrations (Wang et al., 2011).

Overall, the surface charge measurements suggest that the repulsive forces between the negatively charged PAA-nZVI particles and the carbonate sand surfaces will be lower than for quartz sand. This assumption is supported by the interaction energy profiles between quartz and carbonate sands and PAA-nZVI particles. We calculated the electrostatic interactions between the particles and the mineral grains according to the DLVO theory (calculated after Christian et al., 2008, Figure 2.4). The height of the repulsive energy barrier decreased with increasing carbonate content and decreasing surface charge, disappearing completely when the proportion of carbonate sand exceeds 50%. In the absence of a repulsive energy barrier, PAA-nZVI should have a strong tendency to deposit onto carbonate-rich porous media.

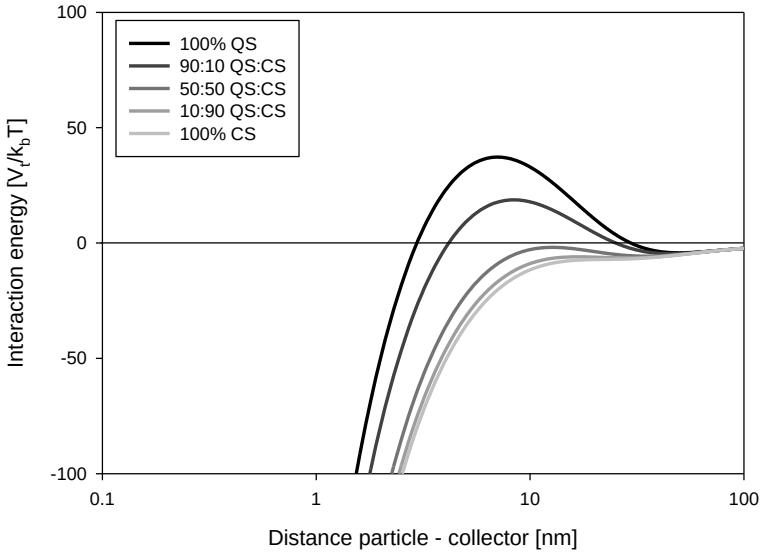

Figure 2.4. Interaction energy profiles calculated after Christian et al. (2008) between PAA-nZVI and porous media containing various amounts of quartz (QS) and carbonate (CS) sand. Input parameters were as follows: zeta potential (porous media) as in Figure. 2.3a, zeta potential (PAA-nZVI) = -40 mV, particle size = 1.1 µm, temperature = 293.15 K, ionic strength = 1 mM, Hamaker constant = 1.62×10^{-20} J (Tiraferri and Sethi, 2009).

2.3.3. Effect of injection velocity on PAA-nZVI deposition and transport

The effect that the injection velocity has on PAA-nZVI deposition and transport was confirmed in two different experimental setups, with pure quartz sand and pure carbonate sand. Like for the previously studied reactive iron nanoparticles (RNIP, Toda Kogyo, Japan) and iron nanoparticles produced by borohydride reduction, the PAA-nZVI transport (NANOFER 25S) depended on the injection velocity, in both quartz and carbonate sands. Doubling the injection velocity from 3×10^{-4} m s^{-1} to 6×10^{-4} m s^{-1} significantly decreased the

deposition and enhanced the PAA-nZVI transport. In quartz sand the breakthrough (C/C_0) increased from 0.32 to 0.70, while in carbonate sand the observed increase was from 0.08 to 0.22 (Figure 2.5). The lower observed deposition at higher injection velocities can be attributed to the smaller volumes of stagnation zones and higher drag forces, as reported for previously investigated nZVI particles (Phenrat et al., 2009a; Phenrat et al., 2010b; Raychoudhury et al., 2010).

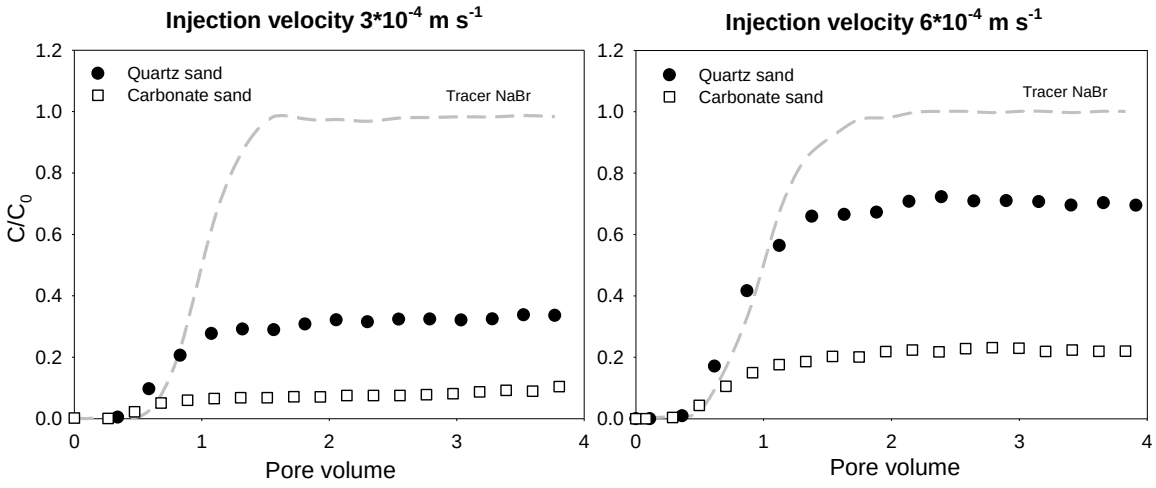

Figure 2.5. Experimental breakthrough curves of the bromide tracer and PAA-nZVI through quartz and carbonate sand at injection velocities of $3x10^{-4}$ m s^{-1} and $6x10^{-4}$ m s^{-1}, respectively. Experimental conditions were as follows: influent iron concentration = ~200 mg L^{-1}, ionic strength = 1 mM $NaHCO_3$, solution pH = 8.3–9.0.

2.3.4. Effect of carbonate minerals in porous media on PAA-nZVI deposition and transport

Five model porous media with increasing proportions of carbonate sand were used to study effects of carbonate minerals on the PAA-nZVI transport.

The results demonstrated that as the proportion of carbonate sand increased the PAA-nZVI deposition also increased and therefore the transport decreased (Figure 2.6). The PAA-nZVI breakthrough (C/C_0) decreased from 0.70 in pure quartz sand to 0.18 and 0.22 in porous media containing 90% and 100% of carbonate sand, respectively (Figure 2.6). The PAA-nZVI breakthrough in the experiments with 90% and 100% of carbonate sand were not different from each other. This suggests that the deposition was dominated by the carbonate surfaces at carbonate loading higher than 90%.

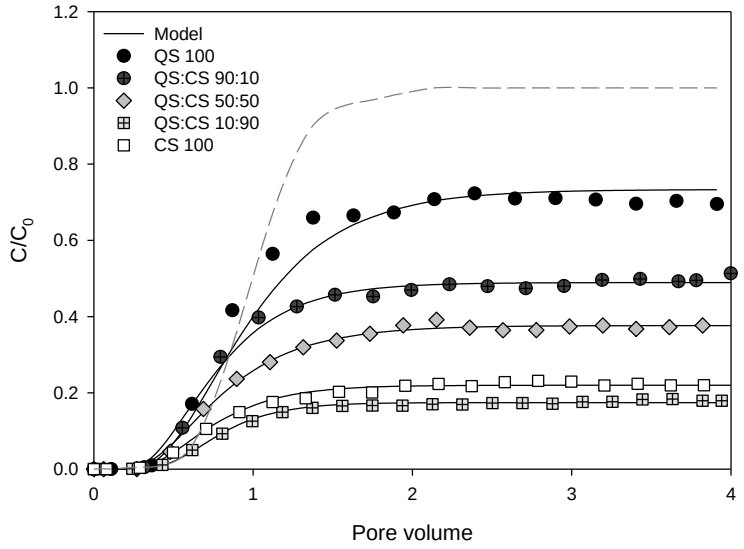

Figure 2.6. Experimental breakthrough curves and model fits of PAA-nZVI in porous media containing various amounts of quartz sand (QS) and carbonate sand (CS). Experimental conditions were as follows: influent iron concentration = ~200 mg L^{-1}, ionic strength = 1 mM $NaHCO_3$, solution pH = 8.3–9.0.

The PAA-nZVI breakthrough occurred slightly ahead of the bromide tracer (Figure 2.6). This reflects the well-documented size exclusion effect, where the PAA-nZVI particles are excluded from the smaller pores and are thus eluted earlier, as previously observed by, e.g., Kretzschmar and Sticher (1997). The breakthrough curves reached a plateau at 1.5 to 2 pore volumes, independent on the investigated porous medium (Figure 2.6), indicating steady-state effluent concentrations. This suggests that, under the experimental conditions used, the PAA-nZVI particles are removed at a constant rate in the porous media, and that the removal is controlled by a first-order kinetic mechanism. The removal of particles at a constant rate allows the use of colloid filtration theory, which is applicable under steady state effluent concentrations (Yao et al., 1971), as well as the convection-dispersion equation with a first-order particle removal term (Chen et al., 2001).

Colloid filtration theory can explain the deposition of particles onto porous media in terms of different transport mechanisms and particle sizes. The calculations of the single-collector contact efficiency (η_0) according to Tufenkji and Elimelech (2004) showed that the values for η_0 were almost the same for all porous media investigated (Table 2.1). This can be attributed to the values of the input parameters used for the η_0 calculation (i.e., mean collector diameter, Darcy velocity, porosity, fluid viscosity, and temperature), all of which were almost identical for the five classes of porous media.

Table 2.1. Transport and deposition parameters of PAA-nZVI particles.

Porous media	η_D	η_I	η_G	η_0	α	k_{CFT}	L_T (99.9)	L_T (50)
						s^{-1}	m	m
100% QS	0.0016	0.0004	0.0134	0.0153	0.20	0.0030	1.55	0.16
90:10% QS:CS	0.0014	0.0003	0.0138	0.0155	0.43	0.0055	0.79	0.08
50:50% QS:CS	0.0013	0.0002	0.0138	0.0153	0.67	0.0068	0.57	0.05
10:90% QS:CS	0.0013	0.0002	0.0138	0.0153	1.24	0.0116	0.32	0.03
100% CS	0.0012	0.0002	0.0141	0.0155	1.20	0.0111	0.34	0.03

Contribution of diffusion (η_D), interception (η_I), and gravitational sedimentation (η_G), single-collector contact efficiency (η_0), attachment efficiency (α), deposition rate coefficient (k_{CFT}), and travel distance to remove 99.9% and 50% of the PAA-nZVI particles (L_T).

The lowest η_0 values were obtained for PAA-NZVI particle sizes between 200 and 500 nm. These correspond to the particle sizes for which the highest subsurface mobility of PAA-nZVI can be expected in an ideal porous media (Elimelech and O'Melia, 1990). The η_0 values increased for particles larger than 500 nm due to the increasing contribution of gravitational sedimentation (Figure 2.7). Gravitational sedimentation (η_G) was therefore recognized as the dominant mechanism for PAA-nZVI deposition in all investigated porous media (Table 2.1), which is attributed to the high density of the used nZVI particles (7.87 g cm^{-3}) and the relatively large size of the nZVI aggregates flowing through the column.

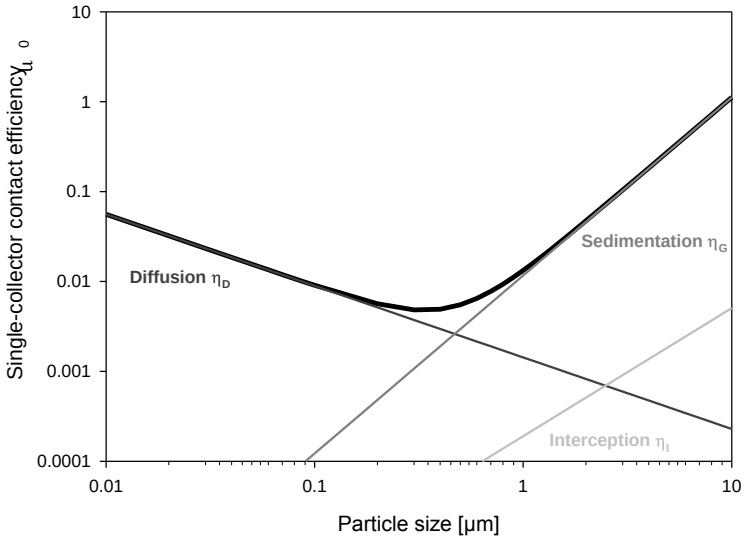

Figure 2.7. Change in single-collector contact efficiency η_0 (calculated after Tufenkji and Elimelech, 2004) with particle size, and contribution of diffusion η_D, interception η_I, and gravitational sedimentation η_G.

The increase in PAA-nZVI deposition with an increasing proportion of carbonate sand is assumed to be a result of favorable particle attachment to carbonate grains. This assumption is supported by the linear increase in the attachment efficiency (α) from 0.2 in pure quartz sand to approximately 1.2 in the porous media containing 90 to 100% carbonate sand (Table 2.1, Figure 2.8a). Values for α greater than 1 are physically impossible, however, particle aggregation during the column experiment can result in overestimation of attachment, as observed previously by Phenrat et al. (2010b). A linear increase with increasing proportion of carbonate sand was also observed for the particle deposition rate coefficient (k_{CFT}), which increased from 0.003 s^{-1} for 100% QS to 0.011 s^{-1} for 100% CS. No difference was observed in the particle deposition rate between sand mixtures with 90% and 100% carbonate sand (Table 2.1).

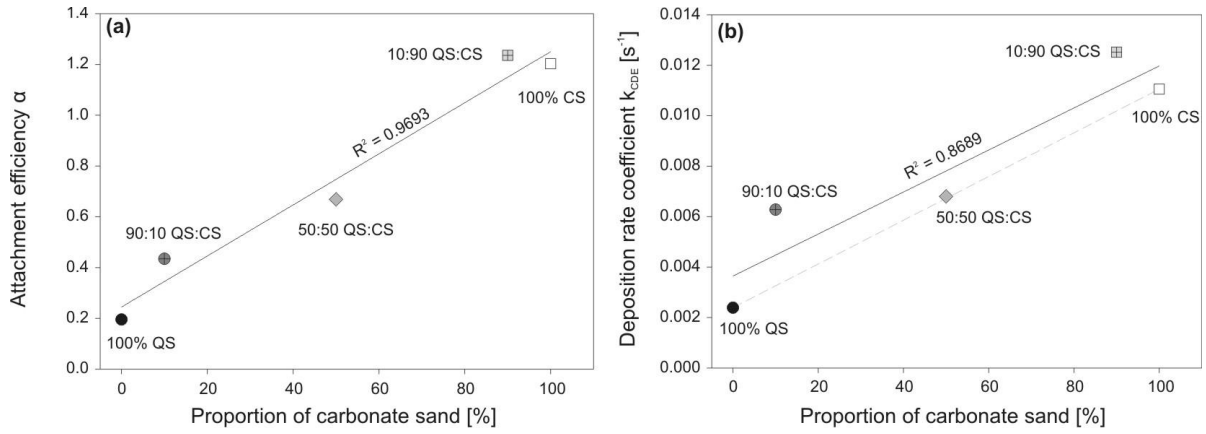

Figure 2.8. Influence of carbonate content on the (a) attachment and (b) deposition kinetics of PAA-nZVI in heterogeneous porous media. The solid lines are linear fits of the results. The dashed line in b indicates the linear combination of the removal rates of pure quartz sand (QS) and pure carbonate sand (CS) sand, according to Equation 2.5.

The transport of PAA-nZVI was further described by fitting the convection-dispersion equation (Equation 2.4) to the experimental breakthrough curves. The results showed an excellent agreement between the experimental and fitted breakthrough curves with r^2 >0.968 (Table 2.2, Figure 2.6), supporting the assumption that the PAA-nZVI deposition was controlled by a first-order kinetic mechanism.

The CXTFIT-fitted first-order deposition rate coefficient (k_{CDE}) ranged from 0.002 to 0.013 s^{-1}, with the highest values recorded in the porous media with 90 and 100% carbonate sand (Table 2.2). Since the hydrodynamic dispersion coefficient differs from zero (Table 2.2), the attachment efficiency was additionally determined using k_{CDE} and Equation 2.2 in order

to exclude dispersion as the dominant transport process. The values for α_{CDE} ranged between 0.16 and 1.33 (Table 2.2). The values for k_{CDE} and α_{CDE} were similar to those for the deposition rate coefficient and attachment efficiency calculated by applying the colloid filtration theory (Table 2.1), indicating that both approaches are applicable for describing the PAA-nZVI deposition kinetics and that dispersion is not the dominating transport process. The particle removal rate coefficients (k_{CDE}) for the five porous media are presented in Figure 2.8b. The results showed that the removal rate increased approximately linearly as the proportion of carbonate sand increased. The linear increase can be explained by the patchwise heterogeneity model (Song et al., 1994), which assumes that the average removal rate is a linear combination of the removal rates onto pure quartz sand ($k_{QS} = 0.0024\ s^{-1}$) and pure carbonate sand ($k_{CS} = 0.0111\ s^{-1}$) (Equation 2.5; dashed line in Figure 2.8b). The removal rates for 10% and 90% carbonate sand were nevertheless slightly higher than the average removal rates (k_{PHM}) calculated using the patchwise heterogeneity model (Table 2.2).

Table 2.2. Properties of the porous media, and results of the convection-dispersion and patchwise heterogeneity models.

Porous media	**d_c**	**n**	**v**	**D**	**k_{CDE}**	**r^2**	**α_{CDE}**	**k_{PHM}**
	mm		$m\ s^{-1}$	$cm^2\ s^{-1}$	s^{-1}			s^{-1}
100% QS	0.68	0.38	$6.75*10^{-4}$	0.061	0.0024	0.968	0.16	0.0024
90:10% QS:CS	0.70	0.40	$6.38*10^{-4}$	0.072	0.0063	0.992	0.49	0.0033
50:50% QS:CS	0.70	0.45	$5.66*10^{-4}$	0.085	0.0068	0.995	0.66	0.0067
10:90% QS:CS	0.70	0.47	$5.42*10^{-4}$	0.041	0.0125	0.996	1.33	0.0102
100% CS	0.75	0.46	$5.53*10^{-4}$	0.067	0.0111	0.992	1.19	0.0111

Mean diameter of the porous media (d_c), porosity (n), pore water velocity (v), hydrodynamic dispersion coefficient for the PAA-nZVI particles (D), removal rate coefficient (k_{CDE}), attachment efficiency (α_{CDE}), and average deposition rate coefficient (k_{PHM}) based on the patchwise heterogeneity model.

The PAA-nZVI travel length was predicted by applying the colloid filtration theory (Equation 2.3) and setting the removal of the particles to 99.9% (close to total removal) or 50% (removal of half of the particles). The maximum predicted travel length in pure quartz sand was 1.55 m (after 99.9% particle removal), but with more than a half of the injected particles travelling no further than 0.16 m (Table 2.1). In the presence of carbonate sand the predicted travel distance was even shorter, ranging between 0.03 m (for 50% particle removal) and 0.34 m (for 99.9% particle removal; Table 2.1). Travel distances (99% particle removal) reported by Saleh et al. (2008) for other surface modified nZVI particles (polyaspartate-,

triblock copolymer-, sodium dodecyl benzyl sulfonate-nZVI) in pure quartz sand were significantly higher than the values in this study, ranging from 0.6 m to ~500 m, depending on the ionic strength and nZVI surface coating. However, Saleh et al. (2008) performed their experiments with the stable nZVI fraction (after sedimentation) at a low nZVI concentration (~30 mg L^{-1}), while in this study the entire polydisperse suspension, as applied in the field, at concentrations ~200 mg L^{-1}, was applied. In addition to the higher concentration, the polydispersity of the nZVI used here may have decreased the transport. Phenrat et al., (2009a) found that the larger nZVI particles aggregated much more readily than the smaller ones, leading to increased aggregation and lower transport. Travel distances reported by Schrick et al. (2004) for polyacrylic acid modified nZVI in pure quartz sand, using very high particle concentrations (5 g L^{-1}), were lower than values in this study, ranging from 9 to 39 cm and depending on the particle size. The high concentration might have contributed to the decreased travel distance. Travel distances (99% particle removal) reported for guar gum-coated nZVI in pure quartz sand (Tiraferri and Sethi, 2009) were comparable with the values in this study. The calculated distances ranged between 0.59 and 2.37 m, depending on ionic strength and injection velocity. The highest value was obtained applying the highest injection velocity, which is therefore considered to be an essential factor in enhancing the transport. Once the injection is terminated and groundwater flow velocity returns to background levels (that are well below those during injection), the PAA-nZVI particles will be retained in the porous media (Phenrat et al., 2010a).

Overall, the linear increase in particle deposition and attachment efficiency with increasing proportions of carbonate sand demonstrated that the attachment and deposition kinetics of PAA-nZVI are controlled by the mineralogical variations within the subsurface. Our results are in agreement with those of Elimelech et al. (2000), who observed a similar linear trend for deposition of colloidal silica particles onto porous media containing various amounts of positively charged patches (aminosilane-modified quartz grains). Our study showed that not only the positively charged minerals (such as iron oxides and the edges of clay minerals) act as favorable deposition sites for nZVI particles, but also carbonate minerals that carry a weak negative surface charge in the pH range typically found in groundwater. Both will decrease the transport of nanoparticles in heterogeneous porous media and therefore need to be taken into account in the design of nZVI-based *in situ* remediation.

It should be noted that higher ionic strength due to the dissolution of calcium carbonate (Appendix, Table A-2) can alter the stability of PAA-nZVI by electrostatic double layer com-

pression and increase its deposition onto the aquifer grains (Petosa et al., 2010). In addition, higher dissolved calcium concentrations can destabilize the PAA-nZVI suspension and therefore decrease transport. This is due to specific adsorption of calcium ions onto nZVI surfaces, as well as complexation of calcium ions by carboxylic groups of the PAA, which results in an associated loss of repulsive negative charges (Ottofuelling et al., 2011; Saleh et al., 2008). The effect of calcium concentration on the PAA-nZVI deposition and transport was evaluated in different experimental setups; with pure quartz and pure carbonate sand, and including three different calcium concentrations (1 mM, 2.5 mM, and 5 mM $CaCl_2$). In quartz sand the PAA-nZVI breakthrough (C/C_0) decreased from 0.36 (in 1 mM $CaCl_2$) to 0.14 (in 5 mM $CaCl_2$), while in carbonate sand the observed decrease was from 0.10 (in 1 mM $CaCl_2$) to 0.03 (in 5 mM $CaCl_2$) (Table 2.3). High aqueous calcium concentrations, which can be expected in carbonate-rich aquifers, are therefore additionally limiting the PAA-nZVI transport, as previously reported by Saleh et al. (2008).

Table 2.3. Changes in breakthrough (C/C_0) of PAA-nZVI through quartz and carbonate sand at three different calcium concentrations. Experimental conditions were as follows: influent iron concentration = ~200 mg L^{-1}, injection velocity = $6x10^{-4}$ m s^{-1}, ionic strength = 1 mM $NaHCO_3$ + 1 mM, 2.5 mM and 5 mM $CaCl_2$, solution pH = 8.3–9.0.

	Calcium concentration	**C/C_0**
Quartz sand	1 mM	0.36
	2.5 mM	0.22
	5 mM	0.14
Carbonate sand	1 mM	0.10
	2.5 mM	0.05
	5 mM	0.03

Similar to the complexation of carboxylic groups in the PAA with dissolved calcium, the PAA can also adsorb on the calcite through complexation of calcium at the sand surface (Geffroy et al., 1999; Taylor and Sigmund, 2010). The latter may result in bridging effects between the PAA-nZVI and carbonate minerals and therefore enhance the particle deposition onto carbonate sand. These interactions and their effects on the nZVI transport need also to be considered when designing a nZVI application in carbonate-rich aquifers.

2.4. Conclusion and implications for field applications

Our study has revealed that the PAA-nZVI (NANOFER 25S) suspension, with a mean aggregate size of approximately 1.4 µm, is polydisperse and not stable. The stable fraction of this suspension (after two hours of sedimentation) contains significantly smaller particles with a diameter of ~235 nm. However, the concentration of nZVI in this stable fraction is only about 10% of the original suspension.

We demonstrated that carbonate minerals in aquifers and with them introduced surface charge heterogeneities, have a strong effect on the transport of a polydisperse suspension of PAA-nZVI. The results showed that even a low proportion of carbonate minerals (10%) in the subsurface may cause an increase in the deposition of PAA-nZVI particles and aggregates, and consequently limit their transport. The favorable deposition of PAA-nZVI particles onto carbonate rather than quartz sand is attributed to the lower negative surface charge of carbonate sand. It should be further noted that surface complexations of PAA coating with calcite might additionally occur, as well as particle aggregation due to dissolved calcium. Both effects are expected to be more pronounced in carbonate-rich porous media and will result in increased particle deposition.

The model simulations based on colloid filtration theory and the one dimensional transport equation showed that the PAA-nZVI attachment efficiency and deposition rate increase linearly with increasing proportions of carbonate sand, under the investigated conditions. The maximum predicted travel distances for PAA-nZVI in carbonate sand was approximately five times shorter than in quartz sand and not more than 0.3 m in our study, which in praxis may reduce chances that the nZVI suspension reaches the contaminated source zone. We acknowledge that the hereby performed small-scale experiments are not direct analogues for large-scale settings. However, the reported differences in nZVI deposition onto quartz and carbonate sands are also likely to manifest themselves at larger scales. The transport distance for nZVI-based particles is therefore likely to be low in carbonate-rich porous media, thus requiring more injection wells in the treatment zone and potentially a larger mass of nZVI, which increases the overall remediation costs. Since carbonate sands are common constituents of aquifers, their effects on nZVI transport needs to be taken into account in the design of nZVI-based remediation.

New strategies are therefore required in order to improve PAA-nZVI transport in such heterogeneous porous media. It might be possible to optimize those nZVI particle properties that

affect their mobility in porous media, or to enhance delivery by improving the injection techniques. Another strategy might be to inject natural polyelectrolytes (with no adverse effects on the environment) prior to, or during the application of nZVI suspensions. Such natural organic polyelectrolytes can adsorb onto the porous media, provide a greater and more uniform negative surface charge and thus minimizing the deposition of negatively charged nZVI particles, as previously demonstrated by Johnson et al. (2009) and Kim et al. (2012). The effects that organic (and biodegradable) polyelectrolyte coatings have on aquifer surfaces will nevertheless need to be considered in future studies, which aim for improved nZVI transport in heterogeneous porous media. Furthermore, the ecotoxicological effects that these coatings may have on the subsurface organisms will also have to be determined. These introduced polyelectrolyte coatings could also promote bacterial growth in the subsurface (Kirschling et al., 2010; Xiu et al., 2010) and subsequently enhance the remediation by combining nZVI treatment with bioremediation.

Acknowledgments

The authors would like to thank Dr. Nadezhda Kataeva (Austrian Institute of Technology) for electron microscope imaging, and NANOIRON, s.r.o. (Czech Republic) for kindly providing aqueous suspensions of NANOFER 25S. The research was funded by the Austrian Federal Ministry of Agriculture, Forestry, Environment and Water; Management by Kommunalkredit Public Consulting, Austria. Author GVL was supported in part by the National Science Foundation (NSF) and the Environmental Protection Agency (EPA) under NSF Cooperative Agreement EF-0830093, through the Center for Environmental Implications of Nanotechnology (CEINT).

3. Mobility enhancement of nanoscale zero-valent iron in carbonate porous media through co-injection of polyelectrolytes

Susanne Laumann, Vesna Micić, Thilo Hofmann; submitted.

Abstract

The mobility of nanoscale zero-valent iron (nZVI) used for *in situ* groundwater remediation is affected by chemical and physical heterogeneities within aquifers. Carbonate minerals in porous aquifers and the presence of divalent cations reduce nZVI mobility. This study assesses the potential for enhancing the mobility of polyacrylic acid coated nZVI (PAA-nZVI) in such aquifers through the co-injection of polyelectrolytes (natural organic matter, humic acid, carboxymethyl cellulose, and lignin sulfonate). When applied at the same concentration, all of the polyelectrolytes produced similar enhancement of PAA-nZVI mobility in carbonate porous media. This increase in mobility was the result of increased repulsion between PAA-nZVI and the carbonate matrix. Lignin sulfonate, an environmentally friendly and inexpensive agent, was identified as the most suitable polyelectrolyte for field applications. The greatest increase in PAA-nZVI mobility was achieved with co-injected lignin sulfonate concentrations $\geq$50 mg L^{-1}; at this concentration the maximum PAA-nZVI travel distance in carbonate porous media was double that in the absence of lignin sulfonate.

3.1. Introduction

Nanoscale zero-valent iron (nZVI) has been proposed as a beneficial agent for *in situ* remediation of aquifers contaminated with chlorinated compounds and heavy metals (Grieger et al., 2010; Zhang, 2003). Successful emplacement of nZVI within the contaminated zone is essential for effective nZVI-based remediation (Crane and Scott, 2012; O'Carroll et al., 2013; Tratnyek and Johnson, 2006). Emplacement is influenced by the nZVI injection velocity (Phenrat et al., 2010b; Raychoudhury et al., 2010) and by the mobility of nZVI in the subsurface. The mobility is limited by particle aggregation, sedimentation, pore blocking, and deposition onto the aquifer grains (Hofmann and von der Kammer, 2009; Ryan and Elimelech, 1996), all of which depend on the particle properties (such as particle size, composition, and surface charge; Phenrat et al., 2007; Phenrat et al., 2009a), as well as on site-specific hydrochemical and hydrogeological parameters (including the groundwater chemistry and the properties of the aquifer material; Johnson et al., 2013; Laumann et al., 2013; Saleh et al., 2008; Yang et al., 2010).

Surface coating of nZVI with anionic polyelectrolytes such as polyacrylic acid (PAA) can hinder nZVI aggregation and deposition onto negatively charged surfaces of aquifer mineral grains (predominantly quartz) through electrostatic and steric repulsion, thereby enhancing nZVI transport (Phenrat et al., 2010b; Raychoudhury et al., 2012; Schrick et al., 2004). The transport of coated nZVI is nevertheless still affected by surface charge heterogeneities encountered in aquifers induced by, for example, natural organic matter (NOM) and mineralogical variations within the aquifer grains (Chen et al., 2001; Ryan and Elimelech, 1996; Yang et al., 2011). It has been demonstrated that weakly negatively charged carbonate minerals in porous aquifers can act as favorable particle deposition sites (Laumann et al., 2013), an effect that has also previously been demonstrated for positively charged aquifer impurities such as iron oxides and the edges of clay minerals (Elimelech et al., 2000; Johnson et al., 1996; Kim et al., 2012).

Carbonate minerals are abundant, with calcite alone making up about 4% of the earth's crust (Heberling et al., 2011; Zhong and Mucci, 1995). Carbonates are therefore common constituents of porous aquifers. It has been shown that, even if only present in low proportions, they can significantly reduce the mobility of nZVI (Laumann et al., 2013). The favorable deposition of coated nZVI particles onto carbonate grains has been attributed to the weak negative surface charge of carbonates and the increase in nZVI aggregation caused by dissolved calcium (Laumann et al., 2013). Groundwater in carbonate-bearing porous aquifers characteristically contains high concentrations of divalent cations, with calcium concentrations of up to 5 mM (Stumm and Morgan, 1996). High ionic strength and high calcium concentrations alter nZVI stability by both electrostatic double layer compression and specific adsorption of calcium ions onto the nZVI surfaces (Ottofuelling et al., 2011; Petosa et al., 2010). This results in a reduction in the electrostatic repulsive forces between the nZVI particles and the aquifer matrix, and hence in reduced nZVI mobility (Saleh et al., 2008).

In order to enhance the emplacement of nZVI in carbonate-bearing porous media it is necessary to improve nZVI mobility. This can be achieved by increasing the repulsion between the nZVI and the carbonate surfaces. Modifying the aquifer grains by means of polyelectrolyte coating can increase the overall surface charge of the aquifer grains and improve nZVI stabilization, thereby resulting in increased nZVI mobility. Previous studies have mainly investigated the effects of polyelectrolytes on the transport of non-coated particles such as iron oxides, copper, and latex microspheres (Flynn et al., 2012; Jones and Su, 2012; Kretzschmar and Sticher, 1997; Pelley and Tufenkji, 2008). Johnson et al. (2009) showed that the mobility

of non-coated nZVI particles in quartz porous media is improved when they are co-injected with NOM. The NOM adsorbs onto the non-coated particles, which results in reduced nZVI aggregation and reduced deposition onto quartz grains. Only limited information is available, however, on the effects that co-injected polyelectrolytes have on the transport of coated nZVI. Kim et al. (2012) showed that an excess of polyaspartate in an nZVI suspension enhances the transport of polyaspartate-coated nZVI in porous media containing kaolinite clay. This was ascribed to the reduced heteroaggregation between kaolinite and nZVI, and to polyaspartate adsorption onto positively charged impurities in the porous media, such as metal oxides and the edges of kaolinite (Kim et al., 2012).

We hypothesize that the co-injection of polyelectrolyte with coated nZVI can similarly enhance nZVI transport in carbonate-bearing aquifers. Carbonate-bearing aquifers are, however, known to contain higher concentrations of dissolved calcium that might induce bridging between the nZVI coating and the polyelectrolyte coating on aquifer grain surfaces (Chen et al., 2006; Dong and Lo, 2013; Phenrat et al., 2010c). This effect could result in increased nZVI aggregation and deposition onto aquifer grain surfaces, and hence in reduced nZVI transport. In contrast, adsorption of the co-injected polyelectrolyte onto the coated nZVI surface might prevent particle destabilization in the presence of dissolved calcium by increasing electrosteric repulsion, as previously observed for other nanoparticles (Liu et al., 2013; Qu et al., 2010). This would increase particle stability and reduce attachment to the collector surfaces. It is therefore essential to take into account these various interactions when evaluating the overall effect that the co-injection of polyelectrolytes has on the mobility of coated nZVI.

In this study we have therefore investigated (1) the effect that different types of co-injected polyelectrolytes have on the transport of PAA-coated nZVI (PAA-nZVI) in carbonate porous media, comparing the results to the effect that they have in quartz porous media. We then selected one of the polyelectrolytes (lignin sulfonate) to study in detail (2) the effect that increasing polyelectrolyte concentration has on PAA-nZVI transport and (3) the combined effect of high dissolved calcium concentrations and co-injected polyelectrolyte on PAA-nZVI transport. To our knowledge this is the first study to have addressed the enhancement of nZVI mobility in carbonate porous media by co-injection of polyelectrolytes. Furthermore, the potential of lignin sulfonate as an environmentally friendly and inexpensive polyelectrolyte in nZVI applications has not previously been recognized. This study may therefore help to close some of the gaps in our knowledge that currently limit the practical use of nanoremediation for *in situ* groundwater remediation.

3.2. Material and methods

3.2.1. Polyelectrolytes

Four different polyelectrolytes were used in this study: Suwannee River NOM (International Humic Substance Society), humic acid (Fluka, Austria), carboxymethyl cellulose (CMC, Sigma Aldrich, Austria), and lignin sulfonate (Otto Dille GmbH, Germany). Both NOM and one of its major components, humic acid, are known to improve the stability and transport of nanoparticles in the environment (Johnson et al., 2009; Jones and Su, 2012; Kretzschmar et al., 1995; Yang et al., 2010). CMC is a water-soluble, environmentally friendly polyelectrolyte, known to effectively stabilize nZVI and increase its transport in porous media (He and Zhao, 2007; He et al., 2009). Lignin sulfonate is water-soluble (Nyman et al., 1986), non-toxic (Milczarek et al., 2013), and has previously been used as a stabilizing agent for silver nanoparticles (Milczarek et al., 2013). As a byproduct of wood pulp production, lignin sulfonate is inexpensive and available in large quantities (Pang et al., 2008). This makes lignin sulfonate advantageous for field applications and we therefore chose this polyelectrolyte for more detailed investigations into the effect that varying polyelectrolyte concentrations, including the high dissolved calcium concentrations that could be expected in carbonate-bearing aquifers, have on PAA-nZVI mobility.

Stock solutions of all selected polyelectrolytes were prepared in 1 mM $NaHCO_3$ and filtered through a 0.45-µm cellulose acetate filter (Millipore, Germany) in order to remove any insoluble impurities (Bai et al., 2009).

3.2.2. Nanoscale zero-valent iron

The PAA-nZVI (NANOFER 25S) was supplied by NANOIRON, s.r.o. (Czech Republic) in the form of an aqueous suspension (pH = 11) with a mean primary particle diameter below 50 nm and a total iron concentration of ~20 wt.% (as given by the producer). The particles had been modified by an iron oxide layer and a PAA coating (Kadar et al., 2011).

The PAA-nZVI suspensions (~200 mg L^{-1} total iron) used in transport experiments and for particle characterization were prepared by suspending NANOFER 25S in a 1 mM $NaHCO_3$ solution (pH = 8.3) containing 50 mg L^{-1} of a polyelectrolyte (NOM, humic acid, CMC, or lignin sulfonate). For the set of experiments with lignin sulfonate, various lignin sulfonate concentrations (10, 25, 50, 250 and 500 mg L^{-1}) were added to the same NANOFER 25S suspension (~200 mg L^{-1} total iron in 1 mM $NaHCO_3$). In order to investigate the effect of dis-

solved calcium on the transport of PAA-nZVI co-injected with lignin sulfonate, the NANOFER 25S particles were suspended in 1 mM $NaHCO_3$ solutions containing 50 mg L^{-1} lignin sulfonate and three different calcium concentrations (1, 2.5, and 5 mM $CaCl_2$). All suspensions were prepared using an ultrasonic bath (Sonorex RK 106, Ø 240 mm, 130 mm high, 120 W indicated power, Bandelin electronic, Germany). The total iron content in suspension (~200 mg L^{-1} in all experiments) was determined by inductively coupled plasma optical emission spectrometry (ICP-OES, Optima 5300DV, PerkinElmer, USA) after acid digestion.

The PAA-nZVI size was determined by analyzing the obscuration time (pulse length, time-of-transition principle) of a particle in different nZVI suspensions illuminated by a rotating laser beam, with a CCD camera positioned behind the measurement vessel (Eytech™, Ambivalue, The Netherlands). The sedimentation of PAA-nZVI was also monitored by measuring the transmittance of monochromatic light (wavelength 880 nm) in the suspensions (TurbiScan LAB, Quantachrome, Germany), as described in Laumann et al. (2013). The resulting sedimentation rates were converted into PAA-nZVI diameters for the settled fraction using Stokes' law (PAA-nZVI density given by the producer: 7.87 g cm^{-3}, fluid density: 1 g cm^{-3}, fluid viscosity: 1 kg m^{-1} s^{-1}).

The electrophoretic mobility of the PAA-nZVI was measured in the stable fraction of the suspension (i.e., the supernatant after two hours of sedimentation) using laser Doppler anemometry (Zetasizer Nano ZS, Malvern Instruments, UK). The electrophoretic mobility was determined in the presence of 1 mM $NaHCO_3$, in the presence of 1 mM $NaHCO_3$ and various polyelectrolytes, and in the presence of 1 mM $NaHCO_3$ with lignin sulfonate and dissolved calcium. The electrophoretic mobility was converted into zeta potential by applying the Smoluchowski relationship (Hunter, 1988).

3.2.3. Porous media

Standard Ottawa sand (20–30 mesh, 0.4–0.85 mm, extra pure, Fisher Scientific, Austria) was used as the quartz porous medium. The quartz sand was acid washed before use in order to remove any metal oxide impurities from the grain surfaces, following the procedure described by Yang et al. (2010). Limestone (with ~97.0% $CaCO_3$, ~2% $MgCO_3$, and <1% aluminum and iron oxides, Appendix Table A-1) was crushed with a jaw crusher and then sieved to between 0.5 and 1 mm, in order to obtain a size fraction as similar as possible to that of the Ottawa sand. The carbonate sand was rinsed with deionized water in order to remove any soluble solids and fine material (Laumann et al., 2013).

The streaming potentials of the porous media were measured using an Electrokinetic Analyzer (SurPASS, Anton Paar, Austria) equipped with a cylindrical cell. The cell was equilibrated by circulating the background solution in alternating directions for a period of ~15 minutes prior to each measurement. The streaming potential was determined in the presence of 1 mM NaCl only, in the presence of 1 mM NaCl and different lignin sulfonate concentrations (10–500 mg L^{-1}) and calcium concentrations (1–5 mM $CaCl_2$). The streaming potential was converted into zeta potential using the Fairbrother-Mastin equation (Fairbrother and Mastin, 1924).

3.2.4. Column experiments

The transport studies were performed in borosilicate glass columns (1 cm i.d., 10 cm length, Omnifit, Germany). A peristaltic pump (Ismatec, Germany) was used to feed background electrolyte and the PAA-nZVI suspensions into the columns. All experiments were carried out under an injection velocity of 6 x 10^{-4} m s^{-1}, which corresponds to injection conditions currently applied in field studies (Phenrat et al., 2010b). Each column was wet packed with model porous media to a height of ~8 cm and flushed with at least ten pore volumes of background solution (1 mM $NaHCO_3$ or 1 mM $NaHCO_3$ with 1, 2.5, and 5 mM $CaCl_2$) in order to remove background turbidity. A tracer test using NaBr was conducted prior to the nZVI and polyelectrolyte injection and effluent bromide concentrations were analyzed by ion chromatography (ICS-1000, Dionex, Austria). The porosities of the media ranged between 0.39 (in quartz sand) and 0.49 (in carbonate sand). Following the elution of the bromide tracer, the PAA-nZVI suspensions (~200 mg L^{-1} total iron) were co-injected with different polyelectrolyte solutions (NOM, humic acid, CMC, and lignin sulfonate), each at concentrations of 50 mg L^{-1}. In a separate set of experiments, different lignin sulfonate concentrations (10, 25, 50, 250 and 500 mg L^{-1}) and dissolved calcium concentrations (1, 2.5, and 5 mM $CaCl_2$) were co-injected with the same PAA-nZVI suspension (~200 mg L^{-1} total iron). Control injections of a pure lignin sulfonate solution (50 mg L^{-1} in 1 mM $NaHCO_3$) and the pure PAA-nZVI suspension (in 1 mM $NaHCO_3$, without any polyelectrolyte) were performed in parallel. In order to reduce nZVI particle aggregation and sedimentation, the PAA-nZVI suspension was sonicated prior to and during the injection in all experiments (ultrasonic bath, Sonorex RK 106, Ø 240 mm, 130 mm high, 120 W indicated power; Bandelin electronic, Germany). The column effluent was collected every 30 seconds and analyzed for total iron. The lignin sulfonate in the control experiment was determined by UV-vis spectroscopy (LAMBDA 35,

PerkinElmer, USA) at a wavelength of 280 nm (Grigg and Bai, 2004; Nanthakumar et al., 2010). The reported data for all column experiments represent the mean of results from duplicate measurements. The experimental transport data were analyzed using colloid filtration theory and a one dimensional convection-dispersion equation (details of the models used are provided in Chapter 2.2.6).

3.3. Results and discussion

3.3.1. Characterization of PAA-nZVI suspension

The laser obscuration time measurements for the pure PAA-nZVI suspension (~200 mg L^{-1} total iron in 1 mM $NaHCO_3$, pH = 8.3) yielded a mean aggregate size of 1.32 ± 1.04 µm (Table 3.1, number distribution). This indicated that the pure PAA-nZVI (NANOFER 25S) suspension is a polydisperse system with a broad particle size distribution, as previously observed by Laumann et al. (2013). The presence of different concentrations of polyelectrolytes (NOM, humic acid, CMC, lignin sulfonate) had no significant effect on the PAA-nZVI aggregate size (Table 3.1, average aggregate size 1.21 µm). The PAA-nZVI aggregate size generally increased in the presence of dissolved calcium (Table 3.1, average aggregate size increased to 3.33 µm) due to nZVI aggregation as a result of reduced electrostatic repulsion. However, no increase in PAA-nZVI aggregate size was observed in the calcium solution containing 50 mg L^{-1} lignin sulfonate, in fact the PAA-nZVI aggregates in this suspension were somewhat smaller than those in the pure PAA-nZVI suspension (Table 3.1, average aggregate size decreased to 1.12 µm). Lignin sulfonate stabilized the PAA-nZVI suspension in the presence of dissolved calcium, probably due to an increase in electrosteric repulsion between PAA-nZVI particles.

The dispersion states of the PAA-nZVI suspensions were further investigated by monitoring particle sedimentation. The Stokes diameter of PAA-nZVI aggregates in the suspensions with various concentrations of polyelectrolytes averaged 1.45 µm, which is comparable to that in the pure suspension (1.52 µm; Table 3.1). The PAA-nZVI diameter increases in the presence of calcium (average size 2.16 µm, Table 3.1), while a slightly smaller size (1.30 µm on average, Table 3.1) was observed for the PAA-nZVI aggregates in the suspension with both calcium and 50 mg L^{-1} lignin sulfonate. The results of the sedimentation test therefore corroborate the results obtained from the laser obscuration time method.

Table 3.1. Size and zeta potential of PAA-nZVI particles in different suspensions and pH of the suspensions.

PAA-nZVI suspension	**Size** (Laser obscuration time)	**Size** (Stokes law)	**Zeta potential**	**pH**
in 1mM $NaHCO_3$ +	μm	μm	mV	
Pure	1.32 ± 1.04	1.52	-49.10 ± 1.12	8.30
50 mg L^{-1} NOM	1.27 ± 1.05	1.38	-52.20 ± 0.80	7.87
50 mg L^{-1} CMC	1.18 ± 0.83	1.52	-52.92 ± 1.15	8.32
50 mg L^{-1} humic acid	1.20 ± 0.80	1.52	-51.55 ± 0.58	8.19
10 mg L^{-1} lignin sulfonate	1.21 ± 0.90	1.52	-45.83 ± 0.49	7.99
25 mg L^{-1} lignin sulfonate	1.17 ± 0.86	1.42	-49.23 ± 0.46	7.96
50 mg L^{-1} lignin sulfonate	1.23 ± 1.01	1.36	-51.67 ± 0.91	8.12
250 mg L^{-1} lignin sulfonate	1.18 ± 0.88	1.48	-51.77 ± 1.25	7.93
500 mg L^{-1} lignin sulfonate	1.26 ± 0.99	1.40	-51.70 ± 0.72	7.57
1 mM $CaCl_2$	2.49 ± 2.59	1.79	-19.58 ± 1.34	8.20
2.5 mM $CaCl_2$	4.33 ± 3.63	2.50	-17.25 ± 0.52	8.17
5 mM $CaCl_2$	3.18 ± 2.94	2.20	-15.62 ± 0.44	8.08
1 mM $CaCl_2$ + 50 mg L^{-1} lignin sulfonate	1.15 ± 0.74	1.45	-20.43 ± 1.42	7.89
2.5 mM $CaCl_2$ + 50 mg L^{-1} lignin sulfonate	1.10 ± 0.61	1.21	-17.27 ± 0.38	8.09
5 mM $CaCl_2$ + 50 mg L^{-1} lignin sulfonate	1.10 ± 0.60	1.23	-17.83 ± 0.70	8.09

The zeta potential of PAA-nZVI, derived from electrophoretic mobility measurements, was -49.1 mV. The presence of the investigated polyelectrolytes at different concentrations did not significantly change the zeta potential of the PAA-nZVI particles (average zeta potential -50.9 mV, Table 3.1), as would be expected because of the strongly negative PAA coating. In the presence of dissolved calcium and at higher ionic strength the zeta potential of the PAA-nZVI particles decreased (average zeta potential -17.5 mV, Table 3.1) as a result of electrostatic double layer compression and possible calcium adsorption onto the nZVI surfaces. This effect has been previously observed for other polymer-coated nZVI particles (Dong and Lo, 2013; Saleh et al., 2008). A similar decrease in zeta potential was also observed when both calcium and 50 mg L^{-1} lignin sulfonate were added (average zeta potential -18.5 mV, Table 3.1).

3.3.2. Surface charge of porous media

The zeta potentials of the two porous media were derived from streaming potential measurements and determined in the presence of different calcium and lignin sulfonate concentrations. Quartz sand was found to be negatively charged (-44.6 mV, Figure 3.1), while the carbonate sand carried a weaker negative charge (-11.3 mV, Figure 3.1), as previously observed by Laumann et al. (2013).

The presence of lignin sulfonate in the background solution did not affect the zeta potential of the quartz sand: it remained between -44.6 mV and -41.4 mV in the presence of 0–500 mg L^{-1} lignin sulfonate (Figure 3.1a). In contrast, the zeta potential of the carbonate sand increased significantly in the presence of lignin sulfonate, from -11.3 mV to -31.2 mV (Figure 3.1a). This suggests that lignin sulfonate adsorbs onto the carbonate grain surfaces thereby increasing the negative surface charge of the carbonate sand. Increasing lignin sulfonate concentrations from 10 to 500 mg L^{-1} did not result in any major change in the zeta potential of the carbonate sand, which remained at an average of -28.6 mV (Figure 3.1a).

With increasing calcium concentration in the background solution (from 1 to 5 mM), the zeta potential decreased for both the quartz and carbonate sands (Figure 3.1b). A high ionic strength together with the presence of calcium results in a reduction of the aquifer grain surface charge, as previously observed by, e.g., Heberling et al. (2011).

When 50 mg $L^{-1}$of lignin sulfonate was added to 1 mM and 2.5 mM calcium solutions the zeta potential of the quartz sand remained similar to that in the pure calcium solutions (Figure 3.1b and c). Nevertheless, when the same amount of lignin sulfonate was added to a solution containing 5 mM calcium an increase in the zeta potential of the quartz sand (from -8.5 mV to -16.5 mV) was observed. The high calcium concentration can facilitate the lignin sulfonate adsorption onto quartz, as previously observed for lignin sulfonate adsorption onto dolomite by Bai et al. (2009).

The zeta potential of the carbonate sand significantly increased when 50 mg $L^{-1}$of lignin sulfonate was added to each calcium containing solution (1 mM, 2.5 mM, and 5mM), irrespectively of the calcium concentration (Figure 3.1b and c). This shows that lignin sulfonate adsorption onto the carbonate grain surface prevents reduction of the carbonate surface charge by the dissolved calcium.

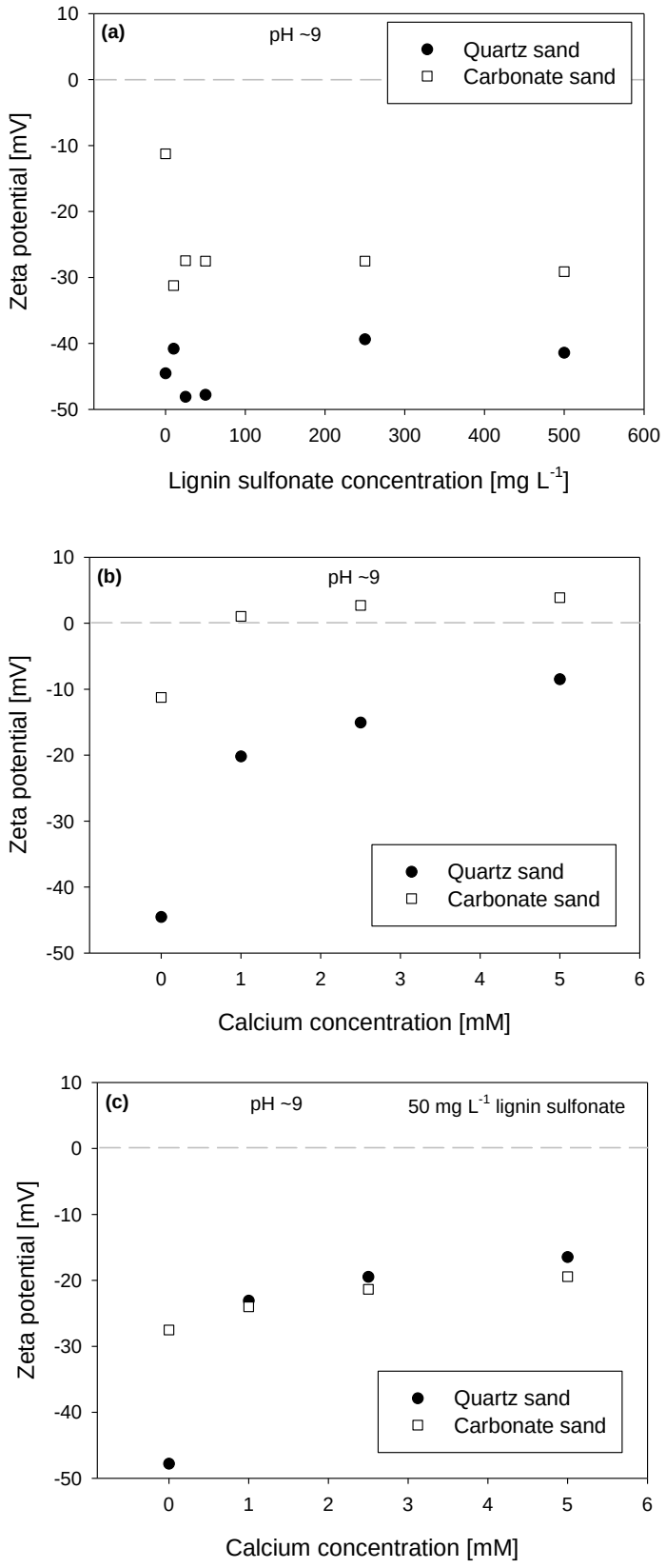

Figure 3.1. Zeta potential of quartz sand and carbonate sand at pH ~ 9 as a function of (a) the lignin sulfonate concentration, (b) the calcium concentration, and (c) the calcium concentration in the presence of 50 mg L^{-1} lignin sulfonate.

3.3.3. Polyelectrolyte interaction with porous media

The interaction between polyelectrolytes and the porous media was studied by injecting a lignin sulfonate solution (50 mg L^{-1} in 1 mM $NaHCO_3$) into columns filled with either quartz sand or carbonate sand.

The breakthrough (C/C_0) of lignin sulfonate varied depending on the porous media (Figure 3.2). In quartz sand, the lignin sulfonate breakthrough matched that of the conservative bromide tracer, demonstrating no significant retardation of lignin sulfonate. Model simulations based on the convection-dispersion equation showed a retardation factor of 1.0 for lignin sulfonate transport in quartz sand (Table A-3, Appendix). Since both lignin sulfonate and quartz sand are negatively charged at a pH of around 8, any surface interactions between these components are inhibited by electrostatic repulsion. This is consistent with previous studies reporting little or no adsorption of other anionic polyelectrolytes (NOM, humic acid) onto quartz surfaces (Johnson et al., 2009; Johnson and Logan, 1996; Lenhart and Saiers, 2003; Mibus et al., 2007).

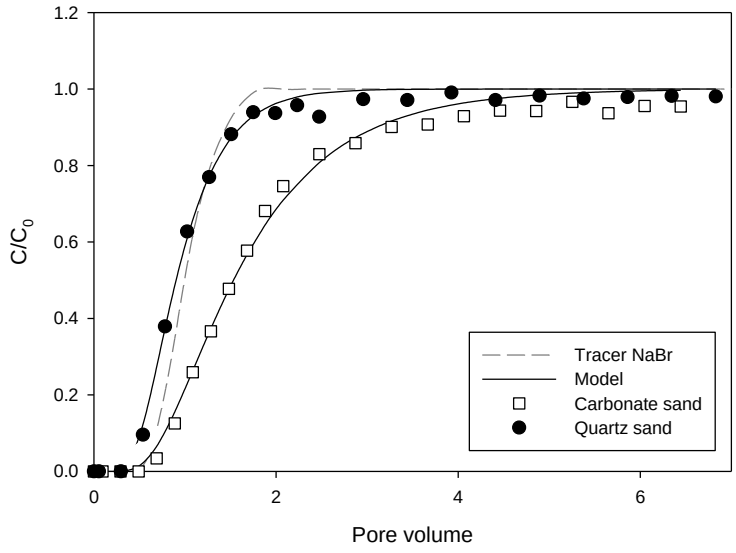

Figure 3.2. Breakthrough curves of lignin sulfonate and the bromide tracer in quartz sand and in carbonate sand (injection velocity: 6 x 10^{-4} m s^{-1}, C_0: 50 mg L^{-1} lignin sulfonate in 1 mM $NaHCO_3$). The solid lines represent model fits for lignin sulfonate transport in porous media using the convection-dispersion equation.

In contrast to quartz sand, the breakthrough of lignin sulfonate in carbonate sand differs from that of the bromide tracer (Figure 3.2), with a retardation factor of 1.78 and a distribution coefficient (K_d) of 0.277 cm^3 g^{-1} (Table A-3, Appendix). This is explained by the adsorption of lignin sulfonate onto the carbonate grain surfaces and is in agreement with the increase in

zeta potential of the carbonate sand in the presence of lignin sulfonate (Figure 3.1a). These observations are also in accordance with the lignin sulfonate adsorption onto porous sandstone and dolomite reported in studies on enhanced oil recovery (Bai et al., 2009; Grigg and Bai, 2004).

3.3.4. Effect of polyelectrolyte co-injection on PAA-nZVI transport

The co-injection of polyelectrolytes (NOM, lignin sulfonate, CMC, and humic acid) at concentrations of 50 mg L^{-1} had no effect on PAA-nZVI transport in quartz sand. The breakthrough of PAA-nZVI with all co-injected polyelectrolytes was similar to that for the pure PAA-nZVI suspension and remained at approximately 0.5 in all the experiments (Figure 3.3a). The attachment efficiency (α, Equation 2.1, Chapter 2.2.6) and the deposition rate coefficient (k_{CDE}, Equation 2.4, Chapter 2.2.6) for PAA-nZVI co-injected with polyelectrolytes were both similar to those for the pure PAA-nZVI suspension (α = 0.3; k_{CDE} = 0.006 s^{-1}, Table A-4, Appendix). This similar deposition and transport behavior in quartz sand for the pure PAA-nZVI suspension and for the suspension co-injected with different polyelectrolytes demonstrates that the repulsion between the polyelectrolytes and the quartz prevents any transport-relevant surface modification of the quartz grains.

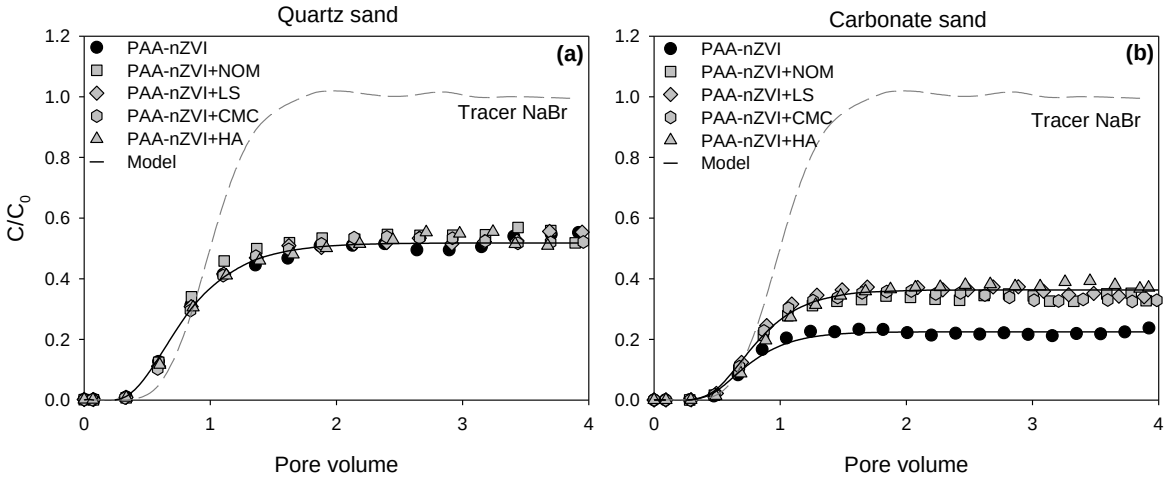

Figure 3.3. Breakthrough curves of PAA-nZVI co-injected with different polyelectrolytes in (a) quartz sand, and (b) carbonate sand (injection velocity: 6 x 10^{-4} m s^{-1}, C_0: 200 mg L^{-1} total iron in 1 mM $NaHCO_3$ and 50 mg L^{-1} polyelectrolyte, HA: humic acid, LS: lignin sulfonate). The solid lines are model fits of the breakthrough curves; for clarity only one is shown in (a) and two in (b).

In contrast, the co-injection of different polyelectrolytes did affect PAA-nZVI transport in carbonate sand. The co-injection of 50 mg L^{-1} of polyelectrolyte increased the breakthrough from 0.20 (for the pure PAA-nZVI suspension) to approximately 0.35, irrespective of the type of polyelectrolyte used (Figure 3.3b). This can be related to the adsorption of the polyelectrolytes onto the carbonate sand, which then increases the repulsion between the PAA-nZVI and the carbonate grain surfaces. The PAA-nZVI attachment efficiency was reduced from 1.0 for the pure suspension to approximately 0.7 for the PAA-nZVI suspension co-injected with polyelectrolytes (Table A-4, Appendix). The deposition rate coefficient was similarly reduced from 0.011 s^{-1} to 0.006 s^{-1} (Table A-4, Appendix). The reduced PAA-nZVI deposition onto the carbonate sand resulted in enhanced particle mobility and therefore greater overall PAA-nZVI travel distance. The maximum predicted travel distance in carbonate sand (at 99.9% of particle removal, Equation 2.3, Chapter 2.2.6) increased from 0.37 m for the pure suspension to 0.56 m for the PAA-nZVI suspension co-injected with polyelectrolytes (Table A-4, Appendix). Although the applied polyelectrolytes differ in their structural and chemical properties (Figure A-1, Table A-5, Appendix), they have the same overall effect on PAA-nZVI mobility in carbonate sand when they are present in concentrations of 50 mg L^{-1} (Figure 3.3b).

3.3.5. Effect of different concentrations of co-injected polyelectrolyte on PAA-nZVI transport

The breakthrough of PAA-nZVI co-injected with different lignin sulfonate concentrations (10–500 mg L^{-1}) in quartz sand remained steady at around 0.5, demonstrating that none of the lignin sulfonate concentrations tested had any effect on PAA-nZVI transport (Figure 3.4). The attachment efficiencies and deposition rate coefficients for the PAA-nZVI particles co-injected with different lignin sulfonate concentrations were also similar to those for the pure PAA-nZVI suspension ($\alpha = 0.3$; $k_{CDE} = 0.006$ s^{-1}, Table A-6, Appendix).

In the experiments using carbonate sand, however, the PAA-nZVI breakthrough increased from 0.20 to 0.30 with 25 mg L^{-1} of co-injected lignin sulfonate, and to 0.37 with 50 mg L^{-1}. The lowest lignin sulfate concentration (10 mg L^{-1}) had no effect on the PAA-nZVI breakthrough while the highest concentration (500 mg L^{-1}) resulted in the highest PAA-nZVI breakthrough (0.40; Figure 3.5).

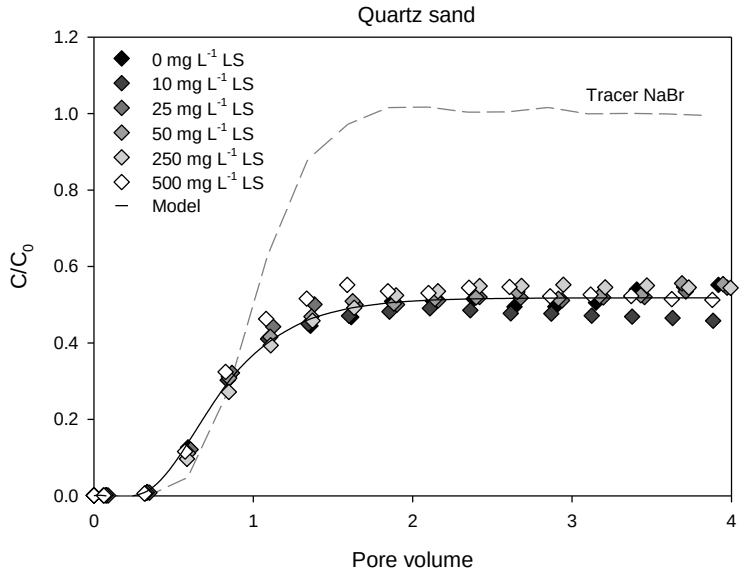

Figure 3.4. Breakthrough curves of PAA-nZVI co-injected with different lignin sulfonate (LS) concentrations in quartz sand (injection velocity: 6 x 10^{-4} m s^{-1}, C_0: 200 mg L^{-1} Fe in 1 mM $NaHCO_3$ and 0 to 500 mg L^{-1} LS). The solid line is a model fit of the breakthrough curve (only one is shown, for the sake of clarity).

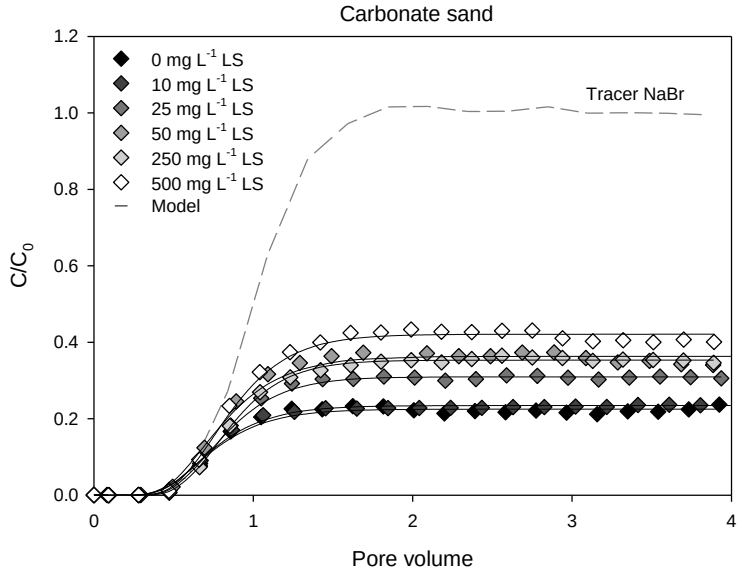

Figure 3.5. Breakthrough curves and model fits of for PAA-nZVI co-injected with different lignin sulfonate (LS) concentrations, in carbonate sand (injection velocity: 6 x 10^{-4} m s^{-1}, C_0: 200 mg L^{-1} total iron in 1 mM $NaHCO_3$ and 0 to 500 mg L^{-1} lignin sulfonate).

The deposition rate coefficient in carbonate sand was reduced from 0.011 for the pure PAA-nZVI suspension to 0.006 s^{-1} for the PAA-nZVI suspension co-injected with 500 mg L^{-1} lignin sulfonate (Table A-6, Appendix). This decrease in PAA-nZVI deposition with increasing

lignin sulfonate concentration is due to the blocking of favorable deposition sites and is matched by a corresponding decrease in attachment efficiency from 1.0 to 0.6 (Figure 3.6). The maximum predicted travel distance for the PAA-nZVI particles (at 99.9% of particle removal) in carbonate sand consequently increased from 0.37 m to 0.64 m in the presence of 500 mg L^{-1} lignin sulfonate. Somewhat shorter travel distances (0.37 m to 0.54 m) were observed for the suspensions containing lower lignin sulfonate concentrations (Figure 3.6). The 10-fold increase in lignin sulfonate concentration from 50 to 500 mg L^{-1} only produced a relatively small (10 cm) increase of the particle travel distance.

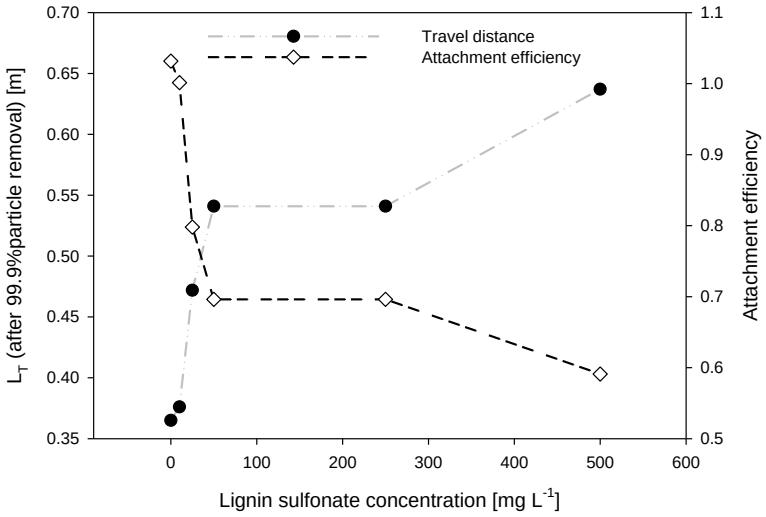

Figure 3.6. Influence of co-injected lignin sulfonate concentration on attachment efficiency (α) and travel distance (L_T) of PAA-nZVI in carbonate sand.

3.3.6. Effect of calcium concentration on the transport of PAA-nZVI co-injected with polyelectrolyte

The effect that increasing calcium concentrations have on the transport of PAA-nZVI co-injected with lignin sulfonate (50 mg L^{-1}) was evaluated for three different calcium concentrations (1, 2.5, and 5 mM $CaCl_2$) and the results were compared with the PAA-nZVI transport with no co-injected lignin sulfonate and in the solely presence of calcium.

The PAA-nZVI breakthrough in quartz sand with 50 mg L^{-1} of co-injected lignin sulfonate decreased from approximately 0.55 in 1 mM $CaCl_2$ to 0.44 in 5 mM $CaCl_2$ (Figure 3.7). This is higher than the PAA-nZVI breakthrough in the presence of calcium only and similar to the PAA-nZVI breakthrough in 1 mM $NaHCO_3$ with neither polyelectrolyte nor calcium present

(Figure 3.3a). This demonstrated that the presence of lignin sulfonate can significantly increase the PAA-nZVI mobility in quartz sand at high calcium concentrations.

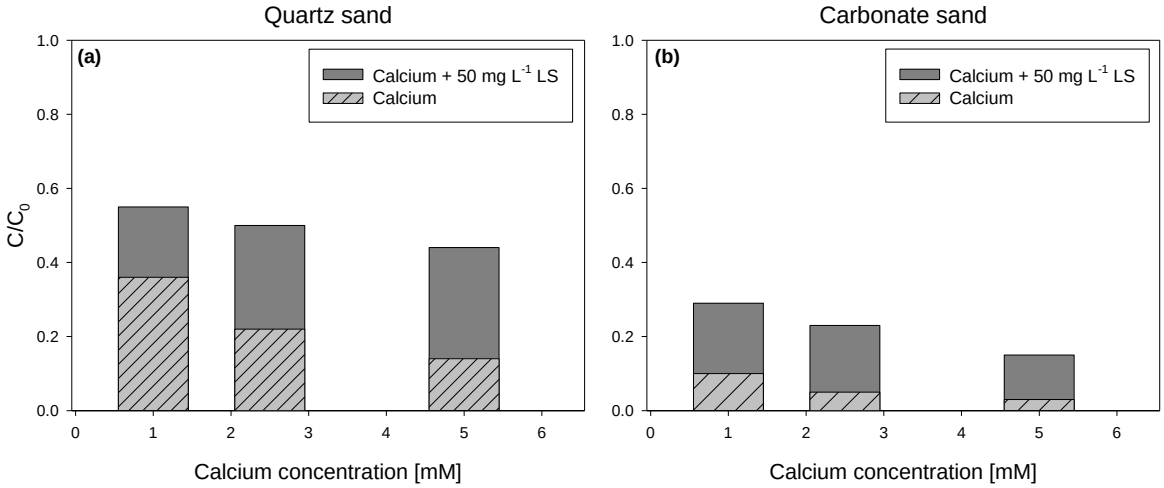

Figure 3.7. Influence of calcium concentration on the PAA-nZVI breakthrough in (a) quartz sand, and (b) carbonate sand, with and without lignin sulfonate (50 mg L^{-1}).

In carbonate sand the breakthrough of PAA-nZVI co-injected with 50 mg L^{-1} lignin sulfonate decreased from 0.29 in 1 mM $CaCl_2$ to 0.15 in 5 mM $CaCl_2$. This is still significantly higher than the PAA-nZVI breakthrough in the presence of calcium only, for which almost no PAA-nZVI breakthrough (0.03) was observed in a 5 mM calcium solution (Figure 3.7). The effect of calcium was, however, more pronounced in the carbonate sand than in the quartz sand.

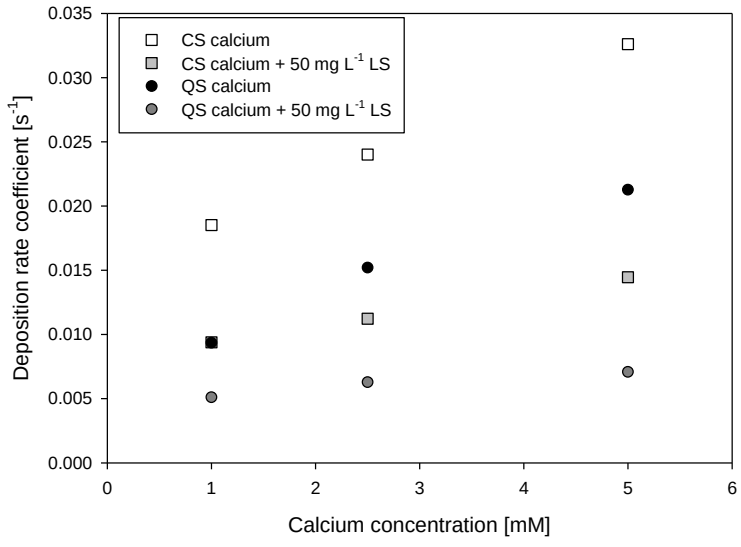

Figure 3.8. Influence of calcium concentration on the deposition kinetics of PAA-nZVI in quartz sand (QS) and carbonate sand (CS), with and without lignin sulfonate (50 mg L^{-1}).

In both the quartz and carbonate sands the deposition rate coefficient (k_{CDE}) for the PAA-nZVI particles increased linearly with increasing calcium concentration, irrespective of whether the background solution contained only dissolved calcium, or dissolved calcium and 50 mg L^{-1} of lignin sulfonate (Figure 3.8). The increase in the deposition rate coefficient with increasing calcium concentrations was, however, less pronounced in the presence of 50 mg L^{-1} lignin sulfonate in both the quartz and carbonate sands (Figure 3.8).

Overall, the results demonstrated that lignin sulfonate is able to increase PAA-nZVI stability (Table 3.1), reducing its attachment to collector surfaces and thereby increasing its mobility in both the quartz sand and the carbonate sand at high ionic strength and high dissolved calcium concentrations (Figure 3.7).

3.4. Implications for field applications

Our investigations have revealed that co-injection of polyelectrolytes can increase PAA-nZVI transport in carbonate sand. The degree of enhancement was similar for all of the polyelectrolytes investigated (NOM, humic acid, CMC, and lignin sulfonate), when applied in the same concentrations. However, lignin sulfonate is considered to be the most promising material for field application due to its availability in large quantities and its low price of about €10 kg^{-1}, which compares favorably with €93 kg^{-1} for CMC, €500 kg^{-1}m for humic acid (Sigma Aldrich), and €3000 kg^{-1} for Suwannee River NOM (International Humic Substances Society). A concentration of 50 mg L^{-1} co-injected lignin sulfonate seems to be the most reasonable quantity in relation to overall material costs and its potential to increase the PAA-nZVI mobility.

Model simulations based on colloid filtration theory and the one dimensional transport equation have shown that the PAA-nZVI attachment efficiency and deposition rate coefficient decrease with increasing co-injected lignin sulfonate concentrations, under the investigated conditions. The maximum predicted travel distance for PAA-nZVI in carbonate sand is almost doubled when co-injected with lignin sulfonate. It should be noted that although the co-injected polyelectrolytes had no observed effect on PAA-nZVI transport in the acid-washed quartz sand, an increase in nZVI mobility would be expect in natural quartz porous media, where positively charged heterogeneities (such as iron and aluminum oxides), and therefore preferential deposition sites for the polyelectrolytes, are invariably present.

In the presence of high dissolved calcium concentrations (up to 5 mM), co-injection of lignin sulfonate has been shown to enhance PAA-nZVI transport irrespective of the type of porous

media. Our results indicate that co-injecting lignin sulfonate at a concentration of 50 mg L^{-1} reduces PAA-nZVI deposition in both quartz and carbonate sands when calcium concentrations are high.

The simplified systems (small-scale column experiments) and well-controlled experimental conditions applied in this study have served to elucidate the interactions between co-injected polyelectrolytes and the PAA-nZVI suspension, as well as the effect that these interactions have on PAA-nZVI transport. Further research on a larger scale will however be required, together with field investigations, to test the applicability of our results to natural (or near-natural) systems.

The application of additional agents such as polyelectrolytes together with the nZVI suspension will inevitably increase remediation costs. Site-specific assessment of hydrochemical and hydrogeological parameters will therefore be required to determine whether or not the improvement in nZVI transport achieved by co-injection of polyelectrolytes will justify the extra effort and cost involved. The effects of the polyelectrolytes on subsurface organisms also need to be evaluated, as they have the potential to promote bacterial growth in the subsurface (Kirschling et al., 2010), thereby enhancing the overall remediation effect by combining nZVI treatment with bioremediation (Su et al., 2012).

Acknowledgments

The authors would like to thank NANOIRON, s.r.o. (Czech Republic) for kindly providing aqueous suspensions of NANOFER 25S. The research was funded by the Austrian Federal Ministry of Agriculture, Forestry, Environment and Water; Management by Kommunalkredit Public Consulting, Austria.

4. Material flow analysis: an effectiveness assessment tool for *in situ* thermal remediation

Susanne Laumann, Vesna Micić, Johann Fellner, David Clement, Thilo Hofmann

Vadose Zone Journal, Vol. 12, No. 1

Reported with permission from ACSESS - Alliance of Crop, Soil, and Environmental Science Societies

Abstract

In situ thermal desorption (ISTD) is a remediation technique that increases the effectiveness of soil vapor extraction through the simultaneous application of heat and vacuum. In this study, ISTD was applied to remove a chlorinated solvent source from unsaturated soil beneath an existing aboveground infrastructure. A material flow analysis (MFA) was applied for the first time to assess the effectiveness of ISTD in the vadose zone and to reveal the total emission of chlorinated solvents into the environment before and during remediation. The principle of matter conservation used in MFA enabled the quantification of chlorinated solvent flows in all matrices affected: soil, groundwater, and soil vapor. The MFA results revealed that the mass removed by ISTD was similar to the mean chlorinated solvent mass estimated to have been present in the soil before remediation, indicating high effectiveness in contaminant removal. The remediation target value in soil vapor was achieved after 9 months of remediation, demonstrating the time efficiency of ISTD for this particular site. The MFA additionally provided an overview of the processes and contaminant transformations occurring in the soil, water, and air compartments during the course of remediation.

4.1. Introduction

Chlorinated solvents, such as tetrachloroethene (PCE) and trichloroethene (TCE), are dense nonaqueous-phase liquids (DNAPLs) and among the most prevalent organic contaminants at industrial sites (U.S. EPA, 2004). Remediation of such contaminated sites is particularly challenging when chlorinated solvents are present in the form of residual droplets or pools in the subsurface beneath existing aboveground infrastructure. Because the dissolution and desorption/diffusion rates of chlorinated solvents are very slow, they represent a long-term source of soil and groundwater contamination (Poulsen and Kueper, 1992; Stroo et al., 2003; Yu, 1995). When the excavation of contaminated soil is too costly or impossible (due to, for ex-

ample, the presence of aboveground infrastructure), a common alternative used for soils affected by volatile and semivolatile organic chemicals (such as PCE and TCE) is soil vapor extraction (Nobre and Nobre, 2004). The effectiveness of soil vapor extraction (SVE) can be hindered by heterogeneities in the soil's permeability, moisture content, and DNAPL distribution, as well as by mass-transfer limitations. The latter is caused by slow desorption/diffusion and the limited volatilization of the contaminants at normal soil temperatures (Brusseau et al., 2010; Heron et al., 1998; Massmann et al., 2000; Park et al., 2005).

Thermally enhanced SVE has been proposed as a way to overcome the mass-transfer limitations (Heron et al., 1998). Heating the soil increases the vapor pressure and the Henry's law constant, resulting in enhanced chlorinated solvent extraction rates.

Heating can be performed by injection of hot air, steam, or water into the soil, by applying an electrical current, or by placing heating elements in the ground. The injection of hot air, steam, or water suffers from the major disadvantage that the heat can only be successfully injected into highly permeable zones (Heron et al., 1998). For complex underground geological systems in which impermeable layers of silt or clay are interspersed with more permeable layers, heating elements offer a better alternative (Triplett Kingston et al., 2010).

In this study, thermal conductive heating, also known as *in situ* thermal desorption (ISTD), was applied for remediation of soil contaminated with chlorinated solvents. This technique involves the simultaneous application of an array of heating elements and SVE wells. Heat is primarily transferred into the soil by thermal conduction from heating elements, which typically operate at temperatures of around 600°C (Stegemeier and Vinegar, 2001).

The effectiveness of ISTD for the removal of chlorinated solvents has, to date, been documented at only a few sites (Heron et al., 2009; LaChance et al., 2006; Triplett Kingston et al., 2010). The performance of this remediation technique has, in most cases, been evaluated solely on the basis of the achievement of the target remediation values. The assessment of the effectiveness of soil remediation is limited to measurements of the contaminant concentration in the soil, taken before and after remediation (Heron et al., 2009; Park et al., 2005; Stegemeier and Vinegar, 2001).

Material flow analysis is a method based on the law of conservation of mass for systematic assessment of the flows and stocks of materials within a system defined in both space and time (Brunner and Rechberger, 2004). It is a frequently applied decision-support tool in waste (Pires et al., 2011; Steubing et al., 2010) and resource management (Klinglmair and Fellner,

2010; Wang et al., 2007), as well as in life-cycle assessment (Brunner and Rechberger, 2004), the latter increasingly being used to study sustainable remediation practices (Kielenniva et al., 2012; Sparrevik et al., 2011; U.S. Sustainable Remediation Forum, 2009). Material flow analysis, to our knowledge, has not been utilized to date to evaluate the performance of a remediation process.

The aim of this study was to use material flow analysis to assess the effectiveness of *in situ* thermal desorption, to determine and visualize the contaminant mass flows between soil compartments, and to determine the total emissions into the hydrosphere and atmosphere both before and during remediation.

4.2. Material and methods

4.2.1. Field site description and remediation goal

The test site is located in the state of Lower Austria. The mean annual temperature in this region is 10°C and the mean annual precipitation ranges from 672 to 838 mm (ZAMG, 2012). At the test site, a former dry-cleaning facility caused subsurface contamination by chlorinated solvents across an area of approximately 400 m^2. The surface area is now being used for commercial purposes and excavation of the contaminated soil was therefore not an alternative.

The subsurface consists of a rock-fill layer (occasionally with sand and gravel) or a layer of gravel and silt extending to maximum depth of 2.5 m below ground surface (bgs), (Figure 4.1, Profile W2). This is underlain by a layer of finer sediments (silt with fine sand or just fine sand) extending to a maximum depth of 4.8 m bgs, followed by a sequence of gravel (to a maximum of 6.8 m bgs), fine sediments (silt and fine sand) to 9.0 m bgs, sand to 11.0 or 15.0 m bgs (Profile W1), and gravel to 15.0 m bgs, followed by an aquiclude of clay and marlstone (Figure 4.1). The groundwater table is between 8.0 and 9.3 m bgs, and the groundwater flow is from southwest to northeast (Figure 4.2).

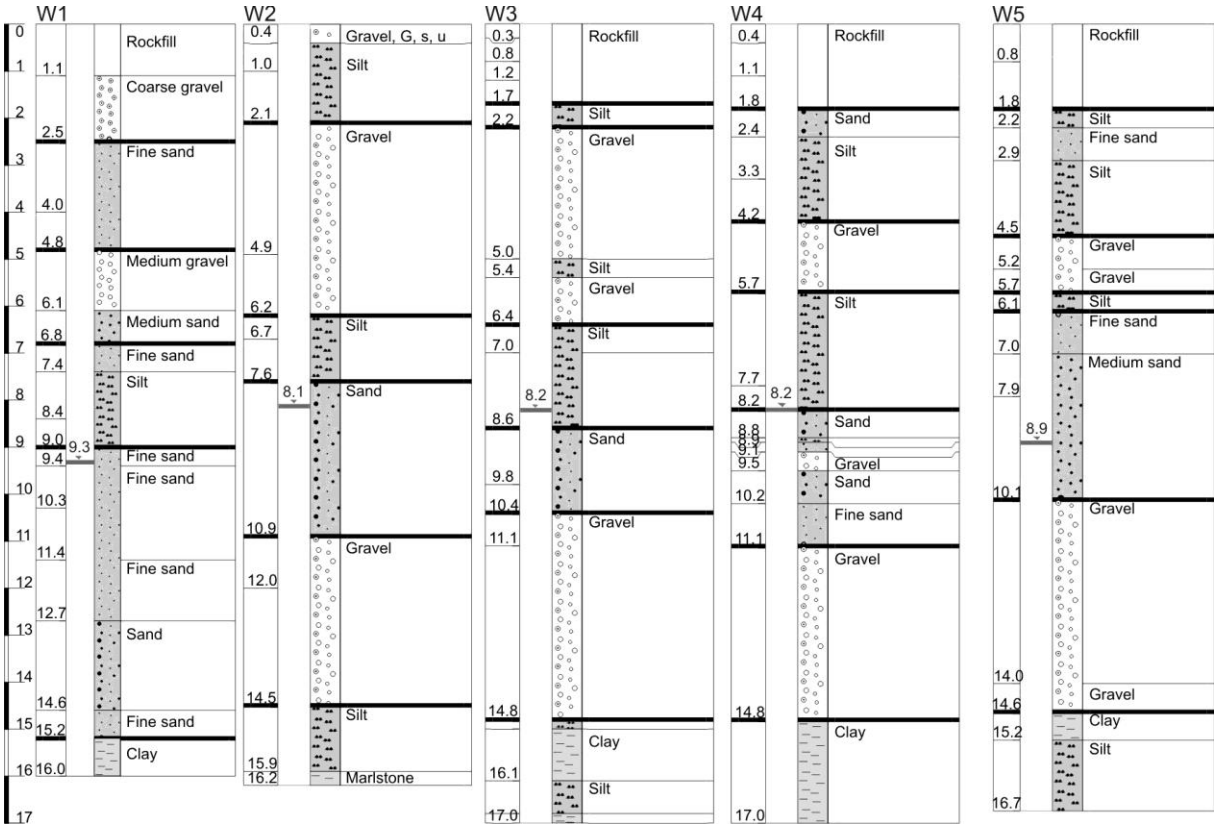

Figure 4.1. Subsurface profiles at the investigated site (for locations refer to Figure 4.2).

The initial site investigation revealed up to 5000 mg m^{-3} (in extraction well E24, Figure 4.2) of chlorinated solvents and their degradation products in soil vapor, including PCE, TCE, 1,1-dichloroethene, *cis*-1,2-dichloroethene, *trans*-1,2-dichloroethene, vinylchloride, 1,1,1-trichloroethane, 1,1-dichloroethane, 1,2-dichlorethane, tetrachloromethane, trichloromethane, and dichloromethane.

The source zone is estimated to have been close to extraction well E24 (Figure 4.2), which had chlorinated solvent concentrations up to 11,600 mg kg^{-1} in the soil at 5 m bgs. In the groundwater observation wells (W2, W3, W4, and W5, Figure 4.2), chlorinated solvent concentrations ranged from 0.9 (in W2) to 2400 μg L^{-1} (in W4).

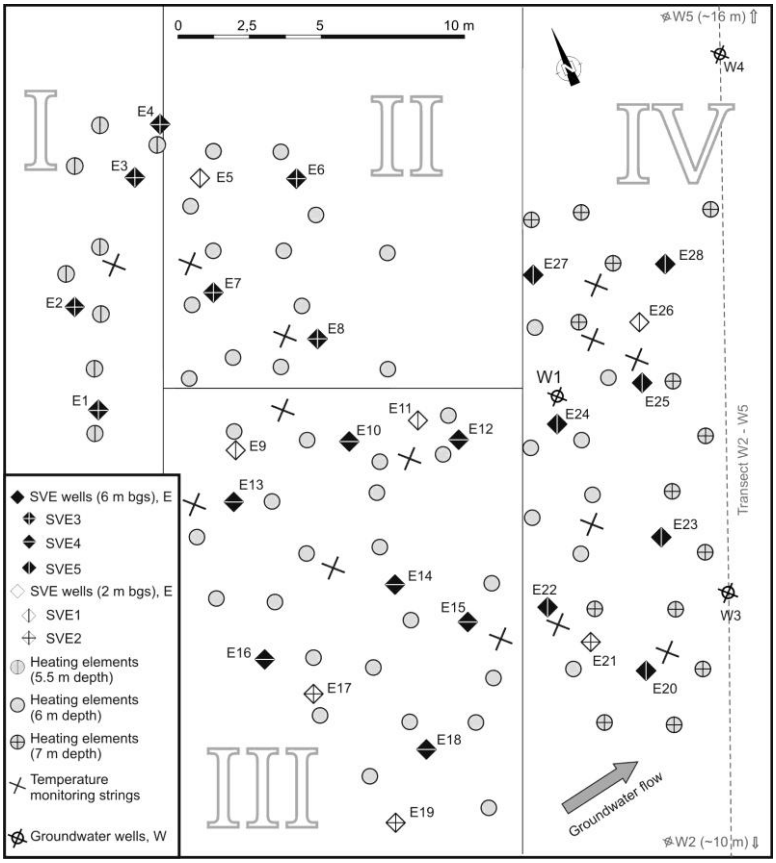

Figure 4.2. Layout of the remediation system, including heating elements, temperature monitoring strings, soil vapor extraction wells, and groundwater monitoring wells (the dashed line indicates the transect between groundwater wells W2 and W5; solid lines represent the test site division into four sections).

The major contaminant in all matrices affected (soil vapor, soil, and groundwater) was PCE (>95% of the chlorinated solvent mass), together with lesser concentrations of TCE and its degradation product dichloroethene. Concentrations of other chlorinated solvents and degradation products were close to or below detection limits (Appendix, Table A-7).

The remediation goal defined by the local environmental agency was to reduce the concentrations in the soil vapor to ≤10 mg m^{-3}. ISTD was applied as a remediation technique only for the unsaturated zone. Contaminated groundwater was captured by a pump-and-treat (P&T) system (in well W1, Figure 4.2) and treated on-site with activated carbon.

4.2.2. Field sampling, analyses, and implementation of *in situ* thermal desorption

Soil samples were collected before remediation from depths between 1.5 and 9 m bgs, which yielded 75 samples from 27 boreholes. Chlorinated solvent concentrations were determined following standard procedures (ÖNORM S 2124, Austrian Standards Institute, 2006). In

brief, ~10-g samples of soil were transferred on-site into precleaned flasks containing 25 mL of methanol for subsequent extraction. After 30 min in an overhead shaker, the headspace samples were analyzed by gas chromatography–mass spectrometry (Agilent Technologies 5973 system). The chlorinated compounds quantified in the soil samples included PCE, TCE, 1,1-dichloroethene, *cis*-1,2-dichloroethene, *trans*-1,2-dichloroethene, vinylchloride, 1,1,1-trichloroethane, 1,1-dichloroethane, 1,2-dichlorethane, tetrachloromethane, trichloromethane, and dichloromethane, later referred to as chlorinated solvents.

We used ordinary kriging to predict the chlorinated solvent concentrations in the soil at unsampled locations and to quantify the uncertainty of the predictions (Goovaerts, 1999). The geostatistical analyses were performed using VESPER software (Minasny et al., 1999). The spatial correlations within the soil sample data were first estimated and modeled using spherical semivariogram analysis. The monitoring data and the spherical semivariogram model were then used to estimate chlorinated solvent concentrations at unsampled locations and to calculate the associated statistical errors.

The design of the ISTD remediation system was based on the total contaminant concentrations in the soil vapor. According to these concentrations, the test site was divided into four sections: Section I with low concentrations, up to 85 mg m^{-3}; Section II with low to intermediate concentrations, up to 900 mg m^{-3}; Section III with intermediate concentrations, up to 1100 mg m^{-3}; and Section IV with high concentrations, up to 5000 mg m^{-3}. The layout of the remediation system, which included heating elements, temperature monitoring strings, vapor extraction wells, and groundwater monitoring wells, is shown in Figure 4.2.

A total of 70 heating elements were installed, operating at depths of 3.5 to 5.5 m bgs in Section I, 3.0 to 6.0 m bgs in Sections II, III, and IV, and 4.0 to 7.0 m bgs in Section IV. Soil temperatures were recorded in 14 temperature-monitoring strings (Figure 4.2), each with temperature sensors set at 1-m intervals.

Soil vapor was extracted from 28 extraction wells. The flows from these wells were combined into five SVE strings according to their locations and extraction depths (Appendix, Table A-8). Chlorinated solvents extracted via SVE strings were monitored up to six times per day during the remediation, using an online gas chromatograph (Meta 3 HE II, Messtechnische Systeme GmbH). Chlorinated solvents from each of the 28 SVE wells were also monitored before soil heating and after 9 months following termination of the ISTD.

The chlorinated solvent mass extracted through each SVE string was determined using the vapor flow rate and the recorded chlorinated solvent concentrations. The extracted vapor was treated on-site with activated carbon, and chlorinated solvent concentrations in the treated effluents were monitored before their release into the atmosphere.

The P&T system installed at the W1 well (Figure 4.2) prevented any eventual groundwater contamination as a result of increased mobilization of chlorinated solvents from the soil during the ISTD. The pumping rate and chlorinated solvent concentrations were recorded and used for mass balance calculations. The extracted groundwater was treated on-site with activated carbon, and chlorinated solvent concentrations were monitored before release into the hydrosphere (i.e., into a nearby creek, not shown in Figure 4.2).

4.2.3. Material flow analysis

Material flow analysis (MFA), as defined by Brunner and Rechberger (2004), applies the law of conservation of mass for the identification and quantification of processes, flows, stocks of materials, and changes in stocks within spatially and temporally defined systems (Hendriks et al., 2000). For details, see Baccini and Brunner (1991). In this study, MFA was used for the first time as a tool for visualizing and evaluating the processes, flows, and stocks of contaminants before and during ISTD, as well as for identifying the intermediate and final sinks of contaminants. The modeling platform used was the STAN software (Cencic and Rechberger, 2008).

System definition

The contaminated test site represented the *system* for the purposes of this study, and its spatial boundary was delineated by the extent of the contamination. The *material* investigated was the mixture of chlorinated solvents and their degradation products, dominated by PCE (>95% of the chlorinated solvent mass). A *process* in MFA is defined as a transport, transformation, or storage of material. The processes at the investigated site included the transport, transformation, and storage of chlorinated solvents within the soil, soil vapor, groundwater, atmosphere, and hydrosphere. *Stocks* in MFA are defined as material reservoirs (masses) within the processes. The stocks in this study were the chlorinated solvent masses within the different processes. Processes are linked by *flows* (mass per time) or *fluxes* (mass per time per unit area) of material (in our case, chlorinated solvents). Flows or fluxes across system boundaries are referred to as *imports* or *exports* (Brunner and Rechberger, 2004).

Material flow analysis was performed in two phases, with Phase 1 covering the period of time from the earliest possible release of the chlorinated solvents to the start of remediation and Phase 2 covering the duration of the remediation.

The temporal system boundary for Phase 1 was taken to be 33 years, which is the time span from the start of operations at the dry-cleaning facility to the start of remediation. For Phase 2, the temporal system boundary was set to 1 year, covering the 9 months duration of the ISTD and a further 3 months required for the soil to cool down to the normal temperature (10–12°C).

Seven relevant processes were identified for Phase 1 (Figure 4.3): the former dry-cleaning facility (1), soil (2), soil vapor (3), groundwater (4), natural attenuation in groundwater (5), the atmosphere (6), and the hydrosphere (7).

These processes are interconnected via six material flows (Figure 4.3): chlorinated solvent emission from the former dry-cleaning facility into the soil (I), chlorinated solvent emission from the soil into soil vapor (II), chlorinated solvent emission from the soil into groundwater (III), chlorinated solvent changes due to natural attenuation in groundwater (IV), chlorinated solvent emission into the hydrosphere (V), and chlorinated solvent emission into the atmosphere (VI).

In Phase 2, eight relevant processes were recognized (Figure 4.5): the former dry-cleaning facility (1), soil (2), soil vapor (3), groundwater (4), natural attenuation in groundwater (5), ISTD and P&T techniques (6), the atmosphere (7), and the hydrosphere (8).

The eight processes were interconnected via 11 flows (Figure 4.5): chlorinated solvent emission from the former dry-cleaning facility into the soil (I), chlorinated solvent emission from the soil into soil vapor (II), chlorinated solvent emission from the soil into groundwater (III), chlorinated solvent changes due to natural attenuation in groundwater (IV), chlorinated solvent emission into the hydrosphere (V), chlorinated solvent emission into the atmosphere (VI), chlorinated solvents extracted via the P&T system (VII), chlorinated solvents extracted via ISTD (VIII), chlorinated solvents captured by activated C (IX), chlorinated solvent emission into the atmosphere following activated C treatment of soil vapor extracted by ISTD (X), and chlorinated solvent emission into the hydrosphere following activated C treatment of groundwater captured by the P&T system (XI).

4.3. Results and discussion

4.3.1. Material flow analysis for phase 1: before remediation

For Phase 1 the material stock in the investigated system was defined as the chlorinated solvent mass stored within the soil (Process 2, Figure 4.3). The export from the system was defined as the combined flows of contaminants from soil vapor and groundwater into the atmosphere and hydrosphere (Fig. 2, Flows V and VI). The initial chlorinated solvent input from the dry-cleaning facility into the system or test site (Fig. 2, Flow I) was back-calculated as the sum of the chlorinated solvent stock in the soil and the total chlorinated solvent exported before the start of remediation.

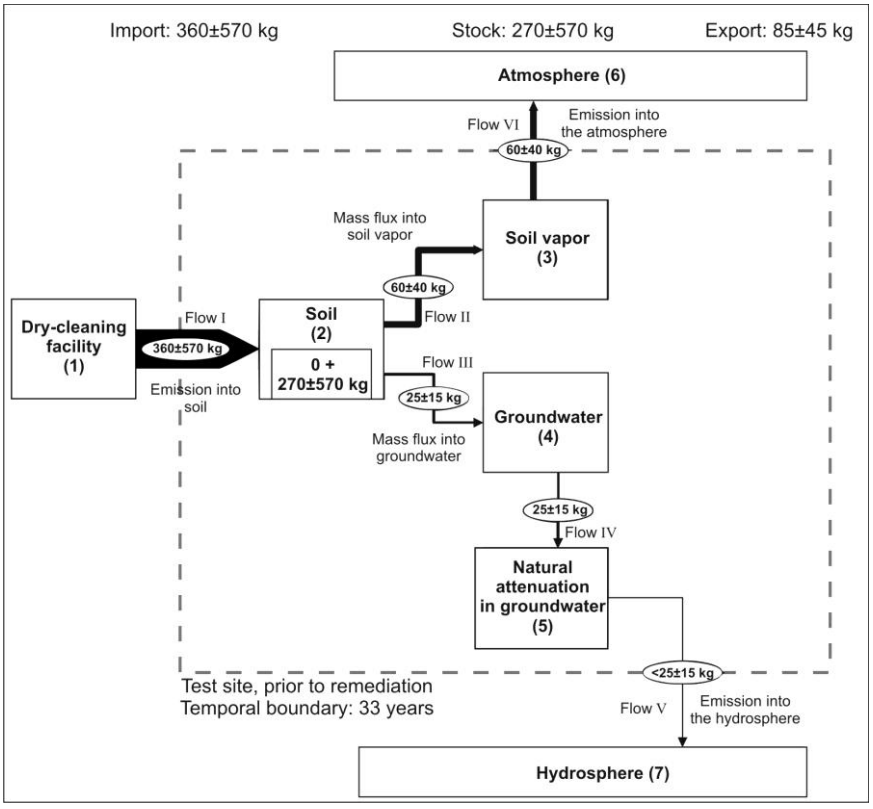

Figure 4.3. Material flow analysis overview for Phase 1, including chlorinated solvent flows, stocks, and processes at the test site for the period prior to remediation (temporal system boundary: 33 years). Processes are depicted as rectangles. Material flows are indicated by arrows.

4.3.1.1. Determination of the chlorinated solvent stock in soil before remediation

The chlorinated solvent stock (mass) in the soil was estimated using the PCE concentrations (>95% of all contaminants) in 75 samples from the soil cores collected before remediation, which ranged from 0.1 to 1979.0 mg kg^{-1}.

The soil was divided into three zones according to the sampling depth: Zone A (1.50–3.25 m bgs), Zone B (3.25–5.00 m bgs), and Zone C (5.00–7.00 m bgs). The concentrations at unsampled locations and their uncertainties were predicted for each zone using ordinary kriging, and then the mean chlorinated solvent concentration and its uncertainty were estimated. The semivariograms, interpolated chlorinated solvent concentrations, and kriging errors for all three zones are shown in the Appendix (figures A-2 to A-9).

The chlorinated solvent mass in each zone was estimated using the mean chlorinated solvent concentration (derived from the measured and predicted values), its uncertainty, the size of the contaminated area (~400 m^2), the thickness of each zone, and the dry soil bulk density (1.80 kg m^{-3}, Table 4.1). The results indicated that the highest chlorinated solvent concentrations were located in Zone B (3.25– 5.00 m bgs), with its peak values falling within Section IV (Figure 4.4).

Table 4.1. Mean chlorinated solvent (CS) concentrations and masses in each zone, together with their uncertainties.

Zone	**Zone thickness** m	**Mean CS concentration and uncertainty** mg kg^{-1}	**Estimated CS mass and uncertainty** Kg
A	1.75	11±14	13±17
B	1.75	168±452	204±548
C	2.00	38±103	53±140

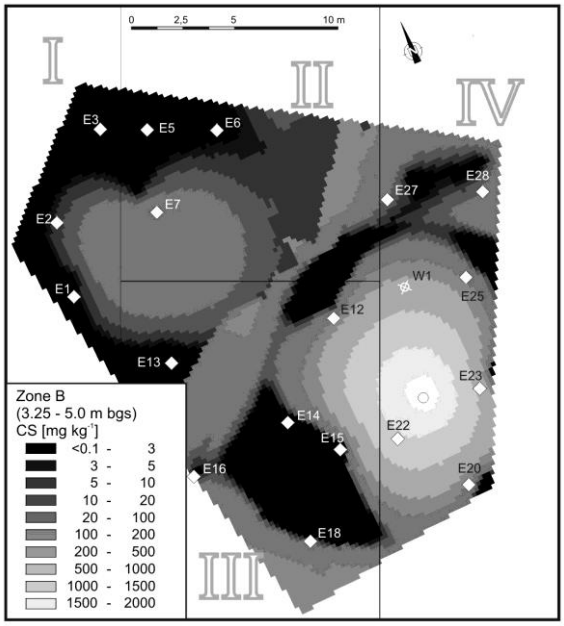

Figure 4.4. Chlorinated solvent (CS) concentrations in Zone B (3.25–5.00 m bgs), based on kriging interpolations.

The total chlorinated solvent mass in the soil, namely the material stock, was calculated as the sum of the masses in all zones, resulting in a total figure of 270 kg ± 570 kg. The high uncertainty is a result of the limited number of soil samples, the steep concentration gradients, and the inhomogeneous contaminant distribution, all of which are commonly observed at contaminated sites (Hofmann et al., 2010; Xie et al., 2011).

4.3.1.2. Assessment of the chlorinated solvent import and export before remediation

The chlorinated solvent flux from soil vapor into the atmosphere (Figure 4.3, Flow VI) was based on the diffusive transport of contaminants. Advective transport due to, for example, barometric pumping as shown by Choi et al. (2002) is not expected to overwhelm the diffusion effects in porous media and therefore was not included in this study.

The chlorinated solvent mass flux (Figure 4.3, Flow VI) was calculated based on a one-dimensional analysis using Fick's first law and the effective diffusion coefficient for the dominating PCE after Millington and Quirk (1961). To account for the most severe contamination, maximum concentrations were applied across the maximum duration of emission (33 years in this study, from the beginning of the dry-cleaning operations until the start of remediation). Parameters, such as the gas diffusion coefficient of PCE, tortuosity, air-filled porosity, chlorinated solvent concentration in the soil vapor, path length, and the size of the contaminated area were varied to account for variations within the subsurface (Appendix Table A-9). The resulting estimates for diffusive vapor flux ranged between 0.6 and 3.0 kg yr^{-1}. During a period of 33 years (the temporal system boundary for Phase 1), the corresponding estimates of contaminant mass emitted to the atmosphere ranged between 20 and 99 kg, with an average of ~60 ± 40 kg (Figure 4.3). The reported uncertainty results from the differences in parameters used for the calculation of the diffusive chlorinated solvent flux, such as the concentration gradient and the size of contaminated area. Because the chlorinated solvents in the soil vapor derived from the soil, the same figure (60 ± 40 kg) was used for the mass emitted from the soil to soil vapor (Figure 4.3, Flow II).

The chlorinated solvent mass flux from the soil via groundwater into the hydrosphere, including natural attenuation in the groundwater (Figure 4.3), was calculated as the sum of the contaminant fluxes in four groundwater wells (W2, W3, W4, and W5) along the W2–W5 transect (Figure 4.2). This involved calculating the contaminant mass flux per well, the average groundwater flux at the test site, the cross-sectional area of the wells, and the average contaminant concentration recorded in the wells (Appendix, Table A-10). The chlorinated sol-

vent concentrations ranged between 0.2 (Well W2) and 2400 μg L^{-1} (Well W4). The chlorinated solvent mass flux across the W2–W5 transect was 2.1 ± 1.3 g d^{-1}. During a period of 33 years, this resulted in ~25 ± 15 kg of chlorinated solvents emitted from the soil to groundwater (Flow III). The uncertainty results from the different aqueous contaminant concentrations at the investigated site (Appendix, Table A-10).

The occurrence of natural attenuation (biodegradation) in groundwater was indicated by a shift in the $\delta^{13}C$ values of PCE and TCE (from samples collected from Wells W3 and W4 to downstream wells outside the test site; data not shown). Natural attenuation was therefore considered to be a relevant process between the groundwater and the hydrosphere (as often observed at industrial sites, e.g., Micić et al., 2007), but because its extent could not be quantified, Flow IV was taken to be equal to Flow III and the chlorinated solvent emission to the hydrosphere (Flow V) was set to <25 ± 15 kg. Natural attenuation in the unsaturated zone was not considered to be a relevant process due to the high PCE concentrations in both the soil and soil vapor, which can be toxic to indigenous bacteria, and the low concentrations of expected degradation products, such as *cis*-dichloroethene and vinylchloride (*cis*-dichloroethene was one to three orders of magnitude less abundant in the soil and soil vapor than in water, while vinylchloride concentrations were below the detection limit in all matrices affected).

The total chlorinated solvent export from the system before remediation was therefore 85 ± 45 kg (the sum of chlorinated solvents emitted from soil vapor and groundwater into the atmosphere and hydrosphere; Figure 4.3, Flows V and VI).

Finally, the back-calculated chlorinated solvent input from the dry-cleaning facility into the system (Figure 4.3, Flow I) was 360 ± 570 kg (the sum of the chlorinated solvent stock and the overall export into the environment), representing the extent of initial contamination.

The results of the MFA for Phase 1 showed that most (~75%) of the chlorinated solvents released into the subsurface by the former dry-cleaning facility remained in the soil, while the remaining ~25% was emitted into the hydrosphere and atmosphere.

4.3.2. Material flow analysis for phase 2: during remediation

For Phase 2, the material stock was defined as the chlorinated solvent mass extracted from the soil and groundwater using ISTD and P&T techniques (Figure 4.5, Flows VII and VIII and Process 6). The export from the system was defined as the chlorinated solvents captured

by activated carbon from soil vapor and groundwater (Flow XI), together with the chlorinated solvents emitted into the atmosphere and hydrosphere directly from the groundwater, including natural attenuation (Flows IV and V) and soil vapor (Flow VI) and the contaminants emitted after the activated carbon treatment of groundwater and soil vapor (Figure 4.5, Flows IX and X). Because direct release of chlorinated solvents into the atmosphere and hydrosphere was prevented (due to the vacuum applied during ISTD and the capture of groundwater by the P&T system), Flows IV, V, and VI were set to zero.

The chlorinated solvent import from the former dry-cleaning facility into the soil was also set to zero because the dry-cleaning facility no longer operated during Phase 2 (Figure 4.5, Flow I).

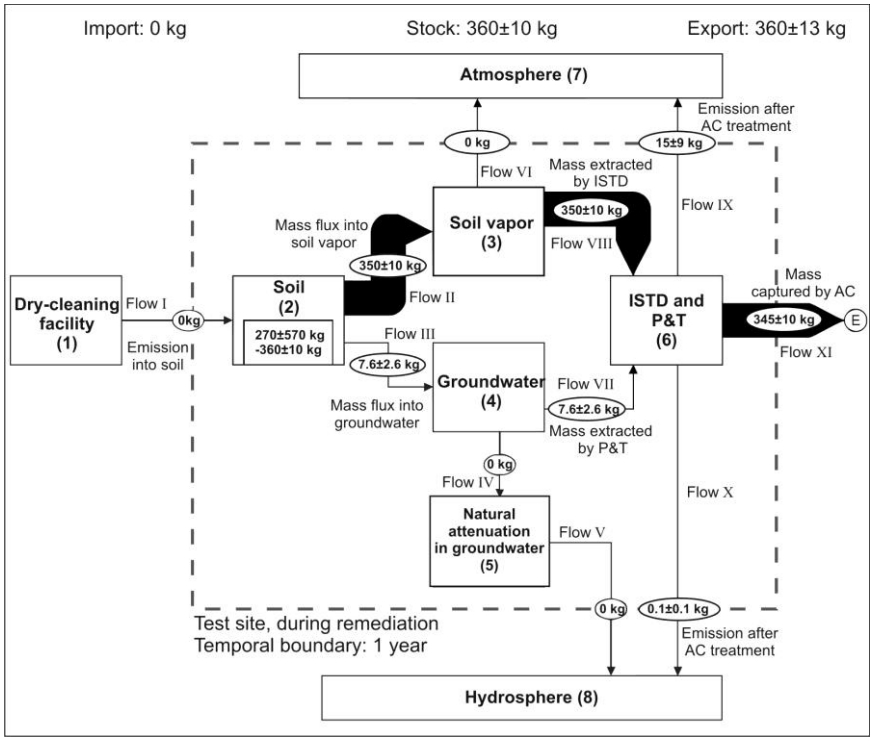

Figure 4.5. Material flow analysis overview for Phase 2, including chlorinated solvent flows, stocks, and processes at the test site for the period of remediation (temporal system boundary: one year). Processes are depicted as rectangles. Material flows are indicated by arrows. AC: activated carbon.

4.3.2.1. Determination of the chlorinated solvent stock during remediation

The chlorinated solvent stock (mass) in the soil was calculated using the chlorinated solvent masses extracted from the soil and groundwater during ISTD and P&T (Figure 4.5, Flows VII and VIII).

The chlorinated solvent mass extracted through ISTD was calculated using the vapor flow rate in the SVE strings and the monitored chlorinated solvent concentrations. The total chlorinated solvent mass flux (the sum of the fluxes from all five SVE strings) reached its maximum of 7 kg d^{-1} after 6 weeks of ISTD. Most of the contaminant mass was extracted by SVE Strings 4 and 5, with the mass flux in the remaining SVE strings being significantly lower (Figure 4.6a). PCE was the most abundant extracted contaminant, comprising up to 95% of the total mass. The remediation target value of 10 mg m^{-3} in soil vapor was reached in all SVE wells after 9 months of ISTD.

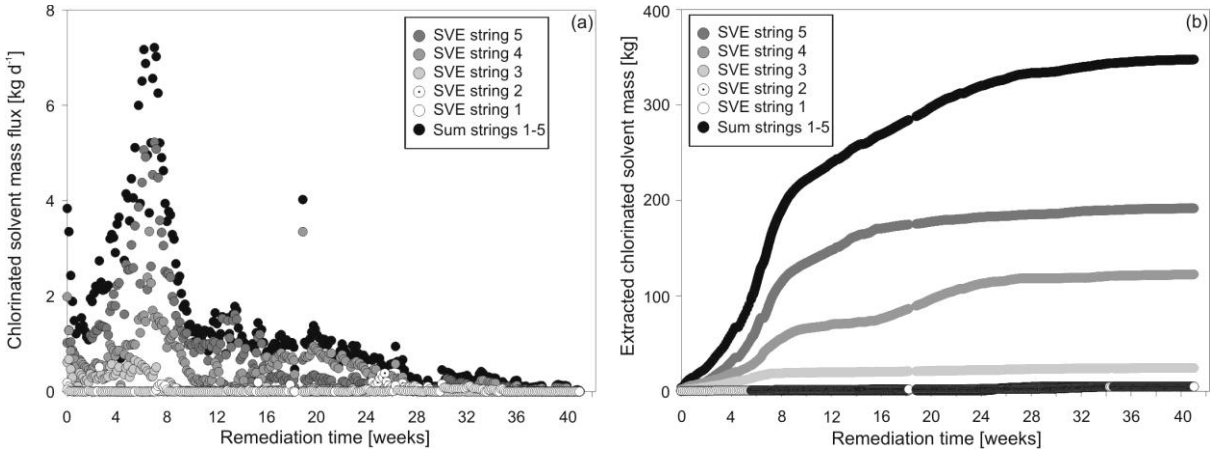

Figure 4.6. (a) Changes in chlorinated solvent mass flux from soil vapor during ISTD; (b) Chlorinated solvent mass extracted in SVE strings during ISTD.

The total chlorinated solvent mass removed from the soil within 1 yr (the temporal boundary for Phase 2) was 350 ± 10 kg (Figure 4.5, Flow VIII). Of this total, 195 kg (56%) was extracted from SVE String 5, 120 kg (35%) from SVE String 4, 25 kg (7%) from SVE String 3, and 5 kg (1%) each from SVE Strings 1 and 2 (Figure 4.6b).

The chlorinated solvent mass extracted through the P&T system (in Well W1, Fig. 1) was determined using the pumping rate and the monitored chlorinated solvent concentrations. The resulting chlorinated solvent mass flux in the groundwater was 20.8 ± 7.1 g d^{-1} (the uncertainty derives from the different aqueous concentrations applied). During a period of 1 year, this resulted in 7.6 ± 2.6 kg of contaminants removed from the groundwater through the P&T system (Figure 4.5, Flow VII). The MFA therefore demonstrated that the majority (98%) of the chlorinated solvents removed from the site was extracted by ISTD, while only 2% was extracted through the P&T system.

The total chlorinated solvent mass extracted from the test site was the sum of the chlorinated solvents extracted by ISTD and P&T, which came to a material stock of ~360 ± 10 kg (Figure 4.5). This calculated stock is similar to the mean chlorinated solvent mass in the soil estimated before the remediation (270 ± 570 kg, Phase 1). Including the uncertainties associated with the mass in the soil (best-case scenario 0 kg and worst-case scenario 840 kg of contaminants in the soil), the recovery of contaminants ranged between 42 and 130%. Taking into account the reasons for the high uncertainty (e.g., steep contaminant concentrations, low sampling density) and the low chlorinated solvent concentrations in soil vapor at the end of the remediation (<10 mg m^{-3}), however, both best- and worst-case scenarios are not realistic at the investigated site. This implies that the high predicted uncertainties in the initial contaminant mass have to be reported and critically evaluated on the basis of the abovementioned obstacles and including the measurable concentrations at the end of the remediation process.

The MFA results for Phases 1 and 2 together with the achievement of the remediation target values in soil vapor therefore implied that the majority of the chlorinated solvents in the soil was successfully extracted.

4.3.2.2. Assessment of the chlorinated solvent export during remediation

The chlorinated solvent emission into the atmosphere during remediation, calculated from the chlorinated solvent concentrations in the soil vapor after the activated carbon treatment and the vapor release rate, was 15 ± 9 kg (Figure 4.5, Flow IX; the uncertainty derives from the different concentrations used for the soil vapor). The total emission of chlorinated solvents from the groundwater into the hydrosphere during Phase 2 was calculated from the chlorinated solvent concentrations in the groundwater (extracted via the P&T system and passed through activated carbon) and the pumping rate, resulting in a significantly lower value of 0.1 ± 0.1 kg (Figure 4.5, Flow X; the uncertainty derives from the different aqueous concentrations applied).

To determine the chlorinated solvent mass captured by the activated carbon, the overall chlorinated solvent mass extracted through ISTD and the P&T system (360 ± 10 kg) was corrected for the chlorinated solvent masses emitted into the atmosphere and hydrosphere (15.1 ± 9.1 kg, this being the sum of Flows IX and X), resulting in a figure of ~345 ± 10 kg.

Finally, the chlorinated solvent exported from the system was calculated as the sum of chlorinated solvents released into the atmosphere and hydrosphere (Flow V = Flow VI = 0 and

Flow IX + Flow X = 15.1 ± 9.1 kg) and the amount captured by the activated carbon (345 ± 10 kg), making a total of 360 ± 13 kg (Figure 4.5).

The MFA results showed that >95% of the chlorinated solvents removed through ISTD and the P&T system was captured by activated Carbon, while only 5% (15.1 ± 9.1 kg) was released into the environment. This demonstrates that even though the ISTD enhanced the contaminant diffusion from the soil, there was only negligible contaminant emission into the environment.

4.4. Conclusions

In situ thermal desorption is a remediation technique that increases the effectiveness of SVE (Heron et al., 1998; Triplett Kingston et al., 2010). In this study, material flow analysis was used for the first time to assess the effectiveness of ISTD for the remediation of soils contaminated with chlorinated solvents and to reveal the total emission of chlorinated solvents into the environment, both before and during remediation.

Material flow analysis was performed for the period before remediation (Phase 1: 33 years) and for the period covering the remediation time and subsequent soil cooling (Phase 2: 1 year). The MFA for Phase 1 showed that an estimated 360 ± 570 kg of chlorinated solvents (predominantly PCE) was released into the soil by the former dry-cleaning facility. The majority of contaminants was captured in the soil (270 ± 570 kg), while 85 ± 45 kg was emitted into the atmosphere and hydrosphere. The high values of relative uncertainty reported are common at contaminated sites for which the sampling density is low in relation to the complex distribution of contaminants (Hofmann et al., 2010). Because an extended sampling program is often not feasible in applied studies of this nature, these uncertainties have to be reported and critically evaluated in the assessment of the remediation process. Although such high uncertainties could be minimized by increasing the sampling density, particularly in those areas with peak contaminant concentrations, this is not possible in most cases due to budgetary limitations.

The mass removed during ISTD, as shown in the MFA, was similar to the mean chlorinated solvent mass estimated by ordinary kriging to have been in the soil initially. Furthermore, only a negligible amount of contaminants was released into the environment as a consequence of the remediation action. The MFA results have therefore shown that the ISTD technique was effective in removing the majority of chlorinated solvents from the soils at this test site,

which was supported by the low soil vapor concentrations by the end of the remediation. The target concentration in the soil vapor (<10 mg m^{-3}) was reached after 9 months of remediation, indicating the time efficiency of this remediation approach.

Our study has shown that MFA is a suitable tool for assessing the effectiveness of a remediation practice by connecting and quantifying the sources, the pathways, and the intermediate and final sinks of the contaminants. The principle of MFA should be applied on a routine basis, providing stakeholders with an overview of the processes and contaminant transformations in soil, water, and air phases during the course of remediation. By accounting for the effects that the remediation activities have on all affected environmental matrices (soil, water, and air), MFA enables decision-makers to evaluate not only the effectiveness of remediation but also its broader environmental impacts. Furthermore, by providing information on total contaminant emissions into the environment during the course of remediation, MFA offers an additional step forward toward achieving the best environmental management practices.

Acknowledgments

We would like to acknowledge Dr. U. Hiester (reconsite- TTI GmbH) for performing the *in situ* thermal desorption, DI G. Schobert for providing the field data, and the Austrian Federal Ministry of Agriculture, Forestry, Environment and Water Management, Keglovits GesmbH, and Kommunalkredit Public Consulting GmbH for providing financial support.

5. Summary and Outlook

Sustainable and effective remediation techniques are needed in order to clean up contaminated land in a cost effective manner and to improve environmental quality. This thesis focused on two selected innovative *in situ* techniques for groundwater and soil contamination: nanoremediation and thermal desorption.

Nanoremediation and in particular the application of nanoscale zero-valent iron (nZVI) has received increasing attention as an efficient *in situ* groundwater remediation technique. However, nanoremediation has not achieved widespread market and regulatory acceptance due to obstacles associated with its performance. The effectiveness of nanoremediation depends to a great extent on the emplacement of nZVI within the contaminated zone, which is limited by the mobility of nZVI in the subsurface. Improved understanding of nZVI mobility in the subsurface under various hydrochemical and hydrogeological conditions is therefore essential for the successful application of nanoremediation.

Surface charge heterogeneities encountered in aquifers induced by, for example, mineralogical variations within the aquifer grains are known to significantly affect the transport and deposition of particles in porous media (Ryan and Elimelech, 1996). Nevertheless, their influence on the nZVI transport has rarely been investigated to date. In particluar carbonate minerals as model porous media have not been employed in any previous study, even though these materials often prevail in aquifers.

Systematic investigations presented in this PhD thesis demonstrated that carbonate minerals in aquifers have a strong effect on the transport of polyacrylic acid coated nZVI (PAA-nZVI). Even a low proportion of carbonate minerals (10%) in the subsurface significantly increased the deposition of PAA-nZVI onto the aquifer grains. The favorable deposition of PAA-nZVI particles onto carbonate rather than quartz sand was attributed to the lower negative surface charge of carbonate sand. High dissolved calcium concentrations, which can be expected in carbonate-rich aquifers, are additionally limiting the PAA-nZVI transport due to increased particle aggregation and deposition onto the aquifer grains.

Transport modeling performed in this thesis revealed that the attachment efficiency and deposition rate coefficient increased linearly as the proportion of carbonate sand in the porous media increased. The maximum predicted travel distances for PAA-nZVI in pure carbonate sand

was not more than 0.3 m, which in practice reduces the chances that the nZVI particles are deliverable to the contaminated source zone in carbonate-rich aquifers.

It is therefore necessary to improve nZVI mobility in carbonate-containing porous media and in the presence of high calcium concentrations. One strategy to increase the nZVI mobility in heterogeneous porous media is the modification of the aquifer grains by means of a polyelectrolyte coating. In this thesis four different polyelectrolytes were used for this purpose: natural organic matter, humic acid, carboxymethyl cellulose, and lignin sulfonate.

The results of this PhD thesis have revealed that co-injection of the chosen polyelectrolytes can increase PAA-nZVI transport in carbonate sand. The degree of enhancement was similar for all of the polyelectrolytes investigated, when applied in the same concentrations. Lignin sulfonate was identified as the most suitable polyelectrolyte for field applications due to its availability in large quantities and its lower market price. The greatest increase in PAA-nZVI mobility was achieved with co-injected lignin sulfonate concentrations of 50 mg L^{-1} or more. The maximum predicted travel distance for PAA-nZVI in carbonate sand was almost doubled when co-injected with lignin sulfonate. Furthermore, the results of this thesis showed that in the presence of high dissolved calcium concentrations (up to 5 mM) co-injection of lignin sulfonate reduces PAA-nZVI deposition in both quartz and carbonate sands.

The small-scale column experiments and well-controlled experimental conditions applied in this PhD thesis have therefore served to elucidate the interactions between (1) the PAA-nZVI particles and the aquifer matrix (quartz sand, carbonate sand, and mixtures of both), (2) the co-injected polyelectrolytes and the aquifer matrix (quartz and carbonate sand), and (3) the co-injected polyelectrolytes and the PAA-nZVI particles. The applied conditions additionally served to assess the effect that these different interactions have on the PAA-nZVI transport.

Up-scaling the results presented in this PhD thesis to predict outcomes in a field system is complicated and associated with high uncertainties. Further research on large-scale settings is therefore required, together with field investigations, to test the applicability of the results presented in this PhD thesis to natural systems. In general, a detailed assessment of the transport and fate of nZVI *in situ* is necessary to assess the performance of the nZVI-based remediation technique. To achieve this, future research has to focus on analytical methods to detect and characterize nZVI particles under subsurface conditions. Johnson et al. (2013) developed a spectrophotometric method to directly quantify the extent of nZVI transport on-site. In combination with a tracer test this approach allows to measure nZVI transport and

changes in groundwater flow during injection (Johnson et al., 2013). Other techniques could be based on nZVI properties (e.g., magnetic susceptibility measurement, Buchau et al., 2010) or changes in dissolved oxygen concentrations, redox potential, and solution pH (Elliott and Zhang, 2001; He et al., 2010; Zhang, 2003).

The nZVI particles investigated in this thesis (commercially available, polyacrylic acid coated nZVI, NANOFER 25S, NANOIRON, s.r.o., Czech Republic) are not stable; in the PAA-nZVI suspension a predominance of large aggregates (~1 µm) was observed. This showed that the surface modification by polyacrylic acid could not prevent extensive nZVI aggregation. Particle aggregation is, however, a major factor limiting nZVI transport. Future work is therefore needed to optimize particle properties with respect to their stability. It should be noted that the costs associated with nZVI synthesis are still relatively high. Ongoing research should therefore consider cost-effective production methods in order to achieve widespread market acceptance of this remediation technique.

An additional critical aspect, especially regarding the regulatory acceptance of the nZVI application for *in situ* groundwater remediation, is the ecotoxicological impact that the nZVI particles, their coatings and the co-injected polyelectrolytes may have on indigenous organisms in aquifers. Kirschling et al. (2010) demonstrated that nZVI does not decrease the microbial abundance in an aquifer and that a polyelectrolyte coating (i.e., polyaspartate) can even stimulate microbial growth. The introduced polyelectrolytes (co-injected or as a particle coating) might therefore enhance the remediation by combining nZVI treatment with bioremediation. However, more such research is needed, especially at a field site, in order to test for any potential negative impact of nZVI particles and simultaneously introduced polyelectrolytes.

***In situ* thermal desorption (ISTD)** has already been applied at several sites contaminated by chlorinated solvents. A detailed assessment of an *in situ* thermal remediation practice is, however, still lacking. In this PhD thesis material flow analysis (MFA), a method based on the law of conservation of mass, has for the first time been used to assess the effectiveness of ISTD treatment of a soil contaminated by chlorinated solvents.

The MFA performed in this PhD thesis enabled quantification of contaminant flows before and during the remediation in all environmental matrices affected (soil vapor, soil, and groundwater). The detailed assessment revealed that the chlorinated solvent mass removed

during the remediation was similar to the amount estimated to have been in the soil before remediation. On the basis of these results the ISTD in soil was judged to have performed effectively at the particular site. This was supported by the achievement of the remediation target value in soil vapor after nine months of remediation, with negligible contaminant release into environment during remediation.

The results presented in this PhD thesis furthermore demonstrated the suitability of MFA as a tool for assessment of effectiveness of a remediation practices. The principle of MFA could be applied on a routine basis, since it allows evaluation of the remediation effectiveness, and also provides an overview of the processes and contaminant transformations occurring in soil-water-air compartments during the course of remediation. In addition, MFA enables assessment of the total emission of chlorinated solvents into the environment, both prior to and during remediation.

Further work on the applicability of MFA for other contaminated sites and innovative remediation techniques is necessary to establish MFA as an assessment tool for remediation practices.

Remediation of emerging contaminants and complex chemical mixtures is challenging and expensive. In order to address these challenges it is necessary to optimize currently available remediation techniques and to continuously develop new clean up strategies. The comprehensive assessment of a remediation performance is one important step in the further development and optimization of sustainable and effective remediation techniques. This assessment should consider all environmental effects of the remediation action in order to achieve the best environmental management practices.

6. References

Austrian Standards Institute, 2006. ÖNORM S 2124: Determination of BTEX/HVHC in solid matter samples after solvent extraction. Vienna, Austria.

Baccini, P., Brunner, P.H., 1991. Metabolism of the anthroposphere. Springer Verlag, Berlin, Germany.

Bai, B., Wu, Y., Grigg, R.B., 2009. Adsorption and Desorption Kinetics and Equilibrium of Calcium Lignosulfonate on Dolomite Porous Media. The Journal of Physical Chemistry C 113, 13772-13779.

Bleyl, S., Kopinke, F.-D., Mackenzie, K., 2012. Carbo-Iron®—Synthesis and stabilization of Fe(0)-doped colloidal activated carbon for in situ groundwater treatment. Chemical Engineering Journal 191, 588-595.

Bradford, S.A., Yates, S.R., Bettahar, M., Simunek, J., 2002. Physical factors affecting the transport and fate of colloids in saturated porous media. Water Resources Research 38, 1327.

Brunner, P.H., Rechberger, H., 2004. Practical handbook of material flow analysis. CRC Press, Boca Raton, FL, USA.

Brusseau, M.L., 1991. Transport of Organic Chemicals by Gas Advection in Structured or Heterogeneous Porous Media: Development of a Model and Application to Column Experiments. Water Resources Research 27, 3189-3199.

Brusseau, M.L., Rohay, V., Truex, M.J., 2010. Analysis of Soil Vapor Extraction Data to Evaluate Mass-Transfer Constraints and Estimate Source-Zone Mass Flux. Ground Water Monitoring & Remediation 30, 57-64.

Brusseau, M.L., Carroll, K.C., Truex, M.J., Becker, D.J., 2013. Characterization and Remediation of Chlorinated Volatile Organic Contaminants in the Vadose Zone. Vadose Zone Journal.

Buchau, A., Rucker, W.M., De Boer, C.V., Klaas, N., 2010. Inductive detection and concentration measurement of nano sized zero valent iron in the subsurface. IET Science, Measurement and Technology 4, 289-297.

Cantrell, K.J., Kaplan, D.I., Wietsma, T.W., 1995. Zero-valent iron for the in situ remediation of selected metals in groundwater. Journal of Hazardous Materials 42, 201-212.

Cencic, O., Rechberger, H., 2008. Material flow analysis with software STAN. Journal of Environmental Engineering and Management 18, 440-447.

Chen, J.Y., Ko, C.-H., Bhattacharjee, S., Elimelech, M., 2001. Role of spatial distribution of porous medium surface charge heterogeneity in colloid transport. Colloids and Surfaces A: Physicochemical and Engineering Aspects 191, 3-15.

Chen, K.L., Mylon, S.E., Elimelech, M., 2006. Aggregation Kinetics of Alginate-Coated Hematite Nanoparticles in Monovalent and Divalent Electrolytes. Environmental Science & Technology 40, 1516-1523.

Chen, Y., Crittenden, J.C., Hackney, S., Sutter, L., Hand, D.W., 2005. Preparation of a Novel TiO2-Based p−n Junction Nanotube Photocatalyst. Environmental Science & Technology 39, 1201-1208.

Choi, J.-W., Tillman, F.D., Smith, J.A., 2002. Relative Importance of Gas-Phase Diffusive and Advective Trichloroethene (TCE) Fluxes in the Unsaturated Zone under Natural Conditions. Environmental Science & Technology 36, 3157-3164.

Christian, P., Von der Kammer, F., Baalousha, M., Hofmann, T., 2008. Nanoparticles: structure, properties, preparation and behaviour in environmental media. Ecotoxicology 17, 326-343.

Chuang, F.-W., Larson, R.A., Wessman, M.S., 1995. Zero-Valent Iron-Promoted Dechlorination of Polychlorinated Biphenyls. Environmental Science & Technology 29, 2460-2463.

Comba, S., Sethi, R., 2009. Stabilization of highly concentrated suspensions of iron nanoparticles using shear-thinning gels of xanthan gum. Water Research 43, 3717-3726.

Crane, R.A., Scott, T.B., 2012. Nanoscale zero-valent iron: Future prospects for an emerging water treatment technology. Journal of Hazardous Materials 211–212, 112-125.

Cundy, A.B., Hopkinson, L., Whitby, R.L.D., 2008. Use of iron-based technologies in contaminated land and groundwater remediation: A review. Science of The Total Environment 400, 42-51.

Domingos, R.F., Baalousha, M.A., Ju-Nam, Y., Reid, M.M., Tufenkji, N., Lead, J.R., Leppard, G.G., Wilkinson, K.J., 2009. Characterizing Manufactured Nanoparticles in the Environment: Multimethod Determination of Particle Sizes. Environmental Science & Technology 43, 7277-7284.

Dong, H., Lo, I.M.C., 2013. Influence of calcium ions on the colloidal stability of surface-modified nano zero-valent iron in the absence or presence of humic acid. Water Research 47, 2489-2496.

Elimelech, M., O'Melia, C.R., 1990. Kinetics of deposition of colloidal particles in porous media. Environmental Science & Technology 24, 1528-1536.

Elimelech, M., Gregory, J., Jia, X., Williams, R.A., 1995. Particle Deposition and Aggregation: Measurement, Modeling and Simulation. Butterworth-Heinemann, Oxford, UK.

Elimelech, M., Nagai, M., Ko, C.-H., Ryan, J.N., 2000. Relative Insignificance of Mineral Grain Zeta Potential to Colloid Transport in Geochemically Heterogeneous Porous Media. Environmental Science & Technology 34, 2143-2148.

Elliott, D.W., Zhang, W.X., 2001. Field assessment of nanoscale bimetallic particles for groundwater treatment. Environmental Science & Technology 35, 4922-4926.

Elliott, D.W., Lien, H.L., Zhang, W.X., 2009. Degradation of lindane by zero-valent iron nanoparticles. Journal of Environmental Engineering 135, 317-324.

European Environment Agency, EEA, 2007. Progress in management of contaminated sites. Report CSI 015, Copenhagen, Denmark.

Fairbrother, F., Mastin, H., 1924. CCCXII.-Studies in electro-endosmosis. Part I. Journal of the Chemical Society, Transactions 125, 2319-2330.

Flynn, R.M., Yang, X., Hofmann, T., von der Kammer, F., 2012. Bovine Serum Albumin Adsorption to Iron-Oxide Coated Sands Can Change Microsphere Deposition Mechanisms. Environmental Science & Technology 46, 2583-2591.

Geffroy, C., Foissy, A., Persello, J., Cabane, B., 1999. Surface Complexation of Calcite by Carboxylates in Water. Journal of Colloid and Interface Science 211, 45-53.

Geological Survey of Austria, 1994. Systematische Untersuchung von Rohstoffvorkommen zur Optimierung der Wertschöpfung, Vienna, Austria.

Georgi, A., Gonzalez-Olmos, R., Köhler, R., Kopinke, F.D., 2010. Fe-zeolites as catalysts for wet peroxide oxidation of organic groundwater contaminants: Mechanistic studies and applicability tests. Separation Science and Technology 45, 1579-1586.

Gillham, R.W., O'Hannesin, S.F., 1994. Enhanced Degradation of Halogenated Aliphatics by Zero-Valent Iron. Ground Water 32, 958-967.

Gonzalez-Olmos, R., Kopinke, F.-D., Mackenzie, K., Georgi, A., 2013. Hydrophobic Fe-Zeolites for Removal of MTBE from Water by Combination of Adsorption and Oxidation. Environmental Science & Technology 47, 2353-2360.

Goovaerts, P., 1999. Geostatistics in soil science: state-of-the-art and perspectives. Geoderma 89, 1-45.

Grieger, K.D., Fjordbøge, A., Hartmann, N.B., Eriksson, E., Bjerg, P.L., Baun, A., 2010. Environmental benefits and risks of zero-valent iron nanoparticles (nZVI) for in situ remediation: Risk mitigation or trade-off? Journal of Contaminant Hydrology 118, 165-183.

Grigg, R.B., Bai, B., 2004. Calcium lignosulfonate adsorption and desorption on Berea sandstone. Journal of Colloid and Interface Science 279, 36-45.

Gu, B., Liang, L., Dickey, M.J., Yin, X., Dai, S., 1998. Reductive Precipitation of Uranium(VI) by Zero-Valent Iron. Environmental Science & Technology 32, 3366-3373.

He, F., Zhao, D., 2007. Manipulating the Size and Dispersibility of Zerovalent Iron Nanoparticles by Use of Carboxymethyl Cellulose Stabilizers. Environmental Science & Technology 41, 6216-6221.

He, F., Zhang, M., Qian, T., Zhao, D., 2009. Transport of carboxymethyl cellulose stabilized iron nanoparticles in porous media: Column experiments and modeling. Journal of Colloid and Interface Science 334, 96-102.

He, F., Zhao, D., Paul, C., 2010. Field assessment of carboxymethyl cellulose stabilized iron nanoparticles for in situ destruction of chlorinated solvents in source zones. Water Research 44, 2360-2370.

Heberling, F., Trainor, T.P., Lützenkirchen, J., Eng, P., Denecke, M.A., Bosbach, D., 2011. Structure and reactivity of the calcite–water interface. Journal of Colloid and Interface Science 354, 843-857.

Hendriks, C., Obernosterer, R., Müller, D., Kytzia, S., Baccini, P., Brunner, P.H., 2000. Material Flow Analysis: A tool to support environmental policy decision making. Case-studies on the city of Vienna and the Swiss lowlands. Local Environment 5, 311-328.

Heron, G., Van Zutphen, M., Christensen, T.H., Enfield, C.G., 1998. Soil Heating for Enhanced Remediation of Chlorinated Solvents: A Laboratory Study on Resistive Heating and Vapor Extraction in a Silty, Low-Permeable Soil Contaminated with Trichloroethylene. Environmental Science & Technology 32, 1474-1481.

Heron, G., Carroll, S., Nielsen, S.G., 2005. Full-Scale Removal of DNAPL Constituents Using Steam-Enhanced Extraction and Electrical Resistance Heating. Ground Water Monitoring & Remediation 25, 92-107.

Heron, G., Parker, K., Galligan, J., Holmes, T.C., 2009. Thermal Treatment of Eight CVOC Source Zones to Near Nondetect Concentrations. Ground Water Monitoring & Remediation 29, 56-65.

Hofmann, T., von der Kammer, F., 2009. Estimating the relevance of engineered carbonaceous nanoparticle facilitated transport of hydrophobic organic contaminants in porous media. Environmental Pollution 157, 1117-1126.

Hofmann, T., Darsow, A., Schafmeister, M.-T., 2010. Importance of the nugget effect in variography on modeling zinc leaching from a contaminated site using simulated annealing. Journal of Hydrology 389, 78-89.

Hunter, R.J., 1988. Zeta Potential in Colloid Science. Principles and Applications. Academic Press, London, UK.

Johnson, P.R., Sun, N., Elimelech, M., 1996. Colloid Transport in Geochemically Heterogeneous Porous Media: Modeling and Measurements. Environmental Science & Technology 30, 3284-3293.

Johnson, P.R., 1999. A Comparison of Streaming and Microelectrophoresis Methods for Obtaining the ζ Potential of Granular Porous Media Surfaces. Journal of Colloid and Interface Science 209, 264-267.

Johnson, R.L., Johnson, G.O.B., Nurmi, J.T., Tratnyek, P.G., 2009. Natural Organic Matter Enhanced Mobility of Nano Zerovalent Iron. Environmental Science & Technology 43, 5455-5460.

Johnson, R.L., Nurmi, J.T., O'Brien Johnson, G.S., Fan, D., O'Brien Johnson, R.L., Shi, Z., Salter-Blanc, A.J., Tratnyek, P.G., Lowry, G.V., 2013. Field-Scale Transport and Transformation of Carboxymethylcellulose-Stabilized Nano Zero-Valent Iron. Environmental Science & Technology 47, 1573-1580.

Johnson, W.P., Logan, B.E., 1996. Enhanced transport of bacteria in porous media by sediment-phase and aqueous-phase natural organic matter. Water Research 30, 923-931.

Jones, E.H., Su, C., 2012. Fate and transport of elemental copper (Cu0) nanoparticles through saturated porous media in the presence of organic materials. Water Research 46, 2445-2456.

Joo, S.H., Zhao, D., 2008. Destruction of lindane and atrazine using stabilized iron nanoparticles under aerobic and anaerobic conditions: Effects of catalyst and stabilizer. Chemosphere 70, 418-425.

Kadar, E., Tarran, G.A., Jha, A.N., Al-Subiai, S.N., 2011. Stabilization of Engineered Zero-Valent Nanoiron with Na-Acrylic Copolymer Enhances Spermiotoxicity. Environmental Science & Technology 45, 3245-3251.

Kanel, S.R., Manning, B., Charlet, L., Choi, H., 2005. Removal of Arsenic(III) from Groundwater by Nanoscale Zero-Valent Iron. Environmental Science & Technology 39, 1291-1298.

Karn, B., Kuiken, T., Otto, M., 2009. Nanotechnology and in situ remediation: A review of the benefits and potential risks. Environmental Health Perspectives 117, 1823-1831.

Khan, F.I., Husain, T., Hejazi, R., 2004. An overview and analysis of site remediation technologies. Journal of Environmental Management 71, 95-122.

Kielenniva, N., Antikainen, R., Sorvari, J., 2012. Measuring eco-efficiency of contaminated soil management at the regional level. Journal of Environmental Management 109, 179-188.

Kim, H.-J., Phenrat, T., Tilton, R.D., Lowry, G.V., 2009. Fe0 Nanoparticles Remain Mobile in Porous Media after Aging Due to Slow Desorption of Polymeric Surface Modifiers. Environmental Science & Technology 43, 3824-3830.

Kim, H.-J., Phenrat, T., Tilton, R.D., Lowry, G.V., 2012. Effect of kaolinite, silica fines and pH on transport of polymer-modified zero valent iron nano-particles in heterogeneous porous media. Journal of Colloid and Interface Science 370, 1-10.

Kirschling, T.L., Gregory, K.B., Minkley, J.E.G., Lowry, G.V., Tilton, R.D., 2010. Impact of Nanoscale Zero Valent Iron on Geochemistry and Microbial Populations in Trichloroethylene Contaminated Aquifer Materials. Environmental Science & Technology 44, 3474-3480.

Klinglmair, M., Fellner, J., 2010. Urban Mining in Times of Raw Material Shortage. Journal of Industrial Ecology 14, 666-679.

Kretzschmar, R., Robarge, W.P., Amoozegar, A., 1995. Influence of Natural Organic Matter on Colloid Transport Through Saprolite. Water Resources Research 31, 435-445.

Kretzschmar, R., Sticher, H., 1997. Transport of Humic-Coated Iron Oxide Colloids in a Sandy Soil: Influence of Ca2+ and Trace Metals. Environmental Science & Technology 31, 3497-3504.

Kretzschmar, R., Sticher, H., 1998. Colloid transport in natural porous media: influence of surface chemistry and flow velocity. Physics and Chemistry of The Earth 23, 133-139.

Kretzschmar, R., Borkovec, M., Grolimund, D., Elimelech, M., 1999. Mobile Subsurface Colloids and Their Role in Contaminant Transport. Advances in Agronomy Volume 66, 121-193.

Kueper, B.H., Wealthall, G.P., Smith, J.W.N., Leharne, S.A., Lerner, D.N., 2003. An illustrated handbook of DNAPL transport and fate in the subsurface. UK Environment Agency R&D Publication 133, Bristol, UK.

Kunkel, A.M., Seibert, J.J., Elliott, L.J., Kelley, R., Katz, L.E., Pope, G.A., 2006. Remediation of Elemental Mercury Using in Situ Thermal Desorption (ISTD). Environmental Science & Technology 40, 2384-2389.

LaChance, J., Heron, G., Baker, R.S., 2006. Verification of an improved approach for implementing in-situ thermal desorption for the remediation of chlorinated solvents. In: Remediation of chlorinated and recalcitrant compounds: Proceedings of the 5th International Conference, Monterey, CA. 22–25 May 2006. Batelle Press, Columbus, USA.

Laumann, S., Micić, V., Lowry, G.V., Hofmann, T., 2013. Carbonate minerals in porous media decrease mobility of polyacrylic acid modified zero-valent iron nanoparticles used for groundwater remediation. Environmental Pollution 179, 53-60.

Lemming, G., Nielsen, S.G., Weber, K., Heron, G., Baker, R.S., Falkenberg, J.A., Terkelsen, M., Jensen, C.B., Bjerg, P.L., 2013. Optimizing the Environmental Performance of In Situ Thermal Remediation Technologies Using Life Cycle Assessment. Groundwater Monitoring & Remediation 33, 38-51.

Lenhart, J.J., Saiers, J.E., 2003. Adsorption of Natural Organic Matter to Air−Water Interfaces during Transport through Unsaturated Porous Media. Environmental Science & Technology 38, 120-126.

Li, X.Q., Elliott, D.W., Zhang, W.X., 2006. Zero-valent iron nanoparticles for abatement of environmental pollutants: Materials and engineering aspects. Critical Reviews in Solid State and Materials Sciences 31, 111-122.

Liu, J., Legros, S., von der Kammer, F., Hofmann, T., 2013. Natural Organic Matter Concentration and Hydrochemistry Influence Aggregation Kinetics of Functionalized Engineered Nanoparticles. Environmental Science & Technology 47, 4113-4120.

Liu, Y., Majetich, S.A., Tilton, R.D., Sholl, D.S., Lowry, G.V., 2005. TCE Dechlorination Rates, Pathways, and Efficiency of Nanoscale Iron Particles with Different Properties. Environmental Science & Technology 39, 1338-1345.

Liu, Y., Lowry, G.V., 2006. Effect of Particle Age (Fe0 Content) and Solution pH On NZVI Reactivity: H2 Evolution and TCE Dechlorination. Environmental Science & Technology 40, 6085-6090.

Liu, Y., Phenrat, T., Lowry, G.V., 2007. Effect of TCE Concentration and Dissolved Groundwater Solutes on NZVI-Promoted TCE Dechlorination and H2 Evolution. Environmental Science & Technology 41, 7881-7887.

Lowry, G.V., Johnson, K.M., 2004. Congener-Specific Dechlorination of Dissolved PCBs by Microscale and Nanoscale Zerovalent Iron in a Water/Methanol Solution. Environmental Science & Technology 38, 5208-5216.

Lowry, G.V., 2007. Nanomaterials for Groundwater Remediation. In: Environmental Nanotechnology – Applications and Impacts of Nanomaterials, Wiesner M.R., Bottero, J.-Y., Mc Graw Hill, New York, USA.

Mackay, D.M., Freyberg, D.L., Roberts, P.V., Cherry, J.A., 1986. A natural gradient experiment on solute transport in a sand aquifer: 1. Approach and overview of plume movement. Water Resources Research 22, 2017-2029.

Mackay, D.M., Cherry, J.A., 1989. Groundwater contamination: pump-and-treat remediation. Environmental Science & Technology 23, 630-636.

Mackenzie, K., Bleyl, S., Georgi, A., Kopinke, F.-D., 2012. Carbo-Iron – An Fe/AC composite – As alternative to nano-iron for groundwater treatment. Water Research 46, 3817-3826.

Massmann, J., Shock, S., Johannesen, L., 2000. Uncertainties in cleanup times for soil vapor extraction. Water Resources Research 36, 679-692.

Mibus, J., Sachs, S., Pfingsten, W., Nebelung, C., Bernhard, G., 2007. Migration of uranium(IV)/(VI) in the presence of humic acids in quartz sand: A laboratory column study. Journal of Contaminant Hydrology 89, 199-217.

Micić, V.,Straub, K., Blum, P., Kappler, A., 2007. Natural attenuation of naphthalene and benzene at a former gasworks site. Water Science & Technology: Water Supply 7, 145-153.

Milczarek, G., Rebis, T., Fabianska, J., 2013. One-step synthesis of lignosulfonate-stabilized silver nanoparticles. Colloids and Surfaces B: Biointerfaces 105, 335-341.

Millington, R.J., Quirk, J.P., 1961. Permeability of porous solids. Transactions of the Faraday Society 57, 1200-1207.

Minasny, B., McBratney, A.B., Whelan, B.M., 1999. VESPER version 1.0. Australian Centre for Precision Agriculture, McMillan Building A05, The University of Sydney, NSW 2006.

Mueller, N.C., Nowack, B., 2010. Nano Zero Valent Iron - the Solution for Water and Soil Remediation?, Report of the ObservatoryNANO. www.observatorynano.eu.

Mulligan, C.N., Yong, R.N., Gibbs, B.F., 2001. Remediation technologies for metal-contaminated soils and groundwater: an evaluation. Engineering Geology 60, 193-207.

Nanthakumar, B., Arinaitwe, E., Pawlik, M., 2010. Adsorption of sodium lignosulfonates on hematite. Adsorption 16, 447-455.

Nobre, M.M.M., Nobre, R.C.M., 2004. Soil vapor extraction of chlorinated solvents at an industrial site in Brazil. Journal of Hazardous Materials 110, 119-127.

Nurmi, J.T., Tratnyek, P.G., Sarathy, V., Baer, D.R., Amonette, J.E., Pecher, K., Wang, C., Linehan, J.C., Matson, D.W., Penn, R.L., Driessen, M.D., 2005. Characterization and properties of metallic iron nanoparticles: Spectroscopy, electrochemistry, and kinetics. Environmental Science & Technology 39, 1221-1230.

Nyman, V., Rose, G., Ralston, J., 1986. The colloidal behaviour of kraft lignin and lignosulfonates. Colloids and Surfaces 21, 125-147.

O'Carroll, D., Sleep, B., Krol, M., Boparai, H., Kocur, C., 2013. Nanoscale zero valent iron and bimetallic particles for contaminated site remediation. Advances in Water Resources 51, 104-122.

Ottofuelling, S., Von Der Kammer, F., Hofmann, T., 2011. Commercial titanium dioxide nanoparticles in both natural and synthetic water: Comprehensive multidimensional testing and prediction of aggregation behavior. Environmental Science & Technology 45, 10045-10052.

Pang, Y.-X., Qiu, X.-Q., Yang, D.-J., Lou, H.-M., 2008. Influence of oxidation, hydroxymethylation and sulfomethylation on the physicochemical properties of calcium lignosulfonate. Colloids and Surfaces A: Physicochemical and Engineering Aspects 312, 154-159.

Park, G., Shin, H.S., Ko, S.O., 2005. A laboratory and pilot study of thermally enhanced soil vapor extraction method for the removal of semi-volatile organic contaminants. Journal of Environmental Science and Health - Part A Toxic/Hazardous Substances and Environmental Engineering 40, 881-897.

Pelley, A.J., Tufenkji, N., 2008. Effect of particle size and natural organic matter on the migration of nano- and microscale latex particles in saturated porous media. Journal of Colloid and Interface Science 321, 74-83.

Petosa, A.R., Jaisi, D.P., Quevedo, I.R., Elimelech, M., Tufenkji, N., 2010. Aggregation and Deposition of Engineered Nanomaterials in Aquatic Environments: Role of Physicochemical Interactions. Environmental Science & Technology 44, 6532-6549.

Phenrat, T., Saleh, N., Sirk, K., Tilton, R.D., Lowry, G.V., 2007. Aggregation and Sedimentation of Aqueous Nanoscale Zerovalent Iron Dispersions. Environmental Science & Technology 41, 284-290.

Phenrat, T., Kim, H.-J., Fagerlund, F., Illangasekare, T., Tilton, R.D., Lowry, G.V., 2009a. Particle Size Distribution, Concentration, and Magnetic Attraction Affect Transport of Polymer-Modified Fe0 Nanoparticles in Sand Columns. Environmental Science & Technology 43, 5079-5085.

Phenrat, T., Liu, Y., Tilton, R.D., Lowry, G.V., 2009b. Adsorbed Polyelectrolyte Coatings Decrease Fe0 Nanoparticle Reactivity with TCE in Water: Conceptual Model and Mechanisms. Environmental Science & Technology 43, 1507-1514.

Phenrat, T., Cihan, A., Kim, H.-J., Mital, M., Illangasekare, T., Lowry, G.V., 2010a. Transport and Deposition of Polymer-Modified Fe0 Nanoparticles in 2-D Heterogeneous Porous Media: Effects of Particle Concentration, Fe0 Content, and Coatings. Environmental Science & Technology 44, 9086-9093.

Phenrat, T., Kim, H.-J., Fagerlund, F., Illangasekare, T., Lowry, G.V., 2010b. Empirical correlations to estimate agglomerate size and deposition during injection of a polyelectrolyte-modified Fe0 nanoparticle at high particle concentration in saturated sand. Journal of Contaminant Hydrology 118, 152-164.

Phenrat, T., Song, J.E., Cisneros, C.M., Schoenfelder, D.P., Tilton, R.D., Lowry, G.V., 2010c. Estimating Attachment of Nano- and Submicrometer-particles Coated with Organic Macromolecules in Porous Media: Development of an Empirical Model. Environmental Science & Technology 44, 4531-4538.

Phenrat, T., Fagerlund, F., Illangasekare, T., Lowry, G.V., Tilton, R.D., 2011. Polymer-Modified Fe0 Nanoparticles Target Entrapped NAPL in Two Dimensional Porous Media: Effect of Particle Concentration, NAPL Saturation, and Injection Strategy. Environmental Science & Technology 45, 6102-6109.

Pires, A., Martinho, G., Chang, N.-B., 2011. Solid waste management in European countries: A review of systems analysis techniques. Journal of Environmental Management 92, 1033-1050.

Poulsen, M.M., Kueper, B.H., 1992. A field experiment to study the behavior of tetrachloroethylene in unsaturated porous media. Environmental Science & Technology 26, 889-895.

Poulsen, T., Massmann, J., Moldrup, P., 1996. Effects of Vapor Extraction on Contaminant Flux to Atmosphere and Ground Water. Journal of Environmental Engineering 122, 700-706.

Qu, X., Hwang, Y.S., Alvarez, P.J.J., Bouchard, D., Li, Q., 2010. UV Irradiation and Humic Acid Mediate Aggregation of Aqueous Fullerene (nC60) Nanoparticles. Environmental Science & Technology 44, 7821-7826.

Raychoudhury, T., Naja, G., Ghoshal, S., 2010. Assessment of transport of two polyelectrolyte-stabilized zero-valent iron nanoparticles in porous media. Journal of Contaminant Hydrology 118, 143-151.

Raychoudhury, T., Tufenkji, N., Ghoshal, S., 2012. Aggregation and deposition kinetics of carboxymethyl cellulose-modified zero-valent iron nanoparticles in porous media. Water Research 46, 1735-1744.

Roland, U., Holzer, F., Buchenhorst, D., Kopinke, F.D., 2007. Results of Field Tests on Radio-Wave Heating for Soil Remediation. Environmental Science & Technology 41, 8447-8452.

Roland, U., Buchenhorst, D., Holzer, F., Kopinke, F.D., 2008. Engineering Aspects of Radio-Wave Heating for Soil Remediation and Compatibility with Biodegradation. Environmental Science & Technology 42, 1232-1237.

Roland, U., Holzer, F., Kopinke, F.D., 2011. Combining Different Frequencies for Electrical Heating of Saturated and Unsaturated Soil Zones. Chemical Engineering & Technology 34, 1645-1651.

Ryan, J.N., Elimelech, M., 1996. Colloid mobilization and transport in groundwater. Colloids and Surfaces A: Physicochemical and Engineering Aspects 107, 1-56.

Saleh, N., Kim, H.J., Phenrat, T., Matyjaszewski, K., Tilton, R.D., Lowry, G.V., 2008. Ionic strength and composition affect the mobility of surface-modified Fe^0 nanoparticles in water-saturated sand columns. Environmental Science & Technology 42, 3349-3355.

Sayles, G.D., You, G., Wang, M., Kupferle, M.J., 1997. DDT, DDD, and DDE Dechlorination by Zero-Valent Iron. Environmental Science & Technology 31, 3448-3454.

Schrick, B., Blough, J.L., Jones, A.D., Mallouk, T.E., 2002. Hydrodechlorination of Trichloroethylene to Hydrocarbons Using Bimetallic Nickel−Iron Nanoparticles. Chemistry of Materials 14, 5140-5147.

Schrick, B., Hydutsky, B.W., Blough, J.L., Mallouk, T.E., 2004. Delivery Vehicles for Zerovalent Metal Nanoparticles in Soil and Groundwater. Chemistry of Materials 16, 2187-2193.

Song, J.E., Phenrat, T., Marinakos, S., Xiao, Y., Liu, J., Wiesner, M.R., Tilton, R.D., Lowry, G.V., 2011. Hydrophobic Interactions Increase Attachment of Gum Arabic- and PVP-Coated Ag Nanoparticles to Hydrophobic Surfaces. Environmental Science & Technology 45, 5988-5995.

Song, L., Johnson, P.R., Elimelech, M., 1994. Kinetics of Colloid Deposition onto Heterogeneously Charged Surfaces in Porous Media. Environmental Science & Technology 28, 1164-1171.

Sparrevik, M., Saloranta, T., Cornelissen, G., Eek, E., Fet, A.M., Breedveld, G.D., Linkov, I., 2011. Use of Life Cycle Assessments To Evaluate the Environmental Footprint of Contaminated Sediment Remediation. Environmental Science & Technology 45, 4235-4241.

Stegemeier, G.L., Vinegar, H.J., 2001. Thermal conduction heating for in-situ thermal desorption of soils, Hazardous & Radioactive Waste Treatment Technologies Handbook, Boca Raton, Florida.

Steubing, B., Böni, H., Schluep, M., Silva, U., Ludwig, C., 2010. Assessing computer waste generation in Chile using material flow analysis. Waste Management 30, 473-482.

Stevenson, F.J., 1994. Humus Chemistry: Genesis, Composition, Reactions. John Wiley & Sons, New York, USA.

Stieber, M., Putschew, A., Jekel, M., 2011. Treatment of Pharmaceuticals and Diagnostic Agents Using Zero-Valent Iron – Kinetic Studies and Assessment of Transformation Products Assay. Environmental Science & Technology 45, 4944-4950.

Stroo, H.F., Unger, M., Ward, C.H., Kavanaugh, M.C., Vogel, C., Leeson, A., Marqusee, J.A., Smith, B.P., 2003. Peer Reviewed: Remediating Chlorinated Solvent Source Zones. Environmental Science & Technology 37, 224A-230A.

Stroo, H.F., Leeson, A., Marqusee, J.A., Johnson, P.C., Ward, C.H., Kavanaugh, M.C., Sale, T.C., Newell, C.J., Pennell, K.D., Lebrón, C.A., Unger, M., 2012. Chlorinated Ethene Source Remediation: Lessons Learned. Environmental Science & Technology 46, 6438-6447.

Stumm, W., Morgan, J.J., 1996. Aquatic chemistry: chemical equilibria and rates in natural waters. Wiley, New York, USA.

Su, C., Puls, R.W., Krug, T.A., Watling, M.T., O'Hara, S.K., Quinn, J.W., Ruiz, N.E., 2012. A two and half-year-performance evaluation of a field test on treatment of source zone tetrachloroethene and its chlorinated daughter products using emulsified zero valent iron nanoparticles. Water Research 46, 5071-5084.

Taylor, J.J., Sigmund, W.M., 2010. Adsorption of sodium polyacrylate in high solids loading calcium carbonate slurries. Journal of Colloid and Interface Science 341, 298-302.

Tiraferri, A., Sethi, R., 2009. Enhanced transport of zerovalent iron nanoparticles in saturated porous media by guar gum. Journal of Nanoparticle Research 11, 635-645.

Tosco, T., Bosch, J., Meckenstock, R.U., Sethi, R., 2012. Transport of Ferrihydrite Nanoparticles in Saturated Porous Media: Role of Ionic Strength and Flow Rate. Environmental Science & Technology 46, 4008-4015.

Tratnyek, P.G., Johnson, R.L., 2006. Nanotechnologies for environmental cleanup. Nano Today 1, 44-48.

Triplett Kingston, J.L., Dahlen, P.R., Johnson, P.C., 2010. State-of-the-practice review of in situ thermal technologies. Ground Water Monitoring and Remediation 30, 64-72.

U.S. Environmental Protection Agency, US EPA, 1996. Pump-and-Treat Ground-Water Remediation - A Guide for Decision Makers and Practitioners. EPA 625-R-95-005, Office of Research and Development, Washington, D.C., USA.

U.S. Environmental Protection Agency, US EPA, 1997a. Analysis of Selected Enhancements for Soil Vapor Extraction. EPA 542-R-97-007, Office of Solid Waste and Emergency Response, Washington, D.C., USA.

U.S. Environmental Protection Agency, US EPA, 1997b. Ground Water Issue, How Heat Can Enhance In-situ Soil and Aquifer Remediation: Important Chemical Properties and Guidance on Choosing the Appropriate Technique. EPA 540-S-97-502, Office of Research and Development, Office of Solid Waste and Emergency Response, Washington, D.C., USA.

U.S. Environmental Protection Agency, US EPA, 1998. Permeable Reactive Barrier - Technologies for Contaminant Remediation. EPA 600-R-98-125, Office of Research and Development, Office of Solid Waste and Emergency Response, Washington, D.C., USA.

U.S. Environmental Protection Agency, US EPA, 2004. In situ thermal treatment of chlorinated solvents: Fundamentals and field applications. EPA 542-R-04-010, Office of Solid Waste and Emergency Response, Office of Superfund Remediation and Technology Innovation, Washington, D.C., USA.

U.S. Environmental Protection Agency, US EPA, 2005. U.S. EPA Workshop on Nanotechnology for Site Remediation. 20-21 October 2005, Washington, D.C., http://epa.gov/ncer/publications/workshop/pdf/10_20_05_nanosummary.pdf.

U.S. Environmental Protection Agency, US EPA, 2008. Nanotechnology for Site Remediation - Fact Sheet. EPA 542-F-08-009, Office of Solid Waste and Emergency Response, Cincinnati, USA.

U.S. Sustainable Remediation Forum, 2009. Sustainable remediation white paper - Integrating sustainable principles, practices, and metrics into remediation projects. Remediation Journal 19, 5-114.

Voudrias, E., 2001. Pump-and-treat remediation of groundwater contaminated by hazardous waste: Can it really be achieved. Global Network for Environmental Science and Technology: the International Journal 3, 1-10.

Wang, C.-B., Zhang, W.-x., 1997. Synthesizing Nanoscale Iron Particles for Rapid and Complete Dechlorination of TCE and PCBs. Environmental Science & Technology 31, 2154-2156.

Wang, L., Xu, S., Li, J., 2011. Effects of Phosphate on the Transport of Escherichia coli O157:H7 in Saturated Quartz Sand. Environmental Science & Technology 45, 9566-9573.

Wang, T., Müller, D.B., Graedel, T.E., 2007. Forging the Anthropogenic Iron Cycle. Environmental Science & Technology 41, 5120-5129.

Xie, Y., Chen, T.-b., Lei, M., Yang, J., Guo, Q.-j., Song, B., Zhou, X.-y., 2011. Spatial distribution of soil heavy metal pollution estimated by different interpolation methods: Accuracy and uncertainty analysis. Chemosphere 82, 468-476.

Xiu, Z.-m., Gregory, K.B., Lowry, G.V., Alvarez, P.J.J., 2010. Effect of Bare and Coated Nanoscale Zerovalent Iron on tceA and vcrA Gene Expression in Dehalococcoides spp. Environmental Science & Technology 44, 7647-7651.

Yang, X., Flynn, R., von der Kammer, F., Hofmann, T., 2010. Quantifying the influence of humic acid adsorption on colloidal microsphere deposition onto iron-oxide-coated sand. Environmental Pollution 158, 3498-3506.

Yang, X., Flynn, R., von der Kammer, F., Hofmann, T., 2011. Influence of ionic strength and pH on the limitation of latex microsphere deposition sites on iron-oxide coated sand by humic acid. Environmental Pollution 159, 1896-1904.

Yao, K.-M., Habibian, M.T., O'Melia, C.R., 1971. Water and waste water filtration. Concepts and applications. Environmental Science & Technology 5, 1105-1112.

Yu, S.C.T., 1995. Transport and fate of chlorinated hydrocarbons in the vadose zone - a literature review with discussions on regulatory implications. Journal of Soil Contamination 4, 25-56.

Zentralanstalt für Meteorologie und Geodynamik, ZAMG, 2012. Klimadaten von Österreich 1971–2000. http://www.zamg.ac.at/fix/klima/oe71-00/klima2000/klimadaten_oesterreich_1971_frame1.htm (accessed 10 Apr. 2012).

Zhan, J., Zheng, T., Piringer, G., Day, C., McPherson, G.L., Lu, Y., Papadopoulos, K., John, V.T., 2008. Transport Characteristics of Nanoscale Functional Zerovalent Iron/Silica Composites for in Situ Remediation of Trichloroethylene. Environmental Science & Technology 42, 8871-8876.

Zhang, W.-X., 2003. Nanoscale Iron Particles for Environmental Remediation: An Overview. Journal of Nanoparticle Research 5, 323-332.

Zhang, W.-X., Elliott, D.W., 2006. Applications of iron nanoparticles for groundwater remediation. Remediation Journal 16, 7-21.

Zhong, S., Mucci, A., 1995. Partitioning of rare earth elements (REEs) between calcite and seawater solutions at 25°C and 1 atm, and high dissolved REE concentrations. Geochimica et Cosmochimica Acta 59, 443-453.

Contributions

Several colleagues and co-authors aided in the writing and research of the published (or submitted) papers presented in this dissertation. A brief description of their contributions is listed below.

Prof. Thilo Hofmann (Department of Environmental Geosciences, University of Vienna) was the primary research advisor. He provided scientific guidance, helped with the interpretation and discussion of results, and contributed to the writing of all chapters.

Dr. Vesna Micić (Department of Environmental Geosciences, University of Vienna) was the co-advisor of this PhD thesis. She provided scientific guidance, helped with the experimental design and with the interpretation and discussion of the results, and contributed to the writing of all chapters.

Prof. Gregory V. Lowry (Center for Environmental Implications of NanoTechnology (CEINT) and Departments of Civil & Environmental Engineering, Chemical Engineering, and Biomedical Engineering, Carnegie Mellon University) provided scientific guidance on the application of nZVI for *in situ* groundwater remediation, assisted with interpretation of the results presented in Chapter 2, and contributed to the writing of Chapter 2.

Dr. Johann Fellner (Institute for Water Quality, Resource and Waste Management, Vienna University of Technology) performed parts of the data analysis in Chapter 4, including material flow analysis and Kriging interpolation, and partly contributed to the writing of Chapter 4.

David Clement (Institute for Water Quality, Resource and Waste Management, Vienna University of Technology) performed parts of the data analysis in Chapter 4, including material flow analysis and Kriging interpolation.

List of Figures

List of Tables

Curriculum vitae

Education

2009 - present	**PhD "Assessment of innovative *in situ* techniques for soil and groundwater remediation"**, Department of Environmental Geosciences, University of Vienna, Supervisors Prof. Thilo Hofmann and Dr. Vesna Micić
2008 - 2009	**Staatsexamen** (state examination) in Food Chemistry, State Office for Consumer Protection, Halle, Germany
2003 - 2008	**Diplom (M.Sc. equivalent) in Food Chemistry**, Institute of Chemistry, Food Chemistry and Environmental Chemistry at the Martin-Luther University Halle-Wittenberg, Germany
2003	**Abitur** (qualification for university entrance), Gymnasium Bad Iburg, Germany

Relevant work experience

2011 - present	Researcher in the NanoSan Project (Application of nanoscale zero-valent iron (nZVI) for *in situ* remediation of groundwater contaminated by chlorinated solvents; funded by the Austrian Federal Ministry of Agriculture, Forestry, Environment and Water Management). *Responsible for design and management of nanoparticle transport studies, writing and editing of project reports, coordination and oversee activities (time planning, organization of meetings, communication with partners, the scientific advisory board and the funding agency), and budget control.*
2009 - 2011	Researcher in the MEMOS Project (Material flow analysis as an effectiveness assessment tool for *in situ* thermal remediation of a chlorinated solvent source zone; funded by the Austrian Federal Ministry of Agriculture, Forestry, Environment and Water Management). *Responsible for collection of field data and data management, writing and editing of the project report, coordinating project meetings, and external communication with project partners.*

Publications

Laumann S., V. Micić and T. Hofmann. Mobility enhancement of nanoscale zero-valent iron in carbonate porous media through co-injection of polyelectrolytes, submitted to Water Research.

Laumann S., V. Micić, G. V. Lowry and T. Hofmann (2013). Carbonate minerals in porous media decrease mobility of polyacrylic acid modified zero-valent iron nanoparticles used for groundwater remediation, Environmental Pollution 179: 53-60.

Laumann S., V. Micić, J. Fellner, D. Clement and T. Hofmann (2013). Material Flow Analysis: An Effectiveness Assessment Tool for In Situ Thermal Remediation, Vadose Zone Journal 12 (1).

Laumann S., V. Micic, M. A. Kruge, C. Achten, R. F. Sachsenhofer, J. Schwarzbauer and T. Hofmann (2011). Variations in concentrations and compositions of polycyclic aromatic hydrocarbons (PAHs) in coals related to the coal rank and origin, Environmental Pollution 159 (10): 2690-2697.

Platform presentations

Laumann, S., V. Micić and T. Hofmann (2013). Polyelectrolyte injection increases mobility of nanoscale zero-valent iron in carbonate sand. Goldschmidt Conference, Florence, Italy.

Laumann, S., V. Micić, D. Schmid and T. Hofmann (2013). Injection of polyelectrolytes enhances mobility of zero-valent iron nanoparticles in carbonate-rich porous media. European Geosciences Union General Assembly, Vienna, Austria.

Laumann, S., V. Micić and T. Hofmann (2012). Transport of zero-valent iron nanoparticles used for remediation in calcareous porous aquifers. FH-DGG Conference, Dresden, Germany.

Appendix

A.1. Carbonate minerals in porous media decrease mobility of polyacrylic acid modified zero-valent iron nanoparticles used for groundwater remediation

A.1.1. Porous media characteristics

Table A-1. Chemical composition of the carbonate sand (CS).

		CS 1	CS 2	CS 3	Mean	Standard deviation
SiO_2	[%]	0,31	0,32	0,31	0,31	0,01
Al_2O_3	[%]	0,19	0,20	0,19	0,19	0,00
Fe_2O_3	[%]	0,06	0,06	0,07	0,07	0,01
CaO	[%]	54,95	54,90	54,62	54,82	0,18
MgO	[%]	1,05	1,01	1,09	1,05	0,04
Na_2O	[%]	0,04	0,03	0,04	0,04	0,00
K_2O	[%]	0,02	0,04	0,03	0,03	0,01
MnO	[%]	<0,01	<0,01	<0,01	<0,01	<0,01
TiO_2	[%]	<0,01	<0,01	<0,01	<0,01	<0,01
P_2O_5	[%]	<0,01	<0,01	<0,01	<0,01	<0,01
Glowing loss	[%]	43,37	43,07	43,38	43,27	0,18
Sum	[%]	100,00	99,64	99,74	99,79	0,19

The chemical composition of the carbonate sand was determined by inductively coupled plasma optical emission spectrometry (ICP-OES, Optima 5300DV, PerkinElmer) after chemical digestion.

A.1.2. Dissolution of the carbonate sand during the column experiment

Table A-2. Changes in electrical conductivity (EC) and pH during the column experiment.

Porous media	Column inflow		Column outflow	
	pH	EC	pH	EC
		µS cm^{-1}		µS cm^{-1}
100% QS	8.32	92	8.35	95
90:10% QS:CS	8.32	92	9.07	104
50:50% QS:CS	8.32	92	9.04	111
10:90% QS:CS	8.32	92	9.03	110
100% CS	8.32	92	9.04	115

A.2. Mobility enhancement of nanoscale zero-valent iron in carbonate porous media through co-injection of polyelectrolytes

A.2.1. Polyelectrolyte interaction with porous media

Table A-3. Results of the convection-dispersion model for lignin sulfonate transport through quartz and carbonate sands.

Porous media	**n**	**v**	**D**	**R**	**r^2**	ρ_b	**K_d**
		$m\ s^{-1}$	$cm^2\ s^{-1}$			$g\ cm^{-3}$	$cm^3\ g^{-1}$
Quartz sand	0.39	6.5×10^{-4}	0.056	0.99	0.995	1.62	/
Carbonate sand	0.49	5.2×10^{-4}	0.070	1.78	0.994	1.38	0.277

Porosity (n), pore water velocity (v), hydrodynamic dispersion coefficient for lignin sulfonate (D), retardation factor (R), and distribution coefficient (K_d).

K_d was determined using the following relationship: $R = 1 + \frac{\rho_b K_d}{n}$, where ρ_b is the bulk density of the media bed: $\rho_b = (1-n)\rho_{quartz/calcite}$ (ρ_{quartz} = 2.65 g cm^{-3}; $\rho_{calcite}$ = 2.71 g cm^{-3}).

A.2.2. Effect of different polyelectrolytes on PAA-nZVI transport

Table A-4. Transport and deposition parameters for PAA-nZVI particles co-injected with different polyelectrolytes in quartz and carbonate sands.

	Polyelectrolyte	**d_c**	**n**	**v**	**D**	**k_{CDE}**	**r^2**	**α**	**L_T(99.9)**
	50 mg L^{-1}	mm		$m\ s^{-1}$	$cm^2\ s^{-1}$	s^{-1}			m
Quartz sand	Pure PAA-nZVI				0.067	0.0060	0.990	0.32	0.82
	NOM				0.067	0.0054	0.993	0.29	0.89
	Lignin sulfonate	0.68	0.38	6.7×10^{-4}	0.059	0.0058	0.998	0.31	0.85
	CMC				0.056	0.0057	0.998	0.31	0.85
	Humic acid				0.059	0.0057	0.992	0.28	0.92
Carbonate sand	Pure PAA-nZVI				0.037	0.0110	0.982	1.03	0.37
	NOM				0.033	0.0076	0.996	0.74	0.51
	Lignin sulfonate	0.75	0.49	5.2×10^{-4}	0.036	0.0072	0.987	0.70	0.54
	CMC				0.036	0.0075	0.987	0.76	0.50
	Humic acid				0.023	0.0068	0.995	0.68	0.56

Mean diameter of the porous media (d_c), porosity (n), pore water velocity (v), hydrodynamic dispersion coefficient for the PAA-nZVI particles (D), deposition rate coefficient (k_{CDE}), attachment efficiency (α), and travel distance to remove 99.9% of the PAA-nZVI particles (L_T).

A.2.3. Properties of the different polyelectrolytes

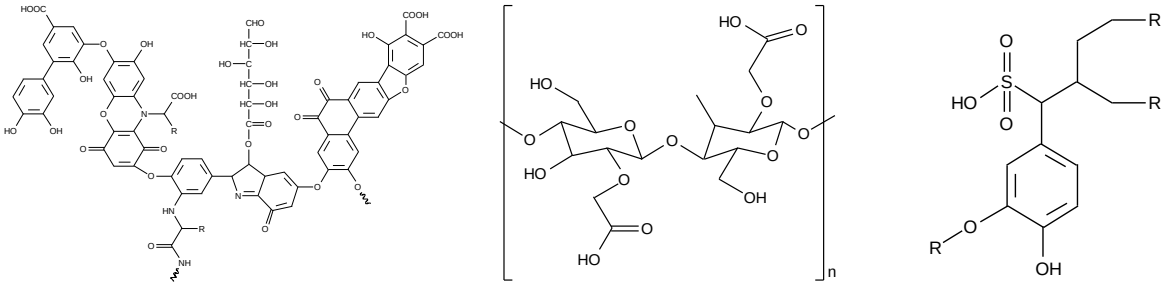

Natural organic matter/Humic acid (after Stevenson, 1994) **Carboxymethyl cellulose** **Lignin sulfonate**

Figure A-1. Molecular structure of NOM/humic acid, CMC, and lignin sulfonate (R describes the basic structures found in lignin). Note that NOM is a complex mixture of plant and microbial residues, with variable structural and functional characteristics. Humic acid is a model substance representing the prevailing functional groups in the NOM structure.

Table A-5. Elemental composition of the four investigated polyelectrolytes.

Polyelectrolyte	C [%]	H [%]	N [%]	S [%]	O [%]
NOM[a]	52.47	4.19	1.10	0.65	42.69
Humic acid	48.73	3.83	0.87	1.25	29.26
Lignin sulfonate	39.14	4.773	1.028	6.254	33.00
CMC	36.77	5.141	0.14	0.252	44.36

The elemental composition (C, H, N, S, O) of the Suwannee River NOM was provided by the International Humic Substance Society. The elemental compositions (C, H, N, S) of the other polyelectrolytes were determined using an Elementar Vario MACRO CHNS analyzer. For oxygen measurements, the polyelectrolytes were combusted in a pyrolysis oven (Hekatech, Germany) and analyzed with an isotope ratio mass spectrometer (DeltaV Advantage, Thermo Scientific, Germany).

A.2.4. Effect of polyelectrolyte concentration on PAA-nZVI transport

Table A-6. Transport and deposition parameters of the PAA-nZVI particles co-injected with different lignin sulfonate concentrations in quartz and carbonate sand.

	Lignin sulfonate concentration	**d_c**	**n**	**v**	**D**	**k_{CDE}**	**r^2**	**α**	**L_T(99.9)**
	mg L^{-1}	mm		m s^{-1}	cm^2 s^{-1}	s^{-1}			m
Quartz sand	0	0.68	0.38	6.7 x 10^{-4}	0.067	0.0060	0.990	0.31	0.82
	10				0.065	0.0066	0.992	0.34	0.75
	25				0.058	0.0058	0.994	0.31	0.85
	50				0.059	0.0058	0.998	0.31	0.85
	250				0.048	0.0055	0.996	0.29	0.90
	500				0.071	0.0056	0.984	0.31	0.85
Carbonate sand	0	0.75	0.49	5.2 x 10^{-4}	0.037	0.0110	0.982	1.03	0.37
	10				0.037	0.0107	0.994	1.00	0.38
	25				0.028	0.0082	0.997	0.80	0.47
	50				0.036	0.0072	0.987	0.70	0.54
	250				0.024	0.0072	0.999	0.70	0.54
	500				0.028	0.0060	0.994	0.60	0.64

Mean diameter of the porous media (d_c), porosity (n), pore water velocity (v), hydrodynamic dispersion coefficient for the PAA-nZVI particles (D), deposition rate coefficient (k_{CDE}), attachment efficiency (α), and travel distance to remove 99.9% of the PAA-nZVI particles (L_T).

A.3. Material flow analysis: an effectiveness assessment tool for *in situ* thermal remediation

A.3.1. Site description

Table A-7. Minimum and maximum chlorinated solvent concentrations in all affected matrices prior to remediation.

Compound	**Soil** mg kg^{-1}	**Soil vapor** mg m^{-3}	**Groundwater** µg L^{-1}
Tetrachloroethene	<0.1 – 1979.0	10.4 – 2617	<0.1 – 1057.0
Trichloroethene	<0.1 – 5.6	<0.5 – 28.4	<0.05 – 14.2
1,1-Dichloroethene	<0.2	<0.5	<0.2
cis-1,2-Dichloroethene	<0.2 – 0.6	<0.5 – 63.4	<0.2 – 105.4
trans-1,2-Dichloroethene	<0.2	<0.5	<0.2 – 0.3
Vinylchloride	<0.1	<0.5	<0.2
1,1,1-Trichloroethane	<0.1	<0.5	<0.05
1,1-Dichloroethane	<2.0	<0.5	<2.0
1,2-Dichlorethane	<2.0	<0.5	<2.0
Tetrachloromethane	<0.1	<0.5	<0.02
Trichloromethane	<0.1	<0.5	<0.1
Dichloromethane	<2.0	<0.5	<2.0

Minimum concentrations were limited by the detection limit for each compound (indicated by <).

A.3.2. Field implementation of *in situ* thermal desorption

Table A-8. Soil vapor extraction (SVE) strings, related SVE wells, their extraction depths (below ground surface, bgs), and their locations within the investigated site.

SVE string	**SVE wells**	**Extraction depth**	**Location**
SVE string 1	E5, E9, E11, E26	1 – 2 m bgs	Section II,III,IV
SVE string 2	E17, E19, E21	1 – 2 m bgs	Section III,IV
SVE string 3	E1, E2, E3, E4, E6, E7, E8	4 – 6 m bgs	Section I,II
SVE string 4	E10, E12, E13, E14, E15, E16, E18	4 – 6 m bgs	Section III
SVE string 5	E20, E22, E23, E24, E25, E27, E28	4 – 6 m bgs	Section IV

A.3.3. Ordinary kriging

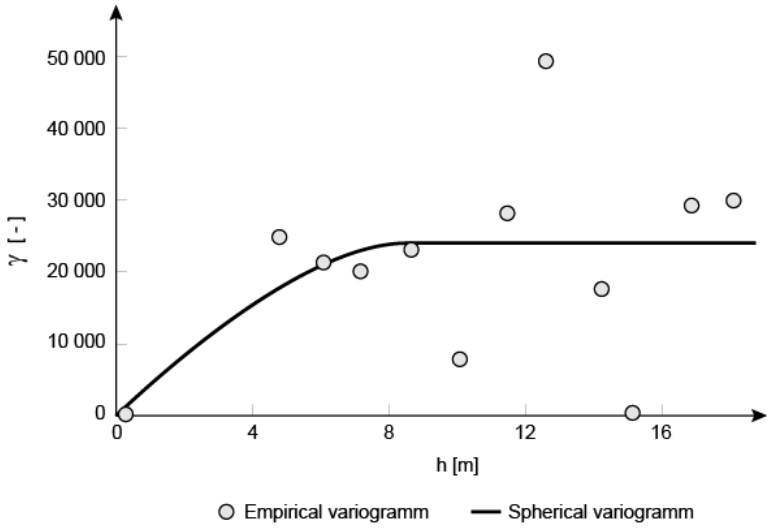

Figure A-2. Semivariogram for chlorinated solvent concentrations in Zone A (1.50–3.25 m below ground surface, bgs)

The best fit to the empirical variograms for all three depth zones (A-C) was achieved by the spherical model. This model is characterized by a linear increase and a smooth transition to the sill (Hofmann et al., 2010).

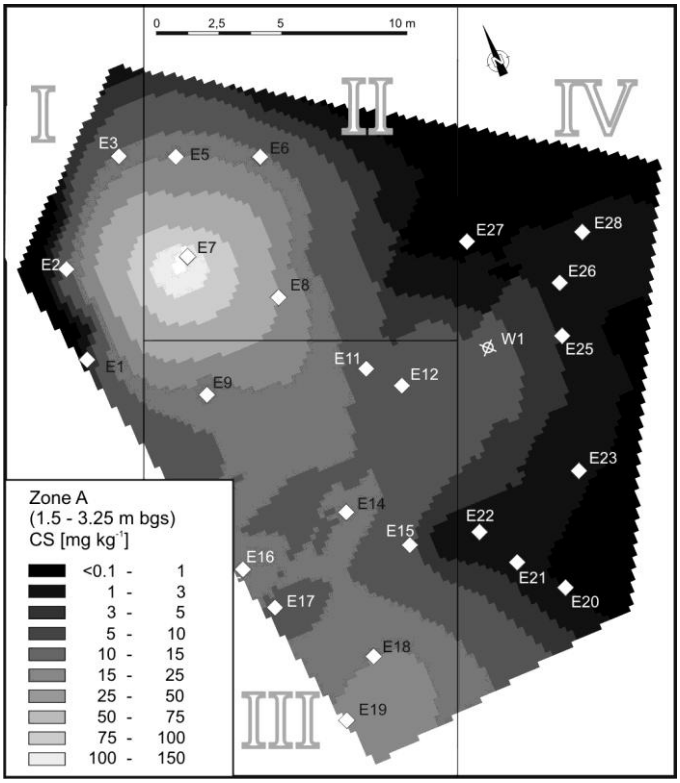

Figure A-3. Interpolated chlorinated solvent concentrations in Zone A (1.50–3.25 m bgs)

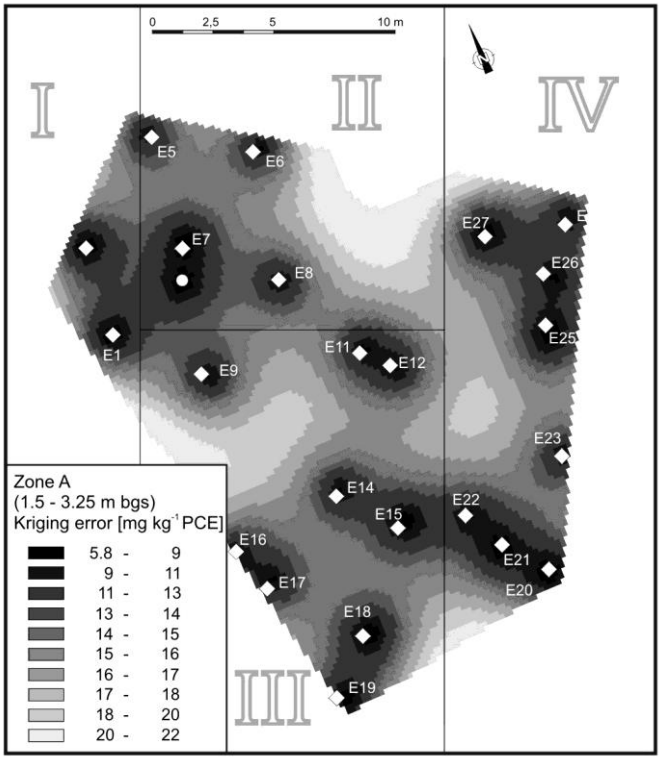

Figure A-4. Error map for chlorinated solvent concentrations in Zone A (1.50–3.25 m bgs)

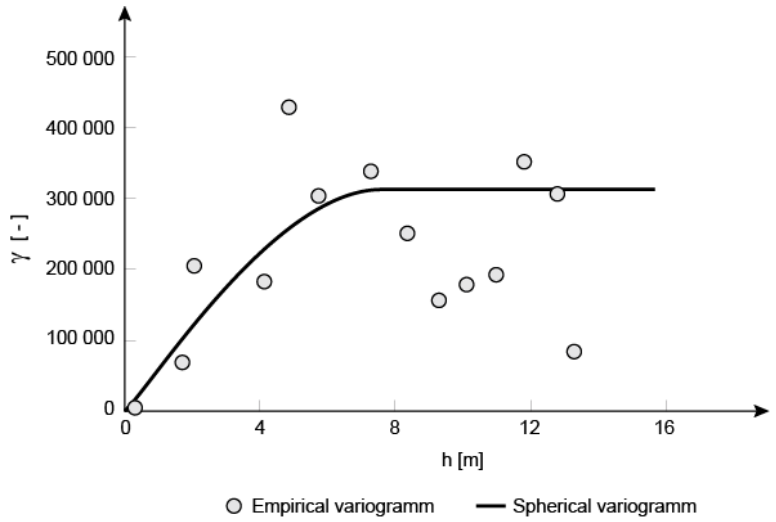

Figure A-5. Semivariogram for chlorinated solvent concentrations in Zone B (3.25–5.00 m bgs)

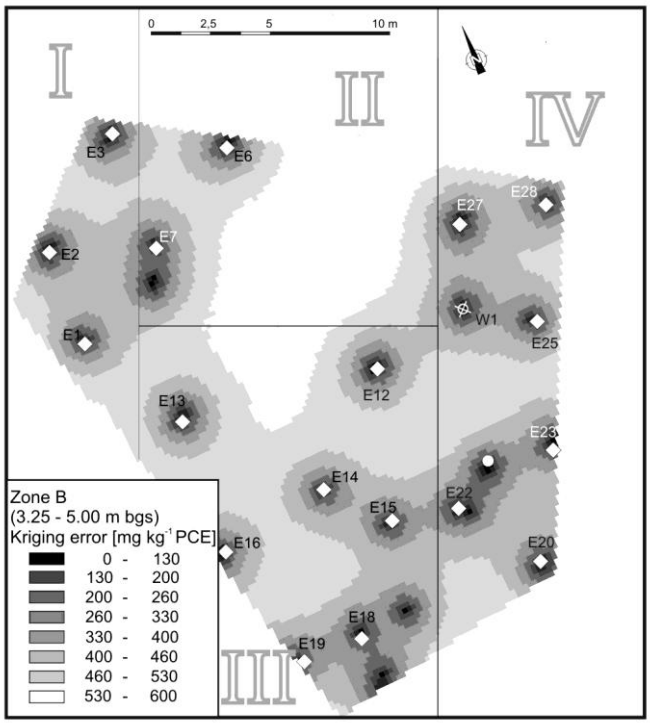

Figure A-6. Error map for chlorinated solvent concentrations in Zone B (3.25–5.00 m bgs)

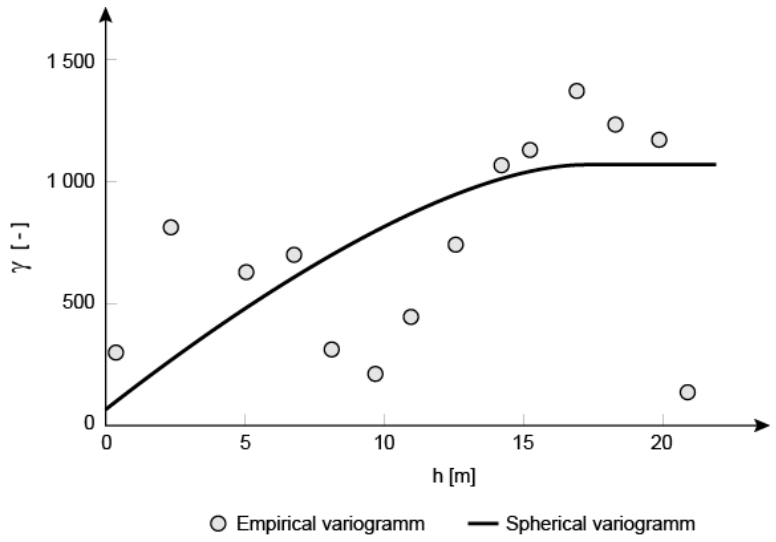

Figure A-7. Semivariogram for chlorinated solvent concentrations in Zone C (5.0–7.0 m bgs)

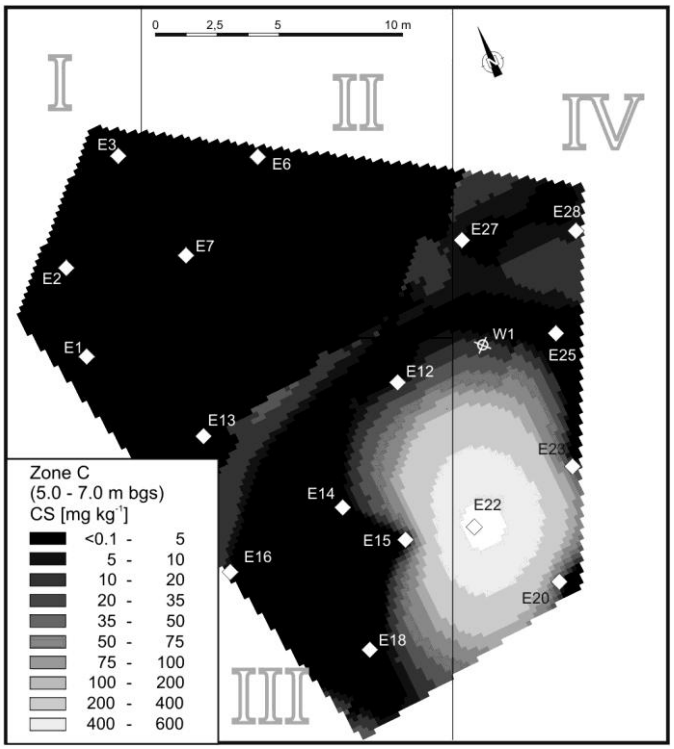

Figure A-8. Interpolated chlorinated solvent concentrations in Zone C (5.0–7.0 m bgs)

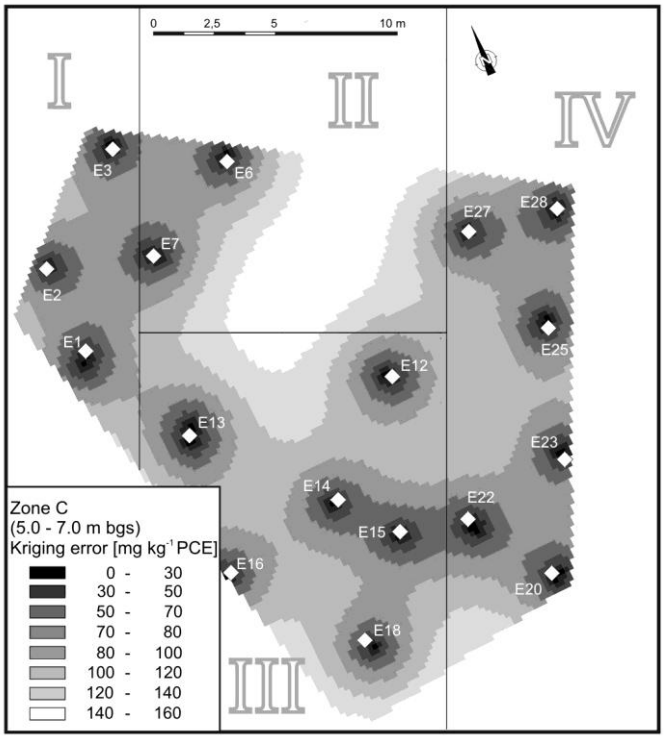

Figure A-9. Error map for chlorinated solvent concentrations in Zone C (5.0–7.0 m bgs)

A.3.5. Chlorinated solvent mass flux from soil vapor into the atmosphere

Fick's first law

$$e_{CS} = -D_{a \cdot eff} \cdot \frac{d\, c_{CS}}{d\, x}$$

e_{CS} – diffusive vapor flux of chlorinated solvents

$\frac{d\, c_{CS}}{d\, x}$ – concentration gradient of chlorinated solvents in soil vapor

The chlorinated solvent concentration gradient was calculated using the minimum and maximum values from the depth at which the highest chlorinated solvent concentrations were recorded (3 to 4 m bgs), while the chlorinated solvent concentration at the ground surface was set to zero.

$D_{a \cdot eff}$ – effective diffusion coefficient after Millington and Quirk (1961)

$D_{a \cdot eff} = D_a \times \tau$ and $\tau = \left(\frac{n_g}{n}\right)^2 \times n^{\frac{4}{3}}$

D_a - molecular gas diffusion coefficient

τ - tortuosity

n_g - air filled porosity

n - overall porosity

Table A-9. Estimated diffusive vapor flux of chlorinated solvents prior to remediation.

	Unit	Maximum values	Minimum values
Gas diffusion coefficient of PCE (D_a)	$m^2\ s^{-1}$	8.0E-06	8.0E-06
Tortuosity (τ)	-	0.060	0.089
Air filled porosity (n_g)	-	0.18	0.22
Overall porosity (n)	-	0.4	0.4
Effective diffusion coefficient ($D_{a \cdot eff}$)	$m^2\ s^{-1}$	4.8E-07	7.1E-07
Chlorinated solvent concentrations in soil vapor (c_{CS})	$mg\ m^{-3}$	3000	1000
Soil vapor extraction depth (x_{ED})	m	3	4
Concentration gradient ($\frac{c_{CS}}{x_{ED}}$)	$mg\ m^{-2}$	1000	250
Diffusive vapor flux of chlorinated solvents (e_{CS})	$mg\ m^2\ d^{-1}$	41	15
Contaminated area (A)	m^2	200	100
Annual CS emission ($E_{CS} = e_{CS} \times A$)	$kg\ a^{-1}$	3.0	0.6
Total CS emission (in 33 years†)	kg	99	20

† Period of 33 years: from the start of the dry-cleaning facility until the start of remediation. CS-chlorinated solvents.

A.3.6. Chlorinated solvent mass flux from groundwater into the hydrosphere

The rate of contaminant mass transfer in groundwater passing the transect (W2 – W5, Fig. 1) was calculated as follows:

$MF = qA \sin\varphi\, C$

MF = mass flux from source zone (g d^{-1})

C = chlorinated solvent concentration (µg L^{-1})

q = specific discharge (m d^{-1}); q = k_f*i; i = hydraulic gradient (~0.004); k_f = hydraulic conductivity (k_f (well W2) = 4.15*10^{-5} m s^{-1}, k_f (well W3) = 4.08*10^{-5} m s^{-1}, k_f (well W4) = 5.26*10^{-5} m s^{-1}, k_f (well W5) = 4.19*10^{-5} m s^{-1})

A = cross-sectional area (width of the transect*aquifer thickness, m^2)

φ = Angle between the transect W2-W5 and the groundwater flow direction

Table A-10. Estimation of the chlorinated solvent mass flux in groundwater passing along the W2–W5 transect prior to remediation.

	Unit	W2	W3	W4	W5	Total/Average
Width of the transect	m	19.80	19.80	19.80	19.80	79
Aquifer thickness	m	6.40	6.60	6.60	5.70	6.3
Cross-sectional area	m^2	127	131	131	113	501
Average chlorinated solvent concentrations	µg l^{-1}	0.3	102	1158	50	328
Estimated uncertainty of average chlorinated solvent concentration	µg l^{-1}	10	70	700	30	
Specific discharge	m d^{-1}	0.014	0.014	0.018	0.015	0.015
Angle φ between transect and groundwater flow direction	°	45	45	45	45	45
Average chlorinated solvent mass flux	g d^{-1}	0.00	0.13	1.93	0.06	2.1
Uncertainty of chlorinated solvent mass flux		0.01	0.09	1.17	0.04	1.3